



UNIVERSITÀ DEGLI STUDI DI TRIESTE

XXXIII CICLO DEL DOTTORATO DI RICERCA IN
SCIENZE DELLA RIPRODUZIONE E DELLO SVILUPPO

PRECISION THERAPY FOR PEDIATRIC BCR-ABL- LIKE ACUTE LYMPHOBLASTIC LEUKEMIA: DEVELOPMENT OF AN IN VITRO SYSTEM FOR DIAGNOSIS AND CLINICAL MONITORING

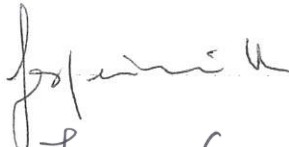
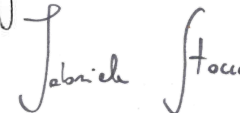

Settore scientifico-disciplinare: **BIO/14**

DOTTORANDA
OKSANA MONTECCHINI

COORDINATORE
PROF. PAOLO GASPARINI

SUPERVISORE DI TESI
PROF. GABRIELE STOCCO

CO-SUPERVISORE DI TESI
PROF. GIULIANA DECORTI

ANNO ACCADEMICO 2019/2020

Index

ABSTRACT	2
RIASSUNTO	4
1 INTRODUCTION	6
1.1 Acute lymphoblastic leukemia and leukemic niche	7
1.1.1 Leukemic niche.....	7
1.1.2 Genomics	9
1.2 BCR-ABL1	10
1.3 BCR-ABL like leukemias	10
1.3.1 ABL pathway.....	13
1.3.2 JAK-STAT pathway	14
1.4 Drugs targeting tyrosine kinase	16
1.5 Diagnostic approaches	17
1.6 Proteomic approach-biosensor	18
2 AIM	20
3 MATERIALS AND METHODS	22
3.1 Cell cultures	23
3.2 Patients	23
3.3 Drug and chemicals/TKI	24
3.4 Cell lysates preparation	24
3.5 Western Blot	24
3.6 Biosensor peptide ABL1 (P_{ABL})	25
3.7 P_{ABL}-Based ELISA assay	25
3.8 P_{JAK2} modeling	26
3.9 JAK2 purification	27
3.10 2D coculture	28
3.11 3D Coculture	29
3.11.1 Flow cytometry.....	30
3.11.2 Microscopy	30
3.12 TLA	31
3.13 Statistical analysis	32
4 RESULTS	33
4.1 Genetic alterations cell lines characterization	34
4.2 P_{ABL} biosensor peptide <i>in vitro</i> functional analysis	35
4.3 P_{ABL} “reporter” region signal specificity validation	36
4.4 Comparison of P_{ABL} and P_{ABLTIDE}	37

4.5	ABL1 kinase activity specificity: inhibitory effect of imatinib and ruxolitinib on P_{ABL}	38
4.7	P1_{JAK2}-P2_{JAK2} peptides and P1_{JAK2}-P2_{JAK2}/JAK2 simulation	42
4.8	JAK2 protein expression and purification	45
4.8.1	Expression	45
4.8.2	SEC purification	46
4.9	Leukemic niche 2D coculture	48
4.10	<i>In vitro</i> primary leukemic cell survival with different concentrations and combinations of growth factors	49
4.11	Primary leukemic cells survival <i>in vitro</i> with combinations of 4 different growth factors	51
4.12	The impact of different culture media on the <i>in vitro</i> survival of primary leukemic cells.	53
4.13	Leukemic niche 3D coculture	55
4.14	Stabilized cell lines survival <i>in vitro</i> measurements by flow cytometry	55
4.15	Stabilized cell lines survival <i>in vitro</i> measurements by microscopy	57
4.16	MSC migration into Puramatrix hydrogel	59
4.17	ALL cells migration in coculture and monoculture into Puramatrix hydrogel	60
4.18	MSC and ALL communication in the 3D architecture	62
4.19	TLA	63
5	DISCUSSION	68
6	CONCLUSION	77
7	REFERENCES	79

ABSTRACT

Pediatric *BCR-ABL like* (BAL) acute lymphoblastic leukemia (ALL) is a novel subtype of leukemias, identified through similarity in gene expression to *BCR-ABL1* positive ALL. BAL is associated with the activation of ABL or JAK-STAT pathways and presents a high risk of early relapse. Since BAL is a subgroup of tyrosine kinase-driven ALL, tyrosine kinase inhibitors (TKIs) might be a therapeutic option for these patients. Here we report a novel peptide biosensor (P_{ABL})-ELISA assay to investigate ABL1 activity in four immortalized leukemic cell lines with different genetic background. The P_{ABL} sequence comprises an ABL1 tyrosine (Y) phosphorylation site and a targeting sequence which increases the specificity for ABL1; additional peptides (Y-site-mutated (P_{ABL-F}) and fully-phosphorylated biosensor ($P_{PHOSPHO-ABL}$)) were included in the assay. After incubation with whole cell lysates, average P_{ABL} phosphorylation was significantly increased (basal *versus* P_{ABL} phosphorylation: $6.84 \pm 1.46\%$ vs $32.44 \pm 3.25\%$, p -value < 0.0001 , two-way ANOVA, Bonferroni post-test, percentages relative to $P_{PHOSPHO-ABL}$ in each cell line). Lines expressing ABL1-chimeric proteins (K562, ALL-SIL) presented the higher TK activity on P_{ABL} ; a lower signal was instead observed for NALM6 and REH ($p < 0.001$ and $p < 0.05$ *versus* K562, respectively). Phosphorylation was ABL1-mediated, as demonstrated by the specific inhibition of imatinib ($p < 0.001$ for K562, NALM6, ALL-SIL and $p < 0.01$ for REH) in contrast to ruxolitinib (JAK2-inhibitor), and occurred on the ABL1 Y-site, as demonstrated by P_{ABL-F} whose phosphorylation was comparable to basal levels. While requiring further optimization and validation in primary leukemic cells to be of clinical interest, the P_{ABL} -based ELISA assay provides a novel *in vitro* tool for screening ABL1 activity in BAL ALL leukemic cells and the potential response to TK inhibitors. In the context of JAK2 pathway, a small sequence belonging to the SH2 domain of STAT5 identified from literature was proposed as peptide biosensor ($P1_{JAK2}$) and from computational studies it provided the specific interactions for binding with JAK2. Interestingly $P1_{JAK2}$ showed higher computationally estimated binding capacity than a second peptide ($P2_{JAK2}$), described in literature. $P1_{JAK2}$ comprises only the reporter and the sequence needs to be optimized. Further analysis with surface plasmon resonance (SPR) will be performed to validate these results. In this thesis the biosensor assay was limited to cell lines, given the difficulties in obtaining and culturing primary human ALL cells. In collaboration with Prof. Den Boer at the Princess Maxima center for Pediatric Oncology (Utrecht, The Netherlands) attempts were made to optimize an *ex vivo* coculture using mesenchymal stromal cells (MSCs) and ALL cells on a two-dimensional (2D) and three-dimensional (3D) system. 2D coculture showed generally no improvement in primary leukemic cells survival. 3D-cocultures provided better results: MSCs migrate into the gel and create complex cluster of cells attracting leukemic cells and, most important, in this complex ALL

cells and MSCs were able to communicate. In this study the 2D system failed to prolong ALL *in vitro* survival and a 3D model mimicking the bone marrow organization might be the best option.

RIASSUNTO

La leucemia linfoblastica acuta (LLA) pediatrica *BCR-ABL like* (BAL) è un nuovo sottotipo di leucemie identificato per similarità nell'espressione genica con la LLA positiva per *BCR-ABL1*. Il BAL è associato all'attivazione delle pathways di ABL o JAK-STAT e ad un alto rischio di ricaduta, ma gli inibitori tirosin chinasi (TKI), potrebbero rappresentare una soluzione terapeutica. Qui riportiamo un saggio ELISA basato su un biosensore peptidico (P_{ABL}) in grado di valutare l'attività chinasi di ABL1. La sequenza di P_{ABL} comprende un sito di fosforilazione della tirosina (Y) ABL1 e una sequenza di targeting che aumenta la specificità per ABL1; ulteriori peptidi (Y-site-mutated (P_{ABL-F}) e un biosensore completamente fosforilato ($P_{PHOSPHO-ABL}$)) sono stati inclusi nel test. Dopo l'incubazione con lisati cellulari, provenienti da 4 linee immortalizzate, la fosforilazione di P_{ABL} media era significativamente aumentata (fosforilazione basale rispetto a P_{ABL} : $6,84 \pm 1,46\%$ vs $32,44 \pm 3,25\%$, valore $p < 0,0001$, ANOVA a due vie, post-test Bonferroni, percentuali relative a $P_{PHOSPHO-ABL}$ in ogni linea). Le linee che esprimono proteine chimeriche di ABL1 (K562, ALL-SIL) presentavano la maggiore attività chinasi su P_{ABL} ; un segnale più basso è stato invece osservato per NALM6 e REH ($p < 0,001$ e $p < 0,05$ versus K562, rispettivamente). Come dimostrato dall'inibizione specifica di imatinib ($p < 0,001$ per K562, NALM6, ALL-SIL e $p < 0,01$ per REH) in contrasto con ruxolitinib (inibitore JAK2), la fosforilazione era mediata da ABL1. A seguito dell'incubazione con P_{ABL-F} la fosforilazione era paragonabile ai livelli basali delle linee, dimostrando l'interazione specifica sulla Y di ABL1. Pur richiedendo un'ulteriore ottimizzazione e convalida nei blasti leucemici, il sistema fornisce un nuovo strumento *in vitro* per lo screening dell'attività di ABL1 nelle leucemie BAL e la risposta ai TKI. Nell'ambito della classe JAK-STAT, è stata identificata una sequenza appartenente al dominio SH2 di STAT5 e proposta come biosensore peptidico ($P1_{JAK2}$). Su di esso sono stati eseguiti studi computazionali che hanno dimostrato lo specifico legame tra il peptide proposto e JAK2. Da notare che $P1_{JAK2}$ ha mostrato una capacità di legame maggiore in paragone ad un secondo peptide ($P2_{JAK2}$), già descritto in letteratura. $P1_{JAK2}$ rappresenta solo la sequenza reporter e necessita quindi di ottimizzazione. Per future analisi funzionali sono stati fatti dei tentativi per esprimere e purificare il dominio chinasi di JAK2, ma dopo 2 tentativi falliti, si è concluso che l'espressione in *E.coli* non è possibile e le future analisi verranno eseguite su un JAK2 commerciale. Viste le difficoltà nel mantenere in colture cellule LLA primarie, in collaborazione con la Prof. Den Boer presso il centro Princess Maxima (Utrecht, Paesi Bassi) sono stati fatti tentativi per ottimizzare una cocoltura ex vivo utilizzando cellule stromali mesenchimali (MSC) e cellule LLA su un piano bidimensionale (2D) e sistema tridimensionale (3D) con lo scopo di utilizzare tali cellule sul biosensore. La cocoltura 2D non ha mostrato generalmente alcun miglioramento nella sopravvivenza dei blasti, mentre al contrario le coculture 3D hanno fornito risultati

interessanti: le MSC migrano nel gel e creano complessi cluster di cellule che attirano le cellule leucemiche e, cosa più importante, in questo complesso le cellule LLA e le MSC sono in grado di comunicare. In questo studio il sistema 2D non è riuscito a prolungare la sopravvivenza *in vitro* delle cellule LLA e un modello 3D che mima l'organizzazione del midollo osseo potrebbe essere l'opzione migliore.

1 INTRODUCTION

1.1 Acute lymphoblastic leukemia and leukemic niche

Acute lymphoblastic leukemia (ALL) is the most frequent type of leukemia occurring in childhood (0-19 years old patients). It exhibits a characteristic peak of incidence in the 1-4 years age group (81.6 cases per million) and a variable disease outcome is associated to age at diagnosis: the best prognosis is observed in the 1-4 years age group (five-year cumulative survival rates: 93%), older patients show increasingly unfavourable outcome (5-9 years: 86%; 10-14 years: 84%; 15-19 years: 68%) whereas infants (<1-year of age) have the worst prognosis of all (60%)⁵⁴.

ALL is a clonal disease arising from the uncontrolled proliferation of lymphohematopoietic B- or T-lineage precursors.

1.1.1 Leukemic niche

Leukemic cells arise from transformation of hematopoietic stem cells (HSCs) or reacquisition of self-renewal capability in committed progenitors. They reside in the local microenvironment of the bone marrow and capable of disrupting normal hematopoietic stem cell niches, creating the so-called leukemic niche⁵⁸. The bone marrow microenvironment comprises different cell types and one of these cell types, mesenchymal stromal cells (MSCs), plays an essential role in regulation of leukemic cell viability⁴⁹.

Leukemic cells are both protected by stroma and able to reprogram stromal cells to transform the niche and reinforce leukemogenesis⁷¹. Moreover, the chemoattractive strategy leading to migration of ALL cells toward MSCs contributed to the creation of a leukemic niche, where MSCs promote survival and chemotherapy resistance to leukemic cells (Figure 1)¹³. Professor Den Boer's group recently demonstrated one of the mechanisms behind this complex system, where tunneling nanotube (TNT) formation from ALL cells toward MSCs play an essential role. TNTs are thin, open-ended membrane protrusions consisting of F-actin, that connect cells and allow communication. Together with other important intercellular communication mechanisms such as extracellular vesicles, gap junctions and integrins, TNTs are involved in leukemia survival and drug resistance¹⁶. Unfortunately, research of leukemia is hampered by the fact that primary ALL cells do not grow or survive very long *in vitro*. The optimization of an *in vitro* system capable to improve and prolong primary ALL cell is under study. Pal and collaborators optimized a coculture of primary ALL cells and human MSCs for the long-term propagation of primary ALL cells⁵⁹, nevertheless *in vitro* leukemic cell proliferation

was low or undetectable even when culture media were supplemented with exogenous growth factors. Bruserud and collaborators tried to standardize an *in vitro* culture condition for human ALL cells: they compared different culture media and different exogenous cytokines in coculture with HFL1 fibroblasts. The highest ALL blast proliferation was detected with HFL1 fibroblasts in serum-free media (StemSpan™ SFEM), and the responses could often be further increased by adding exogenous Flt3-L+IL3+SCF. However, they selected patients with high peripheral blood blast counts and these results may be representative only for this population⁵¹. In contrast, Cox and collaborators suggested a system where ALL primary cells growth *in vitro* was not supported by a stromal layer²⁸. Hence, it remains unclear whether or not ALL cells survival can be promoted *in vitro* and what conditions are required. Recent studies suggest that a three-dimensional system mimicking the structure in the bone marrow, may better support ALL cells *in vitro* survival. Natural or synthetic hydrogels such as collagen, fibrin, Puramatrix and Matrigel are biocompatible and have proven to be widely applicable for 3D tissue constructs^{6,11}. So far, ALL cells 3D models are lacking; however a 3D system was optimized for primary multiple myeloma (MM), which is closely related to leukemia²⁷. Braham et al, showed that healthy MSCs do have the capability to support and maintain primary myeloma cells for a prolonged period of time using a 3D model. The 3D coculture between MM primary cells and MSCs closely mimicked MM marrow physiology and therefore provided a model to explore growth of MM clones associated with drug resistance and minimal residual disease⁶.

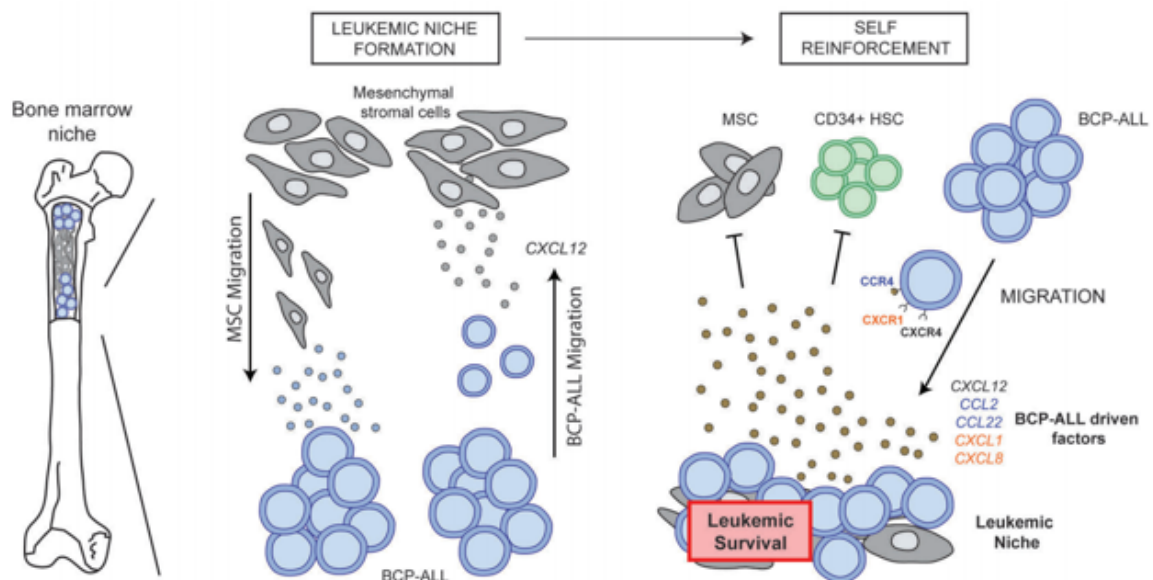


Figure 1: **Proposed model for leukemic niche formation.** BCP-ALL (B cells precursor-ALL) cells migrate toward MSCs and when they are in close proximity, a leukemic microenvironment is created that specifically attracts other BCP-ALL cells. From de Rooij, Polak et al.; Haematologica. 2017.

1.1.2 Genomics

Nowadays the overall survival rates of pediatric ALL after chemotherapy have improved significantly, around 80% of cases have a good outcome²⁴. This is primarily due to optimization of conventional chemotherapeutic drug regimens combined with risk-directed therapies^{23,98}, based also on cytogenetic and molecular characterization of common abnormalities in pediatric ALL subtypes. However, still 15-20% of pediatric patients relapse due to genetic alterations present throughout the course of treatment in subclones or to the acquisition of new mutations, both resulting in resistance to therapy⁶⁰. The causes of the leukemia development both in adult and children are little known, recently the study of large ALL cohorts speculates a genetic predisposition for leukemia. These genes are interestingly related to DNA repair (BLM, ATM, NBS1, MLH1, MSH2, MSH6 and PMS2) or genes known to serve as somatic ALL genes (e.g. genes influencing transcription such as PAX5, RUNX1, ETV6, PHF6, EZH2, NSD1, CREBBP, EP300 or cell signaling such as PTPN11, SH2B3, NF1). However, it is still poorly understood how these germline alterations influence the clinical response and outcome^{46,83}. Technical advances in genomic profiling (such as whole-genome sequencing, exome sequencing and RNA sequencing) have highlighted the heterogeneity and complexity of ALL genetic landscape. B-immunophenotype ALL (B-ALL) represents 85% of paediatric ALL cases and the hallmark of its pathogenesis are genetic alterations in B-lymphoid precursor cells, often by changes in chromosome number and chromosome translocation. In particular chromosome translocations are the result of breaks in different chromosomes or different regions of the same chromosome, resulting in chimeric fusion genes with transforming properties. They are recognized as driver events and consequently B-ALL patients are classified by their chromosomal rearrangements leading to fusion genes with different prognostic impact⁶⁵: patients carrying *ETV6-RUNX1* t(12;21)(p13;q22) (25% of B-ALL) or *TCF3-PBX1* t(1;19)(q23;p13) (6%) have a favourable outcome, while those carrying *MLL*-rearrangements such as t(4;11)(2%) or t(9;22) leading to *BCR-ABL1* t(9;22)(q34;q11) (5%) have a worse prognosis. Numerical aberrations (aneuploidy) consist in gains (25-30% of cases, hyperdiploidy with >50 chromosomes) or losses (5-8%, hypodiploidy with <44 chromosomes) of whole chromosomes due to errors at chromosome pairing and crossing-over and lead to a good and poor prognosis respectively. About 20% of B-ALL with neither of the previous aberrations are classified as B-others⁶⁹.

1.2 *BCR-ABL1*

In haematological diseases, mainly in chronic myeloid leukemia (CML, 90%) and less commonly in ALL (25–30% of adults and 3–5% of children), the *ABL1* gene is translocated from chromosome 9 to chromosome 22, in a 5.8-kb region called breakpoint cluster region (*BCR*)⁶⁸. Depending on the insertion position in *BCR*, several *BCR-ABL1* fusion (Philadelphia or Ph) genes can be generated whose encoded proteins can be distinguished on the basis of their molecular weight. The two most important are p210 and p190: the first is longer and occurs when the *BCR* breakpoint is located between exons 13 and 14 or exons 14 and 15; the second involves a breakpoint between *BCR* exons 1 and 2. Both p210 and p190 *BCR-ABL1* chimeric proteins retain the *BCR* coiled-coil domain and the tyrosine residue required for oligomerization; the *BCR-ABL1* dimers formed then catalyzed their auto-phosphorylation, thus resulting in a constitutively activated enzyme with transforming oncogenic activities. P210 is expressed in 90% of CML cases, whereas in ALL, 75% of *BCR-ABL1* positive patients express the p190 rearrangement¹².

BCR-ABL1 ALL have a dismal prognosis when cured with conventional polychemotherapy: in the case of AIEOP-BFM (Associazione Italiana di Ematologia ed Oncologia Pediatrica Berlin-Frankfurt-Munster) protocols, the 5-years event free survival (EFS) was ~30%, and the outcome could be significantly improved (EFS ~70%) only after the incorporation of imatinib, a first-generation *ABL1* tyrosine kinase inhibitor (TKIs) that targets the product of the *BCR-ABL1* transcript, in the intensive therapeutic scheme^{32,50,73}. Indeed, nowadays most protocols in pediatric *BCR-ABL1*-positive ALL patients have added a TKI to a standard induction regimen, and second-generation TKIs have been developed for patients exhibiting resistance to imatinib, although they have not been clearly associated with superior outcomes compared to imatinib as first-line treatment⁷⁰.

1.3 *BCR-ABL like* leukemias

BCR-ABL like leukemias were identified in 2009, by two independent groups^{10,37}. Den Boer and collaborators used a genome-wide gene expression array on 190 newly diagnosed untreated ALL patients enrolled in the German Cooperative ALL (COALL)-92/97 and in the Dutch Childhood Oncology Group (DCOG)-ALL8/9 studies. They elaborated a predictive model for classification of patients into the major subtypes of pediatric ALL that was then validated in an independent DCOG cohort of 107 patients. Hierarchical clustering of ALL subtypes by gene expression signatures clearly distinguished lineage-T, *MLL*-rearranged, *E2A*-rearranged, *TEL-AML1*, hyperdiploid and *BCR-ABL1* ALL in both the discovery and validation cohort; interestingly, a

significant part of previously unclassified B-ALL cases (~30%) were clustered together with the *BCR-ABL1* although these patients did not harbor the t(9;22)(q34;q11.2) translocation¹⁰. Mullighan and collaborators from St. Jude Children's Research Hospital examined 221 patients with B-ALL treated in the Children's Oncology Group P9906 study. They described a signature based on the prediction analysis of microarrays (PAM) classifier consisting of 257 gene probe sets trained on *BCR-ABL1* positive cases, where *IKZF1* occurred in a substantial proportion of patients with *BCR-ABL1* negative B-ALL with a significant similarity in signature of *BCR-ABL1* positive patients³⁷.

This newly discovered group of patients were classified as *BCR-ABL like*: they represented ~20% of B-ALL considering both pediatric and adult patients, had higher relapse rate (37% versus 16% compared to other precursor B-ALL cases in the discovery cohort) and poor prognosis (5-year EFS: 59.5% versus 84.4% of *BCR-ABL1*-negative ALL); their blasts showed an increased *in vitro* resistance to L-asparaginase and, to a lesser extent, to daunorubicin²⁰. *BCR-ABL like* (Philadelphia like or Ph-like) prevalence increased with age and ranged from 10% in ≤ 9 years old ALL children to 27% in 21-39 years old ALL patients, as described in a large multicentric cohort of 1725 precursor B-cell ALL patients enrolled under multiple clinical protocols⁸⁹. Besides being similar in their expression profile to *BCR-ABL1*, *BCR-ABL like* blasts are characterized by a plethora of genetic abnormalities in B-cell development genes, such as those encoding proteins involved in cell signaling (e.g. *ABL1*, *JAK2*), in tumor-suppressor functions (e.g. *ETV6*), in lymphoid differentiation (e.g. *PAX5*), in cell surface receptors (e.g. *CRLF2*, *PDGFRB*)⁶⁵. These alterations are mainly fusions with tyrosine kinase (TK) genes, leading to the activation of either ABL (ABL-class), JAK-STAT (JAK-class) pathways⁷⁴ or a smaller group involving Ras pathway¹⁷. The most common mechanism of activation is through genomic rearrangements that either cause overexpression of receptors (*CRLF2*, *EPOR*, *PDGFRB* and *CSF1R*) or a constitutive activation of a cytokine receptor or a kinase (*ABL1*, *ABL2*, *JAK1*, *JAK2*) with different partner genes^{45,100} (Figure 2).

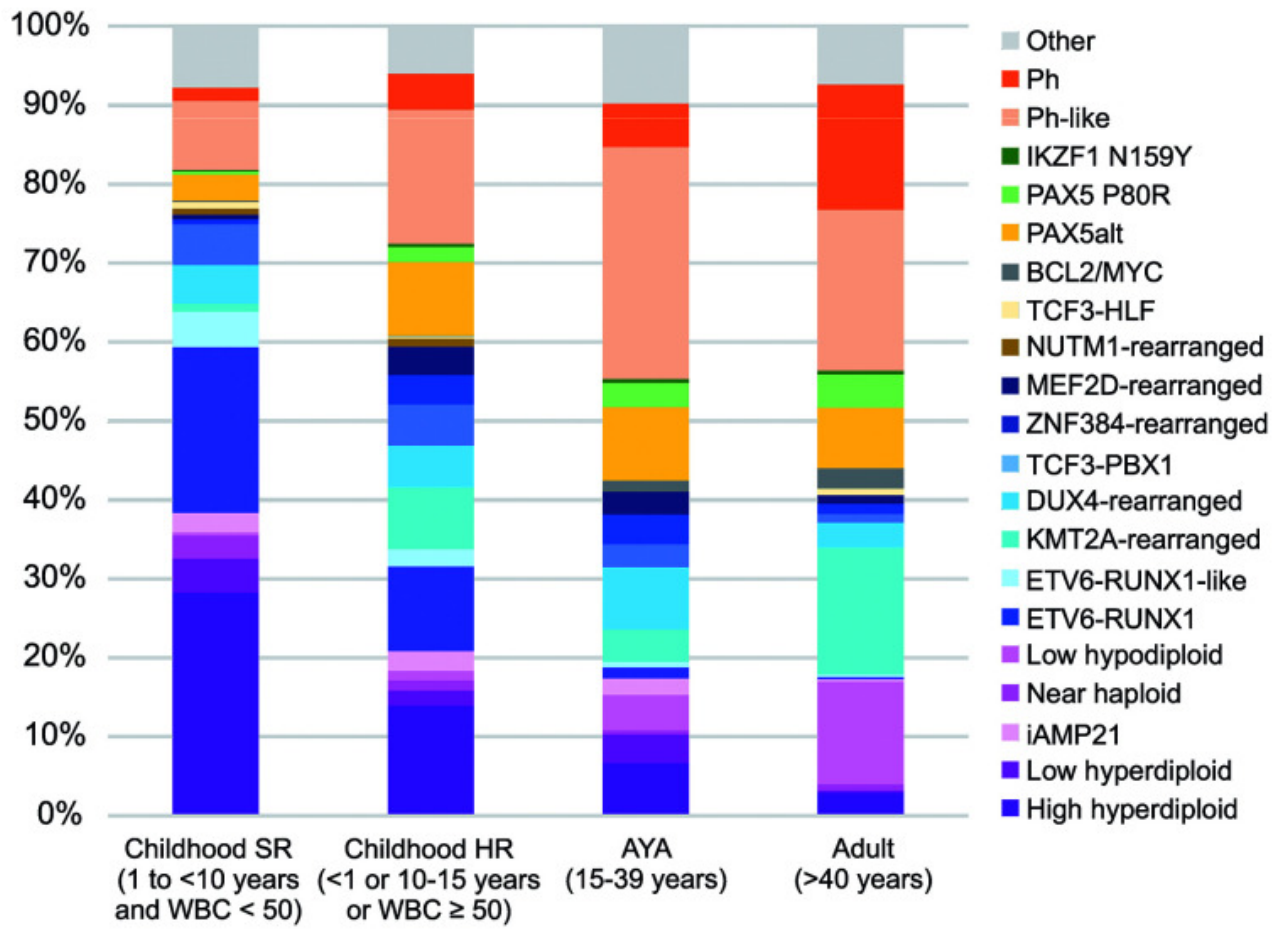


Figure 2: **Distribution of B-ALL subtypes**. SR= standard risk; HR= high risk; WBC= white blood cell count; AYA: adolescent and young adult. From Inaba et al.; Haematologica. 2020.

1.3.1 ABL pathway

ABL belongs to the Abelson non-receptor tyrosine kinase family and plays a role in many key processes linked to cell growth and survival⁶⁸. The protein is ubiquitously expressed and the Rous sarcoma virus oncogene, SRC, Homology (SH) domain, located at the ABL N-terminal, has a tyrosine kinase catalytic domain and two other domains with the major role for protein-protein interactions (N-term SH3, SH2 and SH1). SH3 is about 60 amino acid residues in length and is composed of five β strands; it is responsible for regulating the activity of ABL kinase and its association with its substrate. SH2 domain contains a large central antiparallel sheet, two flanking α helices, and follows a general pattern of β - α - β - β - β - β - α and is important for substrate interaction; allowing ABL to both interact with and phosphorylate its selected targets. Finally, the SH1 domain contains the phosphorylation catalytic domain and has an overall bilobal structure, with a small ATP-binding N-terminal lobe and a large peptide-binding C-terminal lobe (Figure 3)⁶⁴. Genetic alterations found in *BCR-ABL like* blasts and activating the ABL1 signaling pathway are fusions involving directly the ABL-class kinase genes (*ABL1*, *ABL2*) or their upstream receptor genes *CSF1R* and *PDGFRB*²². So far, at least six genes other than *BCR* are known to fuse to *ABL1*, in particular *ETV6*, *ZMIZ1*, *EML1*, *NUP214*, *SFPQ* and *RCSD1*. These fusions are mostly rare except for *NUP214-ABL1*, which has been reported in T-cell ALL with an incidence of 5%¹². The *EBF1-PDGFRB* gene fusion accounts for <1% of B-cell precursor acute lymphoblastic leukemia (ALL) cases. ABL1 tyrosine kinase is constitutively activated by the juxtaposition of the partner gene which favors dimerization or tetramerization and subsequent autophosphorylation. Once it is phosphorylated, ABL1 becomes active and can interact with cytoplasmic molecules, phosphorylating them and leading to disruption of key cellular processes. The dysregulated tyrosine kinase activates signals that contribute to cytokine-independent growth, resistance to apoptosis and genetic instability. Examples include the perturbation of the Ras/MAPK (mitogen- activated protein kinase) cell pathway, the JAK/STAT (Signal Transducer and Activator of Transcription) signaling and the PI3K/mTOR pathway⁶⁷.

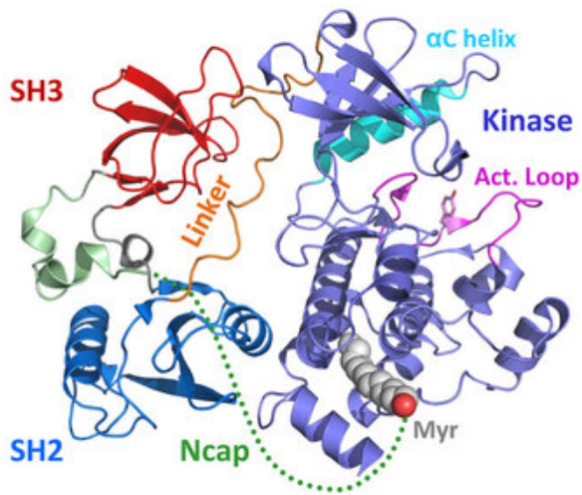


Figure 3: **Domain organization of Abl kinases.** The protein kinase consists of a myristoylated (Myr) N-cap region, followed by SH3 and SH2 domains, the SH2/kinase linker and the tyrosine kinase domain. The unstructured portion of the myristoylated N-cap that engages the C-lobe of the kinase domain is shown as a dotted line. In the kinase domain, the positions of helix α C and the activation loop (Act. Loop) are rendered in cyan and magenta, respectively. The side chain of the activation loop autophosphorylation site (Tyr412) is also shown. From Panjarian et al.; J Biol chem 2015.

1.3.2 JAK-STAT pathway

JAK-STAT pathway operates downstream of >50 cytokines and growth factors and constitutes a rapid membrane-to-nucleus signaling to control processes such as cell proliferation and development of the hematopoietic system through gene transcription⁶¹. The protein structures of all four Jak family members share seven conserved Jak Homology (JH) domains. The C-terminal JH1 domain is a highly conserved kinase domain which contains the activation loop, primary phosphorylation sites (Y1007 and Y1008 in Jak2), and the ATP binding site (K882 in Jak2). JH2 is the pseudo kinase domain, which has similar structural properties to the kinase domain, but lacks catalytic activity (Figure 4)⁹. The intracellular activation occurs when ligand binding induces the multimerization of membrane receptor subunits. Receptor dimerization results in the juxtapositioning of the constitutively associated JAK kinase. The recruitment of JAKs results in their phosphorylation⁵⁶. This activation upon phosphorylation results in increased JAK kinase activity. Activated JAKs then phosphorylate the intracellular receptor domains, which provide binding sites for the recruitment of SH2 domain-containing signaling molecules, such as STATs³³. STATs are latent cytoplasmic transcription factors that become active after recruitment to an activated receptor complex. Recruited STATs are phosphorylated and subsequently dimerize, translocate to the nucleus and bind specific DNA regions promoting transcription of genes associated with cell proliferation. Thus, the JAK/STAT pathway provides a direct mechanism to translate an extracellular signal into a transcriptional response.

Among the most common genetic alterations found in *BCR-ABL like* blasts with activation of the JAK-STAT signaling, there are fusions, mutations or deletions in the *JAK1* and *JAK2* kinase genes, or in some of their upstream cytokine receptor genes, in particular cytokine receptor-like factor 2 (*CRLF2*), interleukin-7 (*IL7*)

receptor and erythropoietin receptor (*EPOR*). A high expression of *CRFL2* is common in leukemic blasts and occurs with an increasing incidence according to age⁸⁹. The overexpression is mostly due to the fusion of the *CRFL2* gene with the upstream constitutively expressed promoter of purinergic receptor P2Y8 (*P2RY8*), as a consequence of pseudoautosomal region 1 (*PAR1*) deletion, or with the immunoglobulin heavy chain gene (*IGH*) locus. The incidence and prognostic relevance of *CRLF2* aberrations were investigated in the context of AIEOP-BFM ALL protocols. A first Italian study in 2012 on 464 B-ALL patients established a cut off level for the *CRFL2* high expression and Kaplan–Meier analysis revealed an inferior 5-years event free survival (EFS) and increased risk of relapse for patients carrying the *P2RY8-CRLF2*; this feature was a poor prognostic factor for 5-year survival estimates regardless of *CRFL2* high expression⁷⁸. A study in a larger cohort of 1105 AIEOP-BFM patients allocated ~80% of the patients carrying *P2RY8-CRLF2* and *CRFL2* gain of copy in the standard and intermediate risk group on the basis of minimal residual disease (MRD), whereas half of *IGH-CRLF2* showed high MRD level and were classified as high risk⁶⁶.

About 20% of the *BCR-ABL* like reveals translocations of the *JAK* gene with different partners²². The activation of *JAK2* is mediated by the oligomerization activity of the partner gene domain. In ETV6-*JAK2*, for example, the oligomerization domain of ETV6, fused with the tyrosine kinase domain of *JAK2*, stimulates the dimerization of *JAK2* and its constitutive activation. The same mechanism is thought to characterize all most other fusions involving *JAK2*, such as *BCR-JAK2*, *SSBP2-JAK2* and others⁵⁵, except for *PAX5-JAK2*, in which the constitutive kinase activity occurs via an unclear mechanism, independent of auto-phosphorylation by dimerization. The paired box transcription factor *PAX5* has an important role in B-cell development. *PAX5-JAK2* is the only nuclear *JAK2* fusion protein, which retains the DNA-binding domain of *PAX5* and deregulates its target genes, suggesting that it may have an impact on both the B-cell transcription program and the activation of *JAK-STAT* signaling pathway⁹³.

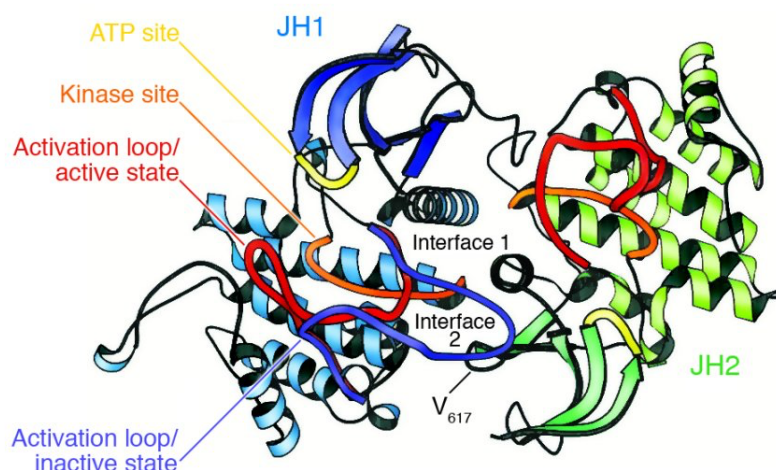


Figure 4: **The Jak2 Protein Structure.** The model depicts the ATP-binding site (yellow), the kinase active site (orange), the activation loop of JH1 in both inactive (purple) and active (red) conformations, and the location of JH2 (green). From Kaushansky. *J Clin Invest* 2005.

1.4 Drugs targeting tyrosine kinase

The addition of targeted therapy with tyrosine kinase inhibitors (TKIs) has significantly improved the outcome of patients with *BCR-ABL1* positive CML¹⁸ and ALL⁹⁹. The high frequency of kinase-activating lesions in *BCR-ABL like* patients, suggests that TKI therapy is likely effective in such patients. TKIs specific to either ABL or JAK pathways have been developed, such as imatinib (ABL-class) and ruxolitinib (JAK-class) and might be a therapeutic option for these unfavourable subgroups of ALL¹⁰⁰. For *BCR-ABL like* ALL cases of the ABL-class, imatinib or dasatinib are used and there is no clear evidence for superiority of one of them yet. Both imatinib and dasatinib pose resistance problems in *BCR-ABL1* positive patients: ABL1 kinase domain mutations have been detected in 30%-90% patients who failed imatinib and in 20%-80% of patients who failed dasatinib; therefore, in myeloid leukemias, other second and third generation TKIs such as nilotinib, bosutinib and ponatinib are currently under investigation. Currently, several studies are underway (clinicaltrials.gov identifiers: NCT02883049, NCT02723994, NCT03117751, NCT02420717, NCT03571321)¹⁹. The therapeutic approach to JAK-class *BCR-ABL like* ALLs is less clear. JAK inhibitors such as ruxolitinib are approved for the treatment of myelofibrosis, but experience in ALL is limited⁸⁰. Leukemic cells with the studied JAK-class fusions of *BCR-ABL like* ALL were responsive in some degree to JAK inhibitors in *in vitro* and xenograft models. Given the constitutive activation of PI3K/mTOR in patients with *BCR-ABL like* ALL, alternative approaches have been tested. The efficacy of PI3K/mTOR inhibitor gedatolisib in coadministration with ruxolitinib for JAK-mutated/CRLF2-rearranged or imatinib for ABL1/PDGRFB-rearranged patient derived xenograft models respectively has been demonstrated²¹ (Figure 5).

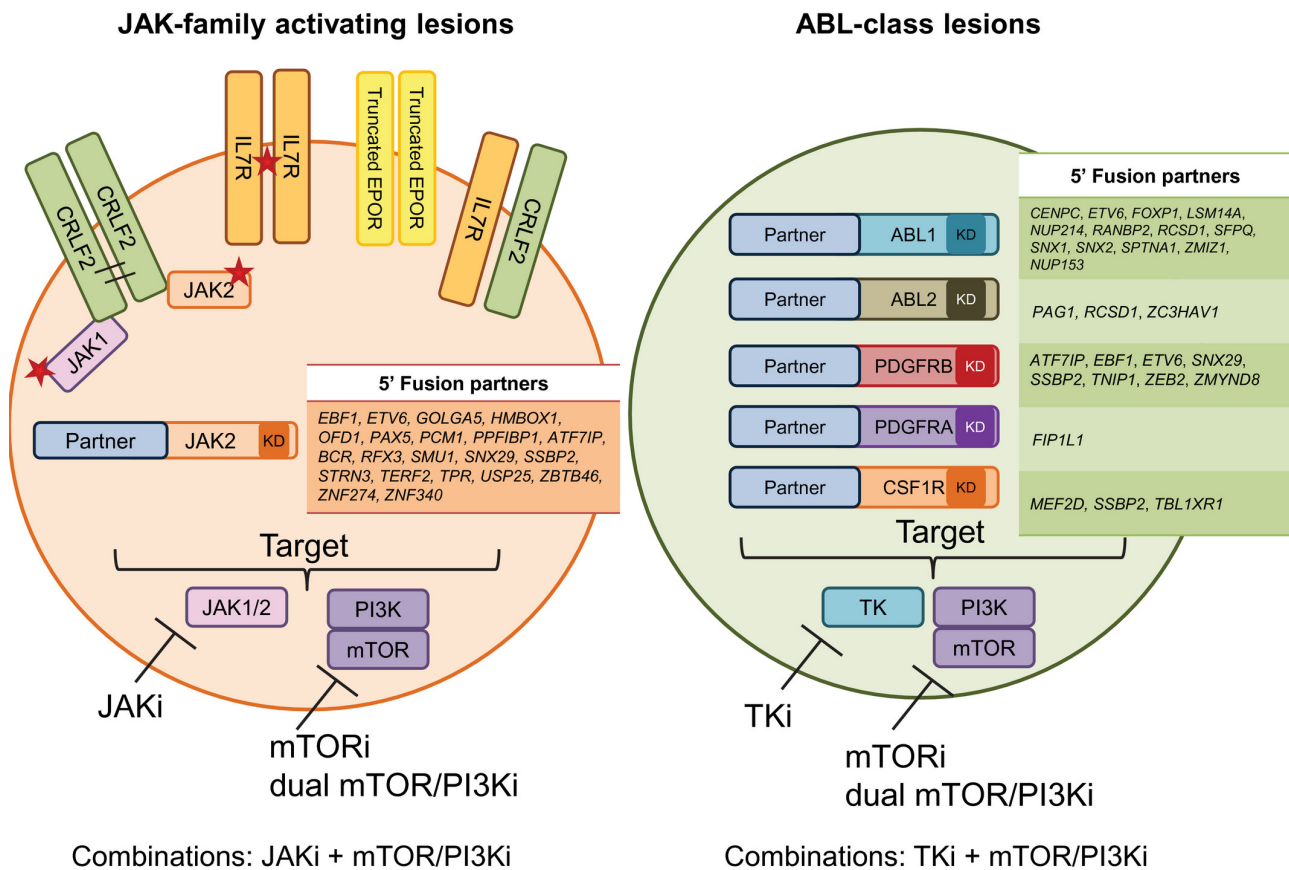


Figure 5: Genetics and therapeutic implications for *BCR-ABL like* acute lymphoblastic leukemia. From Chiaretti et al.; Cancer 2019.

1.5 Diagnostic approaches

BCR-ABL like ALL are extremely heterogeneous in their genetic background and the most comprehensive approach to detect fusions requires genomic assays like exome, whole genome and whole transcriptome sequencing, which are expensive and require specialized bioinformatic knowledge and facilities⁷⁷. Therefore, continued efforts have been performed in the latest years to better describe the frequencies of the occurring genetic lesions in *BCR-ABL like* ALL and investigate their prognostic significance. The final aim is to focus on the most important genetic alteration characterizing this group of leukemias to develop dedicated diagnostic methods for their detection; these novel reliable genetic markers could be employed for improving the risk classification system and thus the therapeutic success in ALL²¹. Nowadays, the determination of specific rearrangements is routinely done by karyotyping or fluorescence in situ hybridization (FISH). These approaches have low resolution, and FISH can test only one known fusion partner at a time. Alternative approaches include RT PCR followed by Sanger sequencing and targeted locus amplification (TLA). Detection

of TK fusions by RT PCR was performed by the St. Jude group and collaborators, with primers specifically designed for those fusions, ^{45,91} and then improved by the Dutch group of prof. Den Boer in the original papers that firstly identified the *BCR-ABL like* subtypes ¹⁰⁰.

TLA is an innovative method that can be used to sequence genes of interest by crosslinking of physically proximal genomic sequences and selective amplification and sequencing of those regions. TLA results in the amplification of sequences at either end of the primer pair, allowing to obtain detailed information of structural variation including novel fusion partners. It is based on the crosslinking of DNA in living or dead cells, that is then fragmented, religated and de-crosslinked to allow formation of circular DNA fragments ⁹⁰.

Any genomic region up to 100 kb can be amplified and sequenced by using one primer pair complementary to a short locus specific sequence. Primers designed for one specific gene of interest are the only variable in the process and allow the complete sequencing and analysis of any region of the DNA. New hypothetical fusions and new partner genes may be, then, discovered. The procedure can also be multiplexed, allowing the analysis of up to 20 genes of interest (technically defined viewpoints) ensuring the analysis of multiple genes or larger loci. Furthermore, TLA allows simultaneous detection of large balanced and unbalanced chromosomal rearrangements as well as single nucleotide variants (SNVs), structural variants and gene fusions in clinically relevant genes. This may enable the choice of a specific treatment, taking into account any mutation that contributes to lymphoid transformation.

1.6 Proteomic approach-biosensor

Currently, practical and fast systems to identify the specific TKIs to treat *BCR-ABL like* patients are missing and a direct assignment of those patients in a target therapy is still an issue. Protein phosphorylation plays a major role in the mechanisms underlying control of cell cycle, differentiation and development. Consequently, disruption of these processes can lead to cell cycle deregulation and uncontrolled cellular proliferation, resulting in malignancy. The development of a modular biosensor methodology allowing the quantification of cellular signalling information about response of TK to inhibitors, might improve the diagnosis, guide the doctor to the choice of the specific TKI and allow clinical monitoring of patients' response, also by identifying patients with primary resistance, which are normally not clinically detected until the recurring disease has progressed ⁹¹. The optimized aminoacidic sequence of an ABL1 substrate is EAIYAAPFAKK (named as "*reporter*" sequence in this thesis), including the consensus motif I/V/-Y-X-X-P/F for ABL1 (where X is any amino acid, Y representing the phosphorylation site). This sequence was found by screening a peptide library for interaction

with purified ABL1^{26,103} and corresponds to the commercially available peptide Abltide (P_{ABL TIDE}). Currently, P_{ABL TIDE} is suitable only for biochemical research use (i.e. enzymatic assays on purified ABL1), and is not intended for clinical and diagnostics applications, because of low specificity for ABL1 among other kinases in primary cells^{7,76}. An additional optimized stretch of amino acids (GGCGGAPTYSPP, named as “targeting” in this thesis) is recognized by the SH3 domain of ABL1 protein and linked to the *reporter* region, resulting in a novel artificial substrate with an increased specificity for ABL1 (P_{ABL}). A similar artificial peptide was initially developed to detect intracellular ABL1 kinase activity in live intact cells^{8 38} and was applied for investigating *BCR-ABL1* in CML³.

In the context of JAK2 biosensor, Professor Parker from University of Minnesota Twin Cities in Minneapolis identified a peptide with sequence GGDNDPDEYITLDEDGGK (P_{2JAK2}). This sequence was identified using proteomic data of endogenous kinase substrates and lanthanide binding sequences to build an “in silico” library from which luminescence-detectable substrates could be selected⁵⁷ but never investigated in functional analysis. Furthermore, based on literature data, a small sequence belonging to the SH2 domain of STAT5 was selected. This sequence has been highlighted following protein microarray studies and provides the specific interaction with JAK2 catalytic domain since it includes the tyrosine (tyrosine Y694) for the specific phosphorylation. This peptide, with sequence LAKAVDGYVKPQI (P_{1JAK2}), may therefore act as a “reporter” region for a second biosensor specific for JAK2¹⁴.

The introduction of dedicated biosensors would represent a novelty in the oncology service identifying the sensitivity to a specific TKI, thus contributing to the rational use of TKIs and to monitor therapy, potentially leading to more favourable clinical outcomes in patients *BCR-ABL like* subgroup, for which current therapies are unsatisfactory. Moreover, creating sets of biosensor peptides with individual enzyme activities could guarantee the detection of many kinases quickly and simultaneously.

2 AIM

The *in vitro* system proposed in this manuscript is based on the recognition and quantification of phosphorylation by tyrosine kinase BCR-ABL *like* using artificial peptide-based substrate. The goal of the project is therefore to lay the foundations for the development of two peptide biosensors capable of recognizing and quantifying the phosphorylation by tyrosine kinases activating the ABL1 and JAK-STAT pathways and perform an *in vitro* screening for available TKIs. The initial analyses were performed using two peptide biosensors, already published by Professor Parker from University of Minnesota Twin Cities in Minneapolis: the first developed to be functional for BCR-ABL1 in chronic myeloid leukemia, the second specific for JAK2 protein but never investigated in functional analysis. A small sequence belonging to the SH2 domain of STAT5 identified from literature data was proposed as a second peptide biosensor. This sequence was highlighted following protein microarray studies and is provided with the specific binding and phosphorylation site for JAK2 (tyrosine Y694). These biosensors will allow to select the best tyrosine kinase inhibitor to be used in *BCR-ABL like* leukemic patients and monitor the effectiveness of the inhibitor chosen during therapy. In this thesis the biosensor assay was limited to cell lines, given the difficulties in obtaining and culturing primary human ALL cells. In collaboration with Prof. Den Boer at the Princess Maxima center for Pediatric Oncology (Utrecht, The Netherlands) attempts were made to optimize an *ex vivo* coculture using a two-dimensional (2D) and three-dimensional (3D) approach, in order to set up conditions that could be applied to test primary ALL cells in several application including our biosensor.

3 MATERIALS AND METHODS

Experiments are divided as following:

- P_{ABL} : the first part comprises the characterization of the genetic alterations in the cell lines used for the project (NALM6, REH, ALL-SIL, K562) and the functional analysis of P_{ABL} with an ELISA assay.
- P_{JAK2} : in the context of JAK-STAT pathway computational analysis were performed to check the binding activity between $P1_{JAK2}/P2_{JAK2}$ and JAK2. Additionally, we tried to purify JAK2 JH1 protein domain for further functional experiments with $P1_{JAK2}/P2_{JAK2}$.
- Leukemic niche: in order to set up conditions that could be applied to test primary ALL cells in several application including our biosensor, we tried to optimize ALL cell viability using a two-dimensional (2D) and three-dimensional (3D) approach.

3.1 Cell cultures

The *in vitro* P_{ABL} -based ELISA assay was optimized on 4 human leukemia cell lines with a focus on *BCR-ABL* like translocation putatively leading to ABL pathway activation: NALM6, harbouring *ETV6-PDGFRB*¹⁵, ALL-SIL, a T-cell lines positive for *NUP214-ABL1* fusion gene also found among *BCR-ABL* like cases ⁷²K562 expressing *BCR-ABL1* (Chronic myeloid leukemia) and the non *BCR-ABL* like REH, positive for *ETV6-RUNX1* (*TEL-AML1*).

3D models were optimized using SupB15 (B-ALL line with *BCR-ABL1*), NALM6 (not detected) and REH (*ETV6-RUNX1*) cell lines stored at the Princes Maxima Centrum in Utrecht.

3.2 Patients

Bone marrow aspirates were obtained from children enrolled in the German Cooperative ALL (COALL)-92/97 and in the Dutch Childhood Oncology Group (DCOG)-ALL8/9 studies with newly diagnosed B-ALL prior to treatment. Mononuclear leukemic cells were collected and processed as previously described ⁷⁵ stored at -80°C and thawed for 2D coculture analysis. MSCs were isolated from bone marrow aspirates obtained from newly diagnosed B-ALL patients (before treatment) and healthy controls. MSCs were processed as described previously ³⁹. Primary ALL cells isolated and collected from patients enrolled in AIEOP BFM ALL 2009 were stored at -80°C and thawed for TLA analysis.

3.3 Drug and chemicals/TKI

Tyrosine kinase inhibitors (TKI) used were: imatinib and ruxolitinib. Imatinib (CDS022173, Sigma-Aldrich, Italy) was dissolved in DMSO although ruxolitinib (11609 Cayman Chemical, USA) in ethanol to reach a concentration of 2mM and 32.6mM respectively. Ruxolitinib was provided by Dr. A. Tommasini from the IRCCS Burlo Garofolo of Trieste.

3.4 Cell lysates preparation

Cell protein lysates was prepared for both Western blot and P_{ABL}-based ELISA assays. The method of extraction has been optimized by Professor Sorio (University of Verona) and requires the use of kinase and phosphatase inhibitors to maintain the integrity of *BCR-ABL1* in K562 cell line. Twenty million cells were lysed in ice with 150 µl of lysis buffer containing 50 mM Tris-HCl (pH 7.4), 1% Triton-X, 150 mM NaCl, 2 mM EDTA, with addition of kinase and phosphatase inhibitors: sodium orthovanadate (Na₃VO₄) 100 µM (S6508, Sigma-Aldrich, Italy), pepstatin 10 nM (77170, Sigma-Aldrich, Italy), phenylarsine oxide (PAO), 20 µM (P3075, Sigma-Aldrich, Italy), benzamidine 1mM (12072, Sigma-Aldrich, Italy), GM-6001 100 µM (CC10, Sigma-Aldrich), CA-074 10 µM (C5732, Sigma-Aldrich, Italy), sodium fluoride (NaF) 10 mM (450022, Sigma-Aldrich, Italy) and DTT 1mM (43819, Sigma-Aldrich, Italy), 1x PhosSTOP tablets (4906845001, Sigma-Aldrich/Merk, Italy). The lysis procedure provided: pipetting 20 times the cell suspension, vortexing and centrifuge at 4°C for 30 min at 13000 g. The collected supernatant was rapidly frozen in liquid nitrogen and stored at -80°C in cryovials. Finally protein yields/concentrations were determined by Bradford analysis (B6916, Sigma-Aldrich, Italy) and absorbance was measured at 570 nm on Microplate Reader EL311 (214891, BioTek Instruments, Inc).

3.5 Western Blot

Whole cell extracts (25 µg) were fractionated by SDS-PAGE using 10% Bolt™ 10% Bis-Tris Plus Gels 12-well (NW00102BOX, Thermo Fisher Scientific, Italy) or NuPAGETM 3 to 8%, Tris-Acetate (EA03752BOX, Thermo Fisher Scientific, Italy) and transferred to nitrocellulose membranes (PB7320, Thermo Fischer Scientific, Italy) using Electrophoresis Power Supply (EPS301, Thermo Fischer Scientific, Italy). After incubation with 5% nonfat milk (non-phospho-protein) or 5% BSA (phospho-protein) in Tris buffered saline (50 mM Tris-Cl, 150

mM NaCl, pH 7,5) with 0.1% Tween-20 (T-TBS) for 1 hour, the membranes were incubated with antibodies against: PDGFRB (1:5000 in T-TBS 5% nonfat milk, ab32570, Abcam), ABL1 (1:500 in T-TBS 5% nonfat milk, ab15130, Abcam), phospho-ABL1 (Y245) (1:1000 in T-TBS 5% BSA, #2861, Cell Signaling Technology), actin (1:3000 in T-TBS 5% nonfat milk, ab218787, Abcam) at 4C, overnight. Membranes were washed and incubated 1 hour at 4C with a 1:10000 dilution in T-TBS 5% nonfat milk of horseradish peroxidase-conjugated anti-rabbit antibodies (AP132P, Merk). Blots were developed with LiteAblo TURBO Extra Sensitive Chemiluminescent Substrate (EMP012001 Euroclone), GBX Developer/Replenisher (P7042, Sigma-Aldrich, Italy) and GBX Fixer/Replenisher (P7167, Sigma-Aldrich, Italy).

3.6 Biosensor peptide ABL1 (P_{ABL})

Table 1 shows biosensor peptide characteristics employed in this study. All biosensor peptides were synthesized by GenScript (GenScript 860 Centennial Ave. Piscataway, NJ08854, USA), with 98% purity. Mass spectrometry was performed to confirm peptide sequence, in the Department of Life Science at the University of Trieste (Professor A. Tossi). Peptide' theoretical molecular weights have been confirmed. P_{ABL} stock was solubilized in MilliQ-water (solubilizing 1 mg/ml) with a final concentration of 338 μ M. P_{ABL-F} and $P_{PHOSPHO-ABL}$ stocks were prepared in DMSO (solubilizing 1 mg/ml) with a final concentration of 340 μ M and 329 μ M respectively. All the solutions were stored at -80°C.

<i>PEPTIDES</i>	<i>SEQUENCE</i>	<i>MOLECULAR WEIGHT</i>
<i>P_{ABL}</i>	<i>EAIYAAPFAKK{Lys(biotin)}GGCGG<u>APTYSPPPPPG</u></i>	2956.41 Da
<i>P_{ABL-F}</i>	<i>EAIFAAPFAKK{Lys(biotin)}GGCGG<u>APTYSPPPPPG</u></i>	2940.41 Da
<i>$P_{PHOSPHO-ABL}$</i>	<i>EAIY(P)AAPFAKK{Lys(biotin)}GGCGG<u>APTYSPPPPPG</u></i>	3036.39 Da

Table 1. **Biosensors peptide ABL1.** Biosensor peptides employed in ELISA assay, their sequence and molecular weight. The reporter sequence is shown in italic, and the targeting sequence is underlined. In the phosphorylation site of ABL1, tyrosine and peptide modifications are shown in red.

3.7 P_{ABL} -Based ELISA assay

The P_{ABL} -based ELISA assay procedure is shown in Figure 6: biosensors peptide P_{ABL} or analogues P_{ABL-F} , $P_{PHOSPHO-ABL}$ contain a biotin tag that allow the anchoring of the peptide to a neutravidin-coated plate (786-766, G-Bioscience, USA).

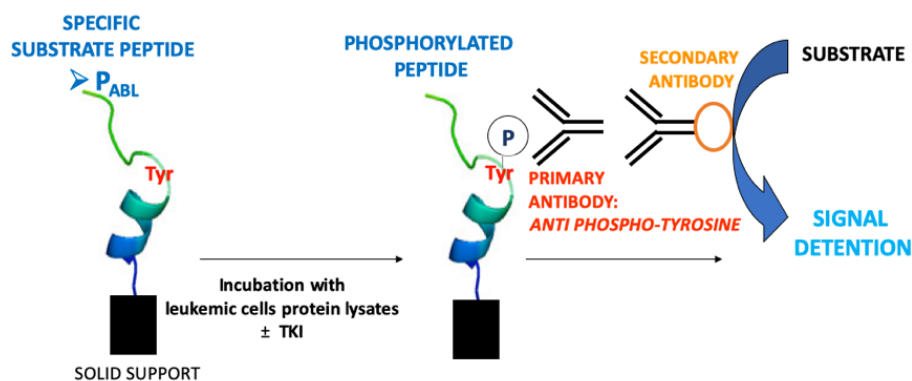


Figure 6. **Summary of P_{ABL}-based ELISA assay.** Biotinylated P_{ABL} is anchored on a neutravidin-coated plate and incubated with leukemic cells protein lysates with or without TKI. Fluorescence is then detected through an anti phospho-tyrosine antibody.

To avoid non specific signals the plate was first washed with a Quencher Buffer (100 μ L/well , PBS Tween 20 0.1% pH 7.4 + 0.4% BSA) for 20 minutes while shaking. 4 μ g of cell lysate (prepared as mentioned above) were incubated with 0.5 μ M of peptide in TKB ((4mM Tris-HCl pH 7.5, 10 mM MgCl₂, 0.1 mM EDTA, 0.01 % TritonX) with 100 μ M ATP, 1x Roche Inhibitors (11697498001, Merck), 2 mM DTT, 0.1 mM Na₃VO₄ and MilliQ-water (final volume 100 μ l)) for 1 h at room temperature (RT). The reaction was measured using an anti phosphorylated tyrosine (dilution 1: 10000 in Quencher Buffer, 1h, RT while shaking (05-1050 4G10 Platinum, EDM Millipore Corporation)) and a secondary antibody ECL Anti Mouse IgG, HRP from goat (dilution of 1: 6000 in Quencher Buffer, 1 h, RT while shaking (5210-0159, Sera-care, USA)). Signal fluorescence analysis was allowed by adding a solution of citrate buffer pH 6.0, 3% H₂O₂, 0.5% Amplex Ultra Reagent Invitrogen (A36006, Thermofischer Scientific, Italy) and measured for 25 times every 0.2 sec (544 nm excitation, 590 nm emission wavelengths). For drug analysis cell lysate were previously incubated for 15 min at RT (imatinib 5 μ M, ruxolitinib 52 nM and 5 μ M). In the analysis P_{ABL} and P_{ABL-F} phosphorylation is expressed as a percentage related to total P_{PHOSPHO-ABL}.

3.8 P_{JAK2} modeling

The starting structure for the STAT5 and JAK2 proteins was obtained from the available RCSB Protein Data Bank (PDB ID 1Y1U and 2B7A, respectively)^{87,94}. The structures of both peptides were created from scratch with UCSF Chimera software¹⁰². Antechamber program from AMBER19¹⁰⁴ was used to assign gaff2 atom types to uncommon residues. All Molecular Dynamics simulations are carried out following a well validated procedure³⁵. Briefly, the system density and volume were relaxed in NPT ensemble maintaining the

Berendsen barostat for 20 ns. After this step 100 or 200 ns of unrestrained NVT production simulation was run for energy calculation purposes. The complexes binding free energy value (ΔG_{bind}) were calculated as the sum of the electrostatic, van der Waals, and solvation contributions following the MM/PBSA approach³⁴. All simulations were carried out using the pmemd and pmemd.CUDA modules of Amber 19 running on a CPU/GPU calculation cluster. Molecular graphics images and trajectory analysis were performed using the UCSF Chimera package (v.1.14)¹⁰².

3.9 JAK2 purification

Sequence JAK2-JH1 expression construct:

MGSSHHHHHSSGENLYFQGHMHMEDRDPTQFEERHLKFLQQLGKGNFGSVEMCRYDPLQDNTGEVVA
VKKLQHSTEEHLRDFEREIEILKSLQHDNIVKYKVCYSAGRRNLKLIMEYLPYGSLRDYQLQHKERIDHIKLL
QYTSQICKGMEYLGTKRYIHRDLATRNILVENENRVKIGDFGLTKVLPQDKEYYKVKEPGESPIFWYAPESLT
ESKFSVASDVWSFGVVLVELFTYIEKSKSPPAEFMRMIGNDKQGQMIVFHLLIELLKNNGRLPRPDGCPDEIYM
IMTECWNNNVNQRPSFRDLALRVDQIRDNMAG*

Protein characteristics:

Mw: 37573.80 (320 aa)

PI: 6.77, protein is negatively charged at pH 8.0

Extinction coefficient: 40340

Absorbance: 1.074

Transformed pET-28a (kanamycin resistance) plasmid containing the sequence encoding JAK2 kinase JH1 domain into *E.coli* strain BL21 (DE3) pLysS competent cells for protein expression, was plated into an agar plate containing 50 $\mu\text{g}/\text{mL}$ kanamycin and grew overnight (O/N) at 37°C. A single colony was selected and grown O/N at 37°C in a shaking incubator at 220 rpm. 25 ml of the O/N culture was inoculated in 2x 1L TB medium (1.2% tryptone, 2.4% yeast extract, 0.5% glycerol) and 2x 1L 2xTY medium (16g/L tryptone, 10g/L yeast extract, 5g/L NaCl) containing 50 $\mu\text{g}/\text{mL}$ kanamycin and grown 37 °C in a shaking incubator at 220 rpm until culture reaches an OD₆₀₀ of 0.5 – 0.7; after 1h the expression was induced with 0.5 mM Isopropil- β -D-1-tiogalattopiranoside IPTG (Fisher Scientific, # 10725471) and left overnight at 25°C. Cells were then collected were added 0.1 % Triton X-100 (200 μl), DNase 1 (Stemcell, produce # 07469, 1/500 v/v – 4 units/ml) and 2 tablets complete protease inhibitor (Fisher Scientific, #15672129), stirred until all cell clumps were well suspended and lysed by sonication (1 sec on, 1 sec off, 1 min sonication in total, amplitude: ~50%). For Ni-affinity chromatography the supernatant was carefully poured and transferred to a 50ml falcon with 20 mM

imidazole (final concentration), and 2 ml (total per media) of Ni Sepharose Excel resin (GE Healthcare Ni Sepharose Excel – Fisher scientific – 12664557). After 2h at 4°C the resin was collected and transferred into two Bio rad polyprep columns (Bio-rad #7311550). JAK2 was eluted with 2ml of elution buffer (20 mM Tris pH7.5, 250 mM NaCl, 1 mM DTT, 250 mM imidazole) and 1.5 ml fractions collected. Fractions were then run on a 12% SDS-PAGE (TGX FastCast Acrylamide kit, 12%). The fraction containing JAK2 from both media were pooled together and added with TEV protease (1:5 w/w, NEB P811S) to cleave His tag and set up dialysis (Thermo fisher, snakeskin, dialysis tubing, 7K MWCO, #10311114). Samples were dialyzed O/N against 2L of TEV buffer (50 mM Tris pH 7.5, 0.5 mM EDTA, 1 mM DTT) at 4 °C, stirring. The dialyzed protein was then concentrated to 1 ml in EMD Millipore Amicon Ultra-4 concentrator (Sigma-Aldrich # UFC801024) with a 10kD cutoff (at 4 °C and 2500g) and a control sample was taken for 12% SDS-PAGE. At this point, 20 mM Imidazole and 500 ul of Ni Sepharose Excel resin were added and let bind for 2 hrs while rotating at 4 °C. Everything was then transferred to a small bio-spin polyprep column (Bio-rad # 731-6008), collected the flow through, and wash with 500 ul extra SEC buffer (20 mM Tris pH7.5, 250 mM NaCl, 1 mM EDTA, 1 mM DTT). Another sample was taken for 12% SDS-PAGE. As a check, what has been bound to the resin was eluted by adding 500 ul of elution buffer (20 mM Tris pH7.5, 250 mM NaCl, 1 mM EDTA, 1 mM DTT, 250 mM Imidazole), and control sample for 12% SDS-PAGE was collected. Sample was finally filtered through Ultrafree-MC Centrifugal Filter (Simga, 0.45 um) and run on a S75 Increase 10/300GL column equilibrated in SEC buffer (20 mM Tris pH7.5, 250 mM NaCl, 1 mM EDTA, 1 mM DTT). Fractions of the SEC run, the pre/post Ni Sepharose resin and the elutions were run on a 12% SDS-PAGE. To test the stability of the purified JAK2, after 1 week at 4 °C fractions were pooled, concentrated and re-run on a S75 Increase 10/300GL column equilibrated in SEC buffer (20 mM Tris pH7.5, 250 mM NaCl, 1 mM EDTA, 1 mM DTT).

3.10 2D coculture

B-others, *ETV6-RUNX1* and *BCR-ABL1* patient' cells, previously shown to survive poorly *in vitro*, were selected and cultured at a concentration of 1.0×10^6 cells/ml in a volume of 140µl in a 96-wells flat bottom plate (manufacturer) with MSC in coculture. 5500 MSC's/well were seeded into the plate, 24 hours prior to the seeding of the primary leukemic cells, (day-1(d-1)). The MSC's were seeded into the plate in Dulbecco's Modified Eagle Medium (DMEM) (Low Glucose/Pyruvate/HEPES, Invitrogen; Ref. no. 22320-022) containing 15% Fetal Calf Serum (FCS) (Integro, Zaandam, The Netherlands), 1.5 µg/ml Fungizone Antimycotic B, 10

$\mu\text{g/ml}$ Gentamycin (Invitrogen; Ref. no. 15290-018 and Invitrogen; Ref. no. 15750-037 respectively), 0.1×10^{-3} M ascorbic acid (Sigma-Aldrich; Ref. no. A7631) and 1 ng/ml recombinant human Fibroblast Growth Factor (FGF) (AbD Serotec; Ref. no. PHP105) (MSC culture medium). After the 24 hours of MSC culture, from now on referred to as d0, 137.500 primary B-ALL cells were seeded into the plate in either RPMI Dutch modified plus 20% of FCS (Integro, Zaandam, The Netherlands), 1% PSF (Penecilin/Streptavidin/Fungizone: Penicilin/Streptomycin (Life Technologies; Ref. no. 15070-063), Fungizone Antimycotic (Invitrogen; Ref. no. 15290-018)), 0.1% L-glutamin (Life technologies; Ref. no. 25030-024), 0.1% ITS (Sigma-Aldrich; Ref. no. 1884-1VL), 10mg/ml Gentamycin ((50 mg/ml) (Invitrogen; Ref. no. 15750-037) of SFEM II with or without 20% of FCS. Growth factors used for viability assays were: IL7 (Miltenyi Biotec; Ref. no. 130-093-937), G-CSF (Sigma Aldrich; Ref. no. GF-412), FLT3LG (Thermo Fisher; Ref. no. PHC9414), TPO (Invitrogen; Ref. no. 34-8685-63), IL3 (Miltenyi Biotec; Ref. no. 130-093-908), SCF (Miltenyi Biotec; Ref. no. 130-093-991), IL2 (Miltenyi Biotec; Ref. no. 130-094-024), TSLP (R&D system; Ref. no. 1398-TS-010). Stock plates with different combination of cytokines at a concentration of 0.4ug/ml for each factor dissolved in 100ul of PBS plus 0.1% Human Serum Albumin (HAS), were previously prepared and added to the coculture at a concentration of 20ng/ml or 50ng/mL. On day3 (d3) the cells were harvested and stained with conjugated antibodies: for staining ALL cells, Brilliant Violet anti-human CD19 (1:50 dilution; Biolegend Ref. no. 302234), for staining MSCs, anti-CD166 AF750, anti-CD73 AF750 and anti-CD146 AF750 (1:100 dilution, R&D System Ref. no. FAB6561S, FAB5795S and FAB932S, respectively). For viability staining, we used Sytox Red Dead Cell stain (1:1000 dilution, Life technologies Ref. no. S34859). Controls involve unstained and single stained coculture cell populations for compensation. Viability measurement was performed based on CytoFLEX S flow cytometry and the analysis was performed on FlowJo® 10.6.2. Survival of primary leukemic cells was analyzed after 72h and normalized to the cell number at start of culture (day 0).

3.11 3D Coculture

Corning® PuraMatrix™ Peptide Hydrogel (Ref. no. 354250) was packaged in one vial containing 1% solution (w/v) of purified synthetic peptide (5 ml per vial). To reduce viscosity of the gel, it was vortexed for 2-3 min and centrifuged for 2 minutes at 2500 rpm. The 0.5 or 0.25% gel concentrations were prepared by dilution with Milli-Q water. 100 ul of this diluted PuraMatrix was slowly added in a well of a 96 well plate (Nunc™ MicroWell™ 96-Well Microplates; Thermo Fisher Ref. no. 167008) by touching the bottom of the well to avoid

a uneven gelation. The gelation was promoted by carefully and slowly adding 200 μ l of MSC medium (DMEM (Low Glucose/Pyruvate/HEPES, Invitrogen; Ref. no. 22320-022) containing 15% FCS (Integro, Zaandam, The Netherlands), 1.5 μ g/ml Fungizone Antimycotic B, 10 μ g/ml Gentamycin (Invitrogen; Ref. no. 15290-018 and 15750-037, respectively), 0.1×10^{-3} M ascorbic acid (Sigma-Aldrich; Ref. no. A7631) and 1 ng/ml recombinant human Fibroblast Growth Factor (FGF; AbD Serotec; Ref. no. PHP105)) to each well (place the end of the pipette tip towards the top of the culture vessel wall). After one hour, the well was washed by carefully removing 150 μ l of media (to avoid gel disruption) and replacing it with new media. After 30 minutes, two more washes were performed to equilibrate the growth environment to physiological pH. When the gelation is completed, 5500 or 10000 MSCs were seeded in a volume of 200 μ l and left to enter the gel for three days. At the third day, ALL cells were added on top of the gel in RPMI 1640 + Glutamax (Gibco, Cat. Nr. 61870-010) with either 20 or 10% of FCS and 1% PSF in a volume of 140 μ l.

3.11.1 Flow cytometry

Three days after coculture, cells were harvested from the gel. Gel was disrupted by pipetting and digested with 250 μ l of concentration Trypsin (manufacturer). The harvest cells were stained with conjugated antibodies to determine cell types for 30 minutes at 4C and then washed two times with PBS. The staining was followed by a viability staining for 20 min at 4C. Viability measurement was performed based on flow cytometry (CytoFlex S, Beckman Coulter) and the analysis was performed on FlowJo® 10.6.2. The following antibodies/dyes were used: for staining ALL cells, Brilliant Violet anti-human CD19 (1:50 dilution; Biolegend Ref. no. 302234), for staining MSCs, anti-CD166 AF750, anti-CD73 AF750 and anti-CD146 AF750 (1:100 dilution, R&D System Ref. no. FAB6561S, FAB5795S and FAB932S, respectively). For viability staining, we used Sytox Red Dead Cell stain (1:1000 dilution, Life technologies Ref. no. S34859).

3.11.2 Microscopy

Cells were stained with one of the dyes of the Vybrant multicolor cell labeling kit (Ref no **V22889**) containing 1,19-dioctadecyl-3,3,39,39-tetramethylindocarbocyanine perchlorate (DiI; yellow), 3,39-dioctadecyloxacarbocyanine (DiO; green) and 1,19-dioctadecyl-3,3,39,39-tetramethylindocarbocyanine

perchlorate (DiD; red;), or with IncuCyte® Cytotox Reagents for Counting Dead Cells (Ref. no. 4633) according to the manufacturer's protocol. Upon staining, MSCs were seeded on top of the hydrogel and incubated at 37°C for three days, followed by the addition of ALL cells. Images of MSC migration inside the gel and MSC-ALL coculture were imaged with a Leica Thunder microscope with a 20x dry objective or a Leica DMI8 microscope with a 10x dry objective. DiO, Dil and DiD were excited with a 488 nm, 561nm and 633 nm lasers respectively. All images were evaluated with Fiji (Image J) 2.1.0/1.53C.

3.12 TLA

As a first step, DNA is fixed in place or crosslinked. Sequences from the same locus (the regions directly around the gene of interest) are crosslinked because crosslinking occurs preferentially between sequences in close physical proximity. TLA protocol then involves digestion of the crosslinked chromatin with the restriction enzyme *NlaIII*, an endonuclease that cleaves double stranded DNA molecules into fragments, recognizing a 4-base-pair site (4-cutter). The cross-linked restriction fragments are then reassembled to form long stretches of DNA consisting of religated DNA fragments originating from the same locus. The newly obtained DNA is de-crosslinked and digested by a second restriction enzyme called *NspI* (5-cutter) that creates fragments of 2 kilo-bases in size and religated obtaining a circular DNA fragment. At the end, the circular DNA, harbouring the gene of interest, is amplified by PCR using anchor-specific, outward-oriented primers pair (Figure 7). The amplified DNA is subsequently sequenced by Next Generation Sequencing technologies.

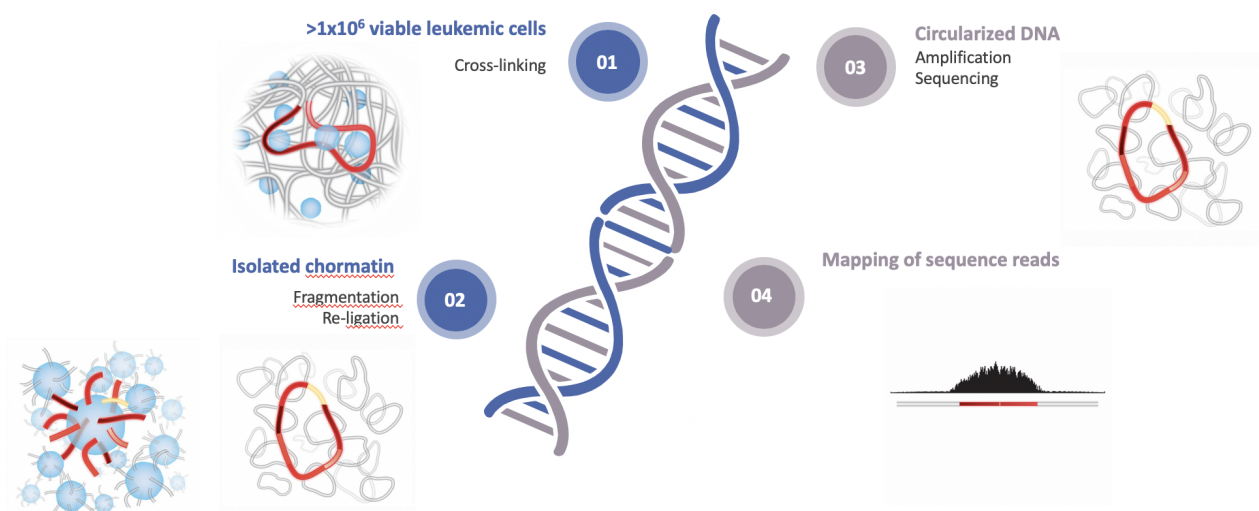


Figure 7: **TLA protocol.** Graphic representation of the phases foreseen by the protocol

3.13 Statistical analysis

In the P_{ABL}-based ELISA assay the analysis of P_{ABL} and P_{ABL-F} phosphorylation is expressed as a percentage related to total P_{PHOSPHO-ABL}. Statistical analysis was performed using two-way ANOVA and Bonferroni multiple comparison test; statistical significance was set at p<0.05.

4 RESULTS

4.1 Genetic alterations cell lines characterization

Leukemia cell lines were analyzed by Western blot to confirm the presence of candidate chimeric proteins. In NALM6 the presence of ETV6-PDGFRB fusion was investigated using an antibody against human PDGFRB. As shown in Figure 8 only in NALM6 a band >200 kDa appeared, corresponding to the presence of oligomeric and multimeric complexes of the chimeric protein. Another band with molecular weight of ~100 kDa, corresponding to PDGFRB (predicted molecular weight 125 kDa), was clearly visible in NALM6 and also in ALL-SIL and to a lesser extent in REH cells, while it was lacking in K562.

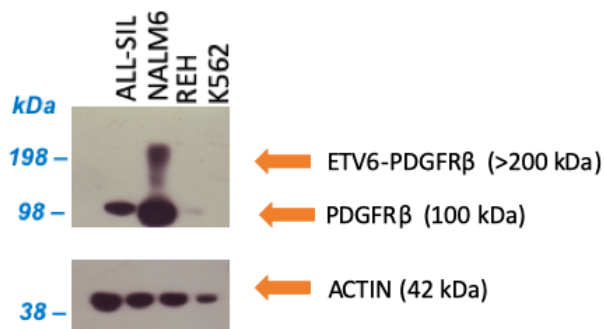


Figure 8. **Characterization of ETV6-PDGFRB fusion protein in NALM6.** Western blot against human PDGFRB (upper panel) and human actin (lower panel) as loading control.

Western blot using antibodies against ABL1 and phospho-ABL1 has been performed as shown in figure 9. ABL1 band (125 kDa) was present in each sample, except in K562, in which a band around 210 kDa corresponding to BCR-ABL1 was visible (Figure 9A); ALL-SIL exhibited a band around 300 kDa corresponding to the chimeric protein NUP214-ABL1. Western blot with anti phospho-ABL1 (pTyr-245) (Figure 9B) showed a band of 210 kDa in K562, corresponding to phosphorylated BCR-ABL1 protein. In ALL-SIL there was no phosphorylation on NUP214-ABL1. In K562 and ALL-SIL a band around 125 kDa appeared, corresponding to phosphorylated ABL1. No specific signals were detectable in NALM6 and REH.

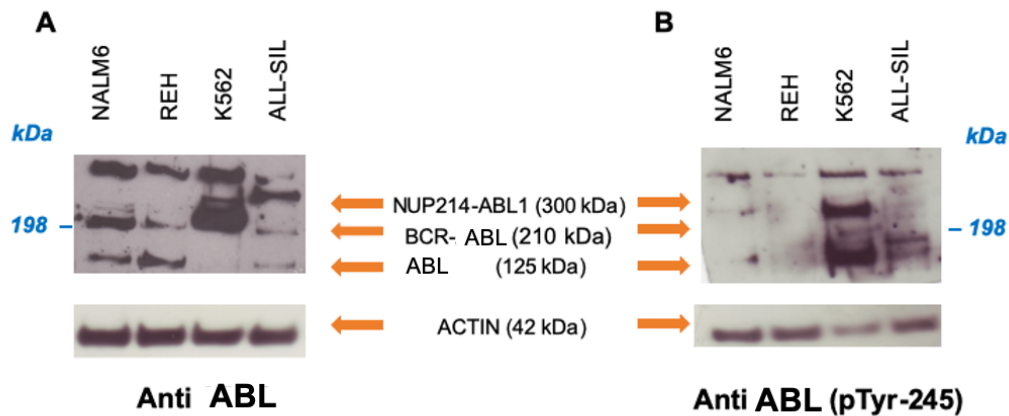


Figure 9. **Characterization of BCR-ABL1 and NUP214-ABL1 fusion proteins.** Western blot against (A) ABL1 and (B) phospho-ABL1. Actin was used as loading control.

4.2 P_{ABL} biosensor peptide *in vitro* functional analysis

The *in vitro* system proposed in this project was based on the recognition and quantification of phosphorylation by aberrantly activated ABL1 in the context of *BCR-ABL like* leukemia using artificial peptide-based substrate. The peptide was previously designed to be specific for ABL1 and contained a reporter region including the catalytic site, a targeting region which increases the specificity for ABL1 and a biotin tag for anchoring the biosensor on neutravidin-coated plates. Phosphorylation was quantified by an ELISA assay on 4 cell lines: 3 ALL lines with different genetic alterations affecting the ABL-pathway (NALM6, a *BCR-ABL like* line harboring *ETV6-PDGFRB*, ALL-SIL a T-ALL with *NUP214-ABL1*; *BCR-ABL1* positive K562 (positive control)) and in contrast to the fourth cell line, REH harboring the *TEL-AML1* fusion. The P_{ABL} - based ELISA analysis showed a significant phosphorylation of the P_{ABL} biosensor probe after incubation with the four leukemic cell lines tested (two-way ANOVA, Bonferroni corrected p-value < 0.0001, Figure 10). Table 2 reports results of the phosphorylated P_{ABL} as percentages relative to the fully phosphorylated $P_{PHOSPHO-ABL}$, used as positive reference value in each cell line. Average basal phosphorylation of lysates was $6.84 \pm 1.46\%$ in absence of biosensor vs $32.44 \pm 3.25\%$ in presence of P_{ABL} . K562 cells presented the highest phosphorylation level (mean fluorescence intensity (FI): 65185.81), similar to the P_{ABL} phosphorylation obtained after incubation with ALL-SIL lysates (mean FI: 53671.62). A lower signal was instead observed for NALM6 (mean FI: 44495.64, p-value < 0.01 *versus* K562) and REH (mean FI: 45352.60, p-value < 0.05 *versus* K562).

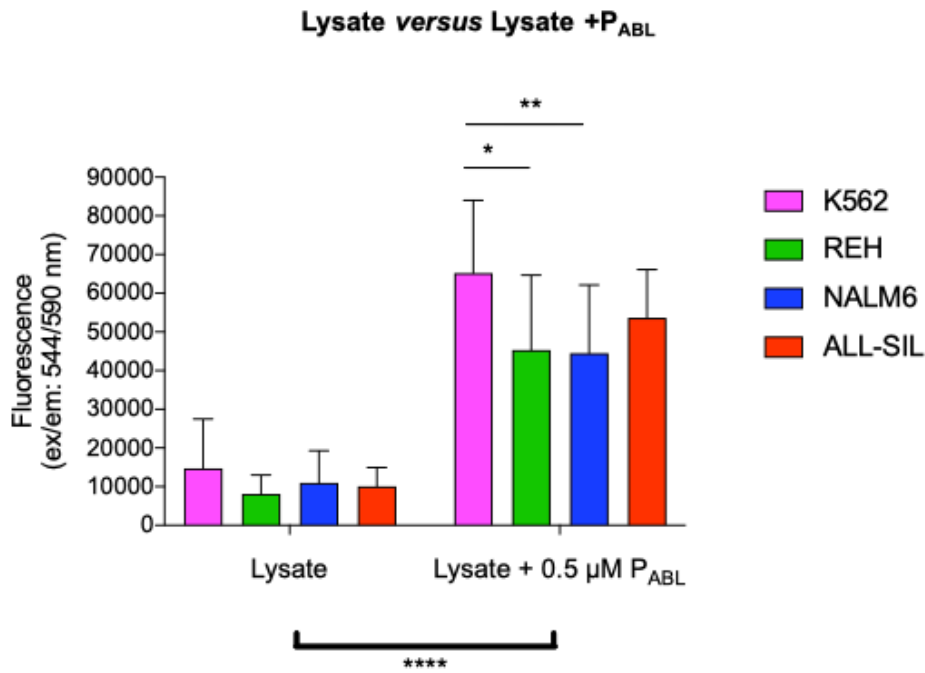


Figure 10. **P_{ABL}-based ELISA assay.** The graph shows data obtained from 12 independent experiments for K562, REH and NALM6 lines and 7 for ALL-SIL lines. Fluorescence values are reported in ordinate. There is a significant increase in terms of phosphorylation levels for all the lines after incubation with the peptide (****, p-value ANOVA 2-way 0.0001). K562 line showed the highest signal, significantly higher compared to the NALM6 (**, p-value ANOVA 2-way Bonferroni post-test for multiple comparison 0.001) and REH lines (*, p-value ANOVA 2-way Bonferroni post-test for multiple comparison 0.05).

	<i>Lysate</i>	<i>Lysate + P_{ABL}</i>
<i>K562</i>	9.35 ± 2.35 % N=12	41.43 ± 3.45 % N=12
<i>REH</i>	5.10 ± 0.88 % N=12	28.40 ± 3.50 % N=12
<i>NALM6</i>	6.93 ± 1.53 % N=12	28.16 ± 3.23 % N=12
<i>ALL-SIL</i>	5.96 ± 1.09 % N=7	31.76 ± 2.79 % N=7

Table 2: **P_{ABL}-based ELISA assay.** Phosphorylation of P_{ABL} biosensor is expressed as a percentage relative to the fully phosphorylated P_{PHOSPHO-ABL}, used as reference.

4.3 P_{ABL} “reporter” region signal specificity validation

The biosensor includes a tyrosine both in the target and in the reporter region. In order to verify the specificity of the phosphorylation signal on the catalytic site, a site-mutated biosensor was tested in the assay (i.e. P_{ABL-F}, with the tyrosine in the “reporter” region replaced by phenylalanine). The levels of P_{ABL-F} phosphorylation were similar among cell lysates and did not differ from the basal fluorescence signals detectable in all cell lines in the absence of peptide (Figure 11 and Table 3).

Lysate versus Lysate +P_{ABL-F}

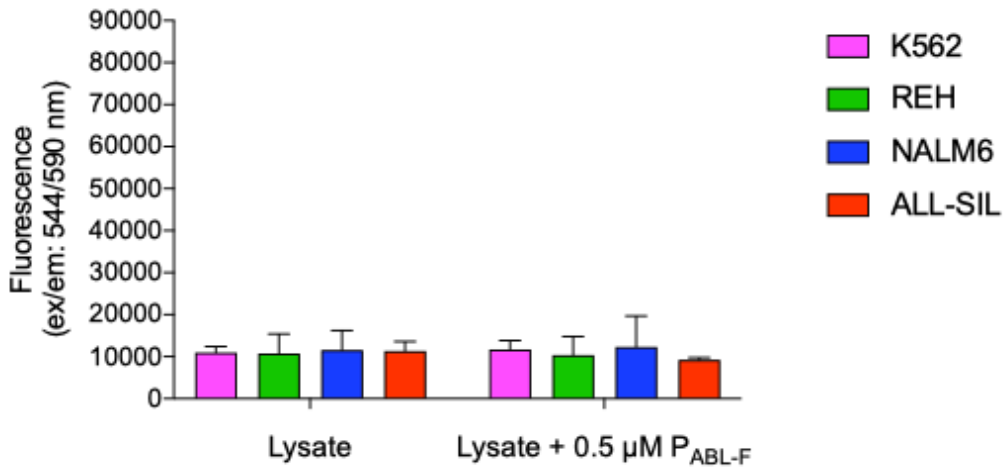


Figure 11. **P_{ABL-F}-based ELISA assay**. The graph shows data obtained from 4 independent experiments. Fluorescence values in ordinate. There is no significant increase in terms of phosphorylation levels for all the lines after incubation with the peptide P_{ABL-F} (two-way ANOVA Bonferroni post-test for multiple comparison).

	Lysate (N=4)	Lysate + P _{ABL-F} (N=4)
K562	4.60 ± 0.92 %	6.24 ± 0.84 %
REH	3.92 ± 1.08 %	5.72 ± 2.01 %
NALM6	3.89 ± 1.08 %	5.57 ± 2.40 %
ALL-SIL	6.11 ± 0.60 %	4.97 ± 0.14 %

Table 3. **P_{ABL-F}-based ELISA assay**. Phosphorylation is expressed as a percentage related to P_{PHOSPHO-ABL}, from 4 different lysates.

4.4 Comparison of P_{ABL} and P_{ABL-TIDE}

An ELISA assay was performed on K562 lysates to compare the P_{ABL} (“*target*” + “*reporter*” sequences) to P_{ABL-TIDE} (“*reporter*” sequence only). P_{ABL} shows a higher phosphorylation compared to P_{ABL-TIDE} (p-value two-way ANOVA, Bonferroni corrected p-value 0.023), with a significant decrease after imatinib (ABL1 specific TKI) pre-treatment of lysates (p-value 0.0027, Figure 12A). Interestingly, no significant changes in phosphorylation level of P_{ABL-TIDE} were observed increasing both the amount of lysate and the probe concentration (Figure 12B).

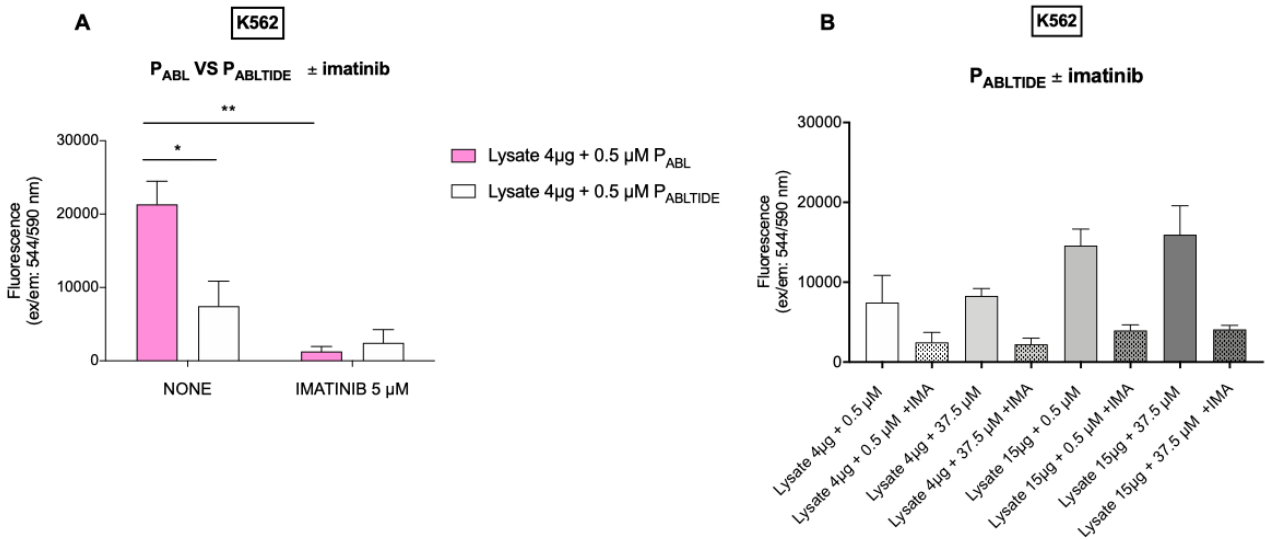


Figure 12. **Peptide-based ELISA assay to detect ABL1 activity in the presence and absence of 5 μM imatinib.** A. Comparison between P_{ABL} and P_{ABL}TIDE phosphorylation levels; B. P_{ABL}TIDE phosphorylation levels incubated with different amount of lysates and probe. The graphs show data obtained from 2 independent experiments. Fluorescence values in ordinate. P-value calculated two-way ANOVA, Bonferroni post-test: * = 0.023; ** = 0.0027). IMA: imatinib.

4.5 ABL1 kinase activity specificity: inhibitory effect of imatinib and ruxolitinib on P_{ABL}

To determine the specificity of ABL1 phosphorylation activity on the probe, cell lysates were pre-incubated with tyrosine kinase inhibitors: imatinib and ruxolitinib. Imatinib was selected as ABL1 specific inhibitor and used at a concentration of 5 μM. Incubation with imatinib showed a significant decrease of phosphorylation levels for all the cell lines (2-way ANOVA p-value < 0.0001) Figure 13 and table 4.

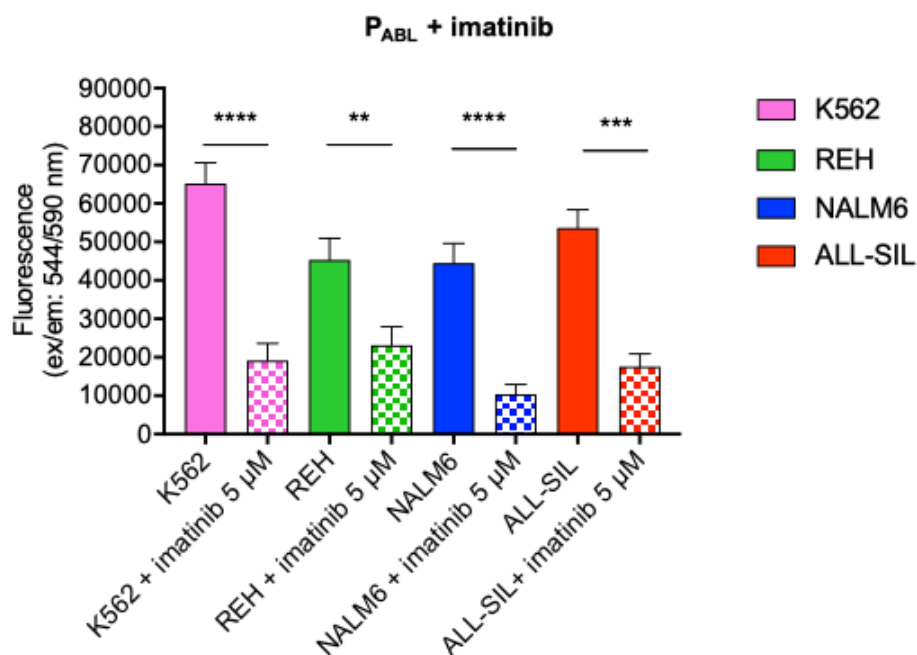


Figure 13. **P_{ABL}-based ELISA assay in the presence of imatinib.** The graph shows data obtained from 9 independent experiments for K562, REH and NALM6 lines and 7 for ALL-SIL lines. Fluorescence values in ordinate. Imatinib determined a significant decrease of phosphorylation levels for all the lines (****, p-value ANOVA 2-way 0.0001). The reduction is particularly evident for those lines activating ABL1 pathway: K562 (****, p-value ANOVA 2-way Bonferroni post-test for multiple comparison 0.0001), NALM6 (****, p-value ANOVA 2-ways Bonferroni post-test for multiple comparison 0.0001), ALL-SIL (***, p-value ANOVA 2-way Bonferroni post-test for multiple comparison 0.0002). REH line the cell line not activating ABL1 pathway, showed a less pronounced effect (**, p-value ANOVA 2-ways Bonferroni post-test for multiple comparison 0.0068)

Following the same protocol, cell lysates were incubated with ruxolitinib, a JAK1/2 specific inhibitor, to evaluate the phosphorylation activity of ABL1 to a non-specific inhibitor, as negative control. Two different concentrations of ruxolitinib were selected (52nM and 5μM). As expected, ruxolitinib did not affect the P_{ABL} phosphorylation at any of the concentrations tested. A decrease in phosphorylation was observed in NALM6, REH and ALL-SIL after incubation with ruxolitinib 5μM but it did not reach statistical significance Figure 14 and table 4.

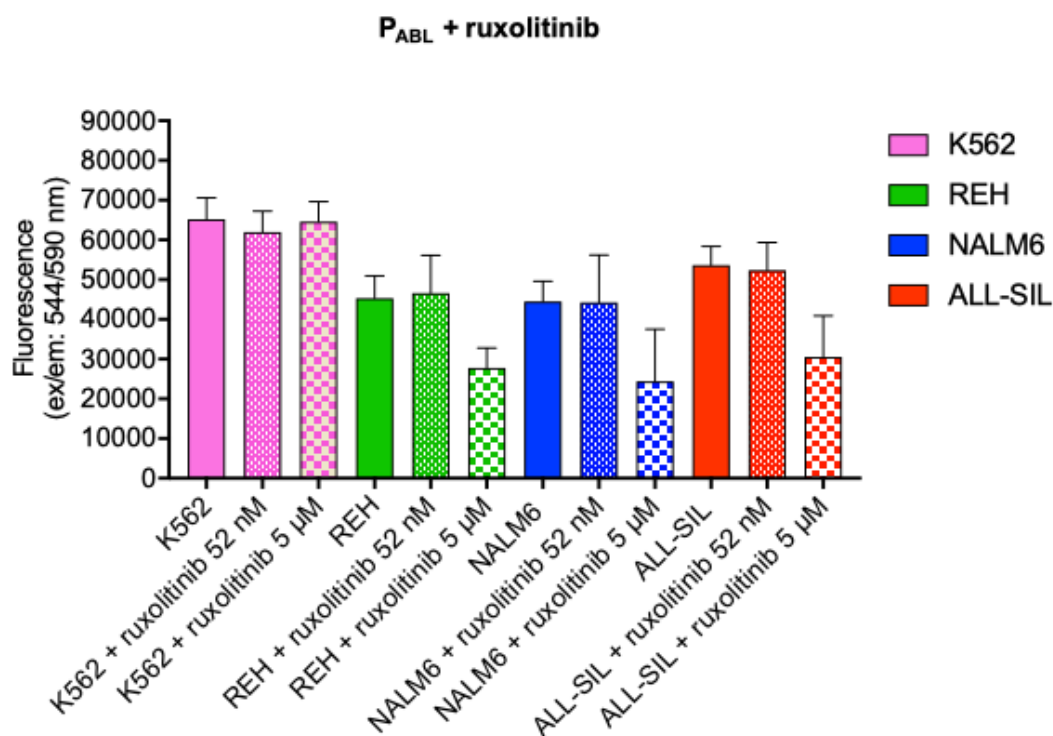


Figure 14. **P_{ABL}-based ELISA assay in the presence of ruxolitinib.** Biosensor phosphorylation was expressed in terms of percentage of fluorescence in comparison to a fully phosphorylated probe. The graph shows data obtained from 6 independent experiments using 52nM of ruxolitinib and 3 independent experiments at 5μM. Fluorescence values in ordinate. None of the cell line determined a significant decrease in terms of phosphorylation.

	<i>LYSATE</i>	<i>LYSATE + P_{ABL}</i>	<i>P_{ABL} + imatinib 5 μM</i>	<i>P_{ABL} + ruxolitinib 52nM</i>	<i>P_{ABL} + ruxolitinib 5 μM</i>
<i>K562</i>	9.35 ± 2.35 % N=12	41.43 ± 3.45 % N=12	12.17 ± 2.83 % N=12	39.41 ± 3.31 % N=6	41.08 ± 3.20 % N=3
<i>REH</i>	5.10 ± 0.88 % N=12	28.40 ± 3.50 % N=12	14.47 ± 3.05 % N=12	29.18 ± 5.97 % N=6	17.42 ± 3.14 % N=3
<i>NALM6</i>	6.93 ± 1.53 % N=12	28.16 ± 3.23 % N=12	6.57 ± 1.62 % N=12	38.02 ± 7.54 % N=6	15.43 ± 8.30 % N=3
<i>ALL-SIL</i>	5.96 ± 1.09 % N=7	31.76 ± 2.79 % N=7	10.40 ± 1.95 % N=7	31.02 ± 4.13 % N=6	18.08 ± 6.12 % N=3

Table 4. **P_{ABL}-based ELISA assay in the presence of imatinib or ruxolitinib.** Phosphorylation of P_{ABL} biosensor is expressed as a percentage relative to the fully phosphorylated P_{PHOSPHO-ABL}, used as reference.

4.6 Molecular simulation (SM) performed for the STA5 / JAK2 complex

As first step the study was focused on understanding the interaction between STAT5 and JAK2 and verifying the position of our candidate peptides. The protein models were obtained optimizing from the available pdb files in the Protein Data Bank (code 2B7A for JAK2 and code 1Y1U for STAT5). It was necessary to computationally refine some missing parts of STAT5 structure, especially in the putative region of interaction with JAK2. By applying a consolidated protein-protein computational docking recipe ^{86,88}, the best conformations obtained were selected among those fitting the best protein-protein interactions energy and belonging to the most populated cluster. Accordingly, the best docking positions were then subjected to an extensive Molecular Dynamics (MD) protocol in explicit solvent in order to actually reproduce the physiological environment in which the STAT5/JAK2 binding occurs (Figure 15).

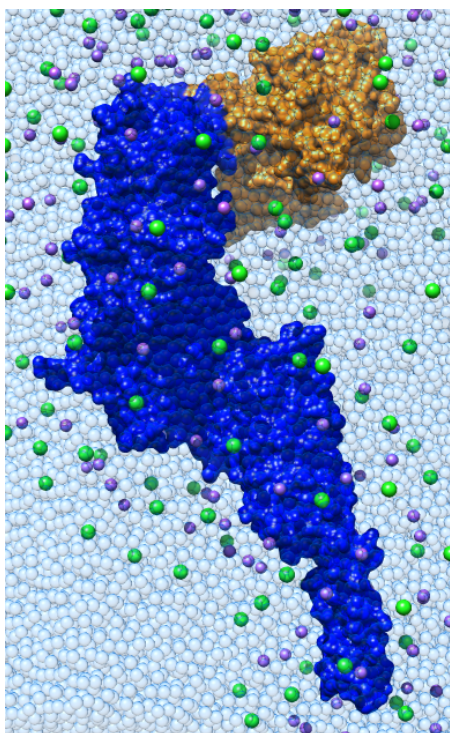


Figure 15. **Molecular simulation between STAT5 and JAK2.** The figure on the left shows the initial STAT5 (blue) / JAK2 (orange) complex in an aqueous solvation box with the addition of Cl⁻ (green) and Na⁺ (purple) counterions to simulate the presence of physiological ionic strength (150 mM NaCl).

Eventually, the simulated complex, after equilibration of the thermodynamic and structural parameters, was subjected to MD for a total time of 200 ns and the binding energy analysis was performed to quantify the interactions between the two proteins.

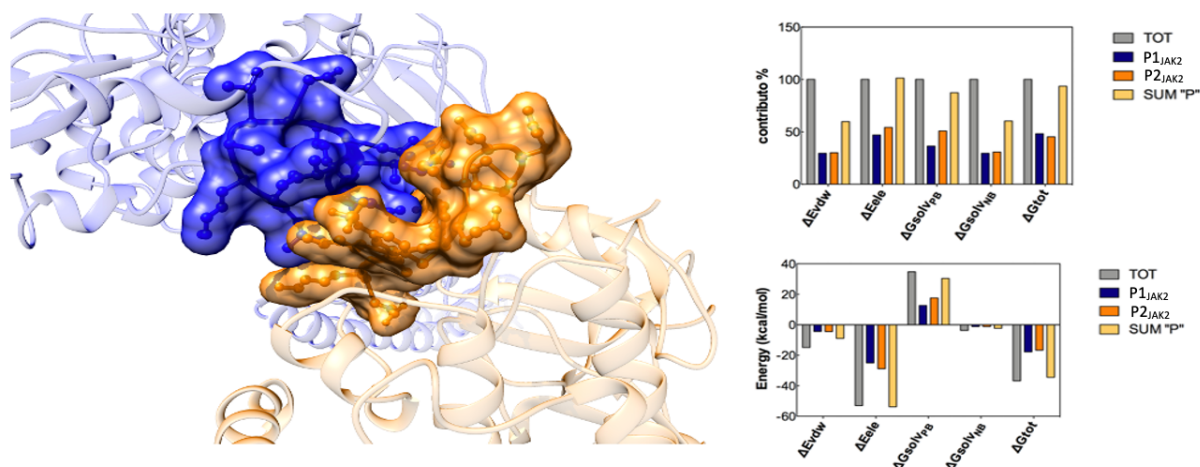


Figure 16. **P1_{JAK2}** and **P2_{JAK2}** provide the main interaction between STAT5 and JAK2. In the left figure, a detail of the link interface between STAT5 (blue) and JAK2 (orange); the amino acids displayed with their vΔW surface are those corresponding to the previously reported peptide sequences. The graphs on the right represent the results of our analysis: the two proteins establish an interaction with a favorable energy as demonstrated by the negative value ΔG_{tot} (-36.73 kcal / mol). Although the greatest contribution is given by ΔE_{ele} (-53.00 kcal / mol), this is partially counteracted by the solvation work ($\Delta G_{solv_{PB}}$) which is positive (+34.82 kcal / mol) and partially contrasts the binding between the two proteins. The hydrophobic interactions (ΔE_{vdw}) are stabilizing and favorable for the binding (-14.87 kcal / mol).

Interestingly the main contributions of interaction come largely from the selected peptides: both P1_{JAK2} and P2_{JAK2} provide the main interactions between STAT5 / JAK2 for their thermodynamics stabilization. The first graph in Figure 16 shows the contributions translated into % of the total. In all components, the sum of the energy (SUM "P") concerning the two peptides, represents at least 60% of the total, ultimate confirmation that the main interaction interface of the STAT5 / JAK2 complex concerned these two specific sequences under these specific conditions.

4.7 P1_{JAK2}-P2_{JAK2} peptides and P1_{JAK2}-P2_{JAK2}/JAK2 simulation

P1_{JAK2} was subjected to MD for a total time of 100 ns, in an explicit solvent (Figure 17A). The trajectory was then analyzed to obtain a conformational model corresponding to the energetically most favorable structures of P1_{JAK2} in aqueous environment (Figure 17B). The conformational model was further processed to obtain the most stable structure (i.e., the most probable) to be compared with the STAT5 / JAK2 complex in which the P1_{JAK2} sequence was within the SH2 domain at the binding interface with the kinase domain of JAK2. The

analysis revealed that the main contributions to the binding are provided by the selected peptide, which perform the main interactions for thermodynamically stabilizing the STAT5 / JAK2 complex.

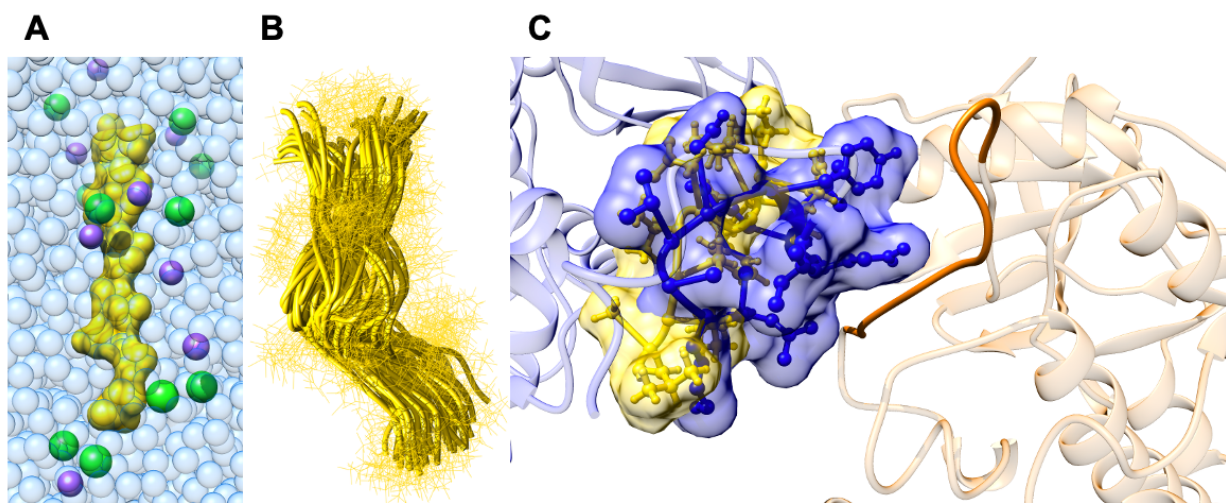


Figure 17. **Molecular simulation of P1_{JAK2}**. Extensive Molecular Dynamics (MD) protocol in explicit solvent (A). P1_{JAK2} was subjected to DM for a total of 100 ns. The trajectory was analyzed to obtain a conformational model corresponding to the energetically most favorable structures of P1_{JAK2} in the aqueous environment (B). The most stable conformational model of P1_{JAK2} compared with the STAT5 / JAK2 complex in which the P1_{JAK2} sequence was within the SH2 domain at the kinase binding interface (C). As can be seen, there is an excellent matching between the corresponding sequence in the complete protein (blue) and the P1_{JAK2} peptide (gold).

The final phase of analysis involved the exclusive interaction of the P1_{JAK2} with JAK2 protein. The resulting P1_{JAK2} / JAK2 complex in an aqueous environment, after equilibration of the thermodynamic parameters, was subjected to MD for a total time of 200 ns at the end of which an energy analysis was performed to quantify the peptide / protein interactions (Figure 18).

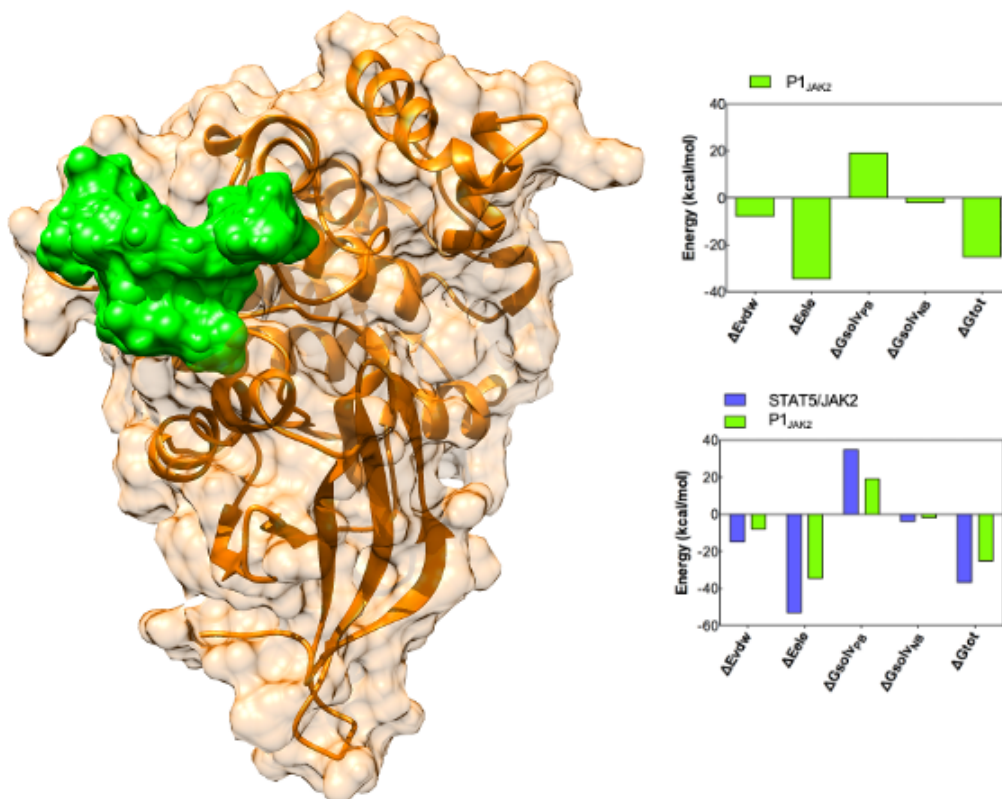


Figure 18: **P1_{JAK2} peptide (green) in the active site of the JAK2 protein.** P1_{JAK2}-JAK2 establish a favorable binding energy (negative ΔG_{tot}). The comparison between the binding energies of the P1_{JAK2} with the JAK2 protein is also reported, as well as the binding interactions occurring between STAT5 and JAK2 (in blue).

The JAK2 binding capability of the previously mentioned P2_{JAK2} peptide was compared to P1_{JAK2} by applying a computational procedure similar to that described for P1_{JAK2} (Figure 19). In turn, the overall binding energies ΔG_{tot} are both negative, but P1_{JAK2} had a more favorable binding energy than P2_{JAK2}.

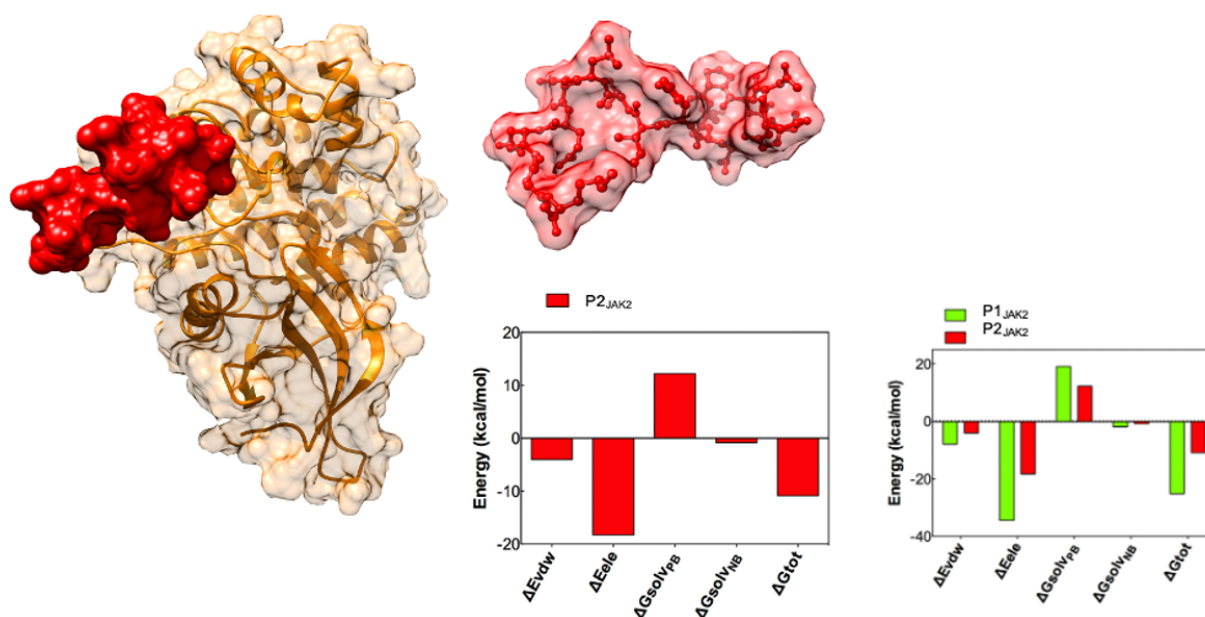


Figure 19: **P1_{JAK2} and P2_{JAK2} comparison.** P2_{JAK2} peptide in red, in the active site of the JAK2 kinase domain with which it establishes a favorable binding energy (negative ΔG_{tot}). The graph shows the comparison between the binding energies of P1_{JAK2} (in green) compared with the binding interactions established by P2_{JAK2} (in red) in complex JAK2.

4.8 JAK2 protein expression and purification

The simulation showed the potential of P1_{JAK2} as future reporter for the new JAK2 biosensor. These results must be validated, and JAK2 Janus kinase 1 (JH1) domain was expressed and purified to recover substrates for future surface plasmon resonance (SPR) experiments. Suzana Aulic from Professor Pricl group at the University of Trieste and visiting scientist at ICGEB, designed an expression plasmid containing the sequence of JH1 kinase domain. The protocol provides the expression in *E. coli* and a consequent size-exclusion chromatography (SEC) purification.

4.8.1 Expression

To start the expression the plasmid was first transformed into BL21 (DE3) pLysS competent cells, plated and a single colony was then isolated to induce expression of JAK2 JH1. The expression product was isolated and loaded into two Bio-rad polyprep columns (Bio-rad #7311550). To check the success of the reaction, 1.5 ml elution fractions were collected and checked on a 12% SDS-PAGE.

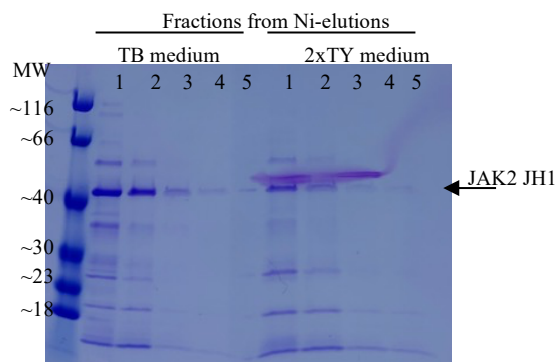


Figure 20: **JAK2 JH1 expression in BL21 (DE3) pLysS competent cells.** The image shows fractions from the 2xTY-media-expression and the TB-media-expression loaded on a 12% SDS-PAGE (TGX FastCast Acrylamide kit, 12%), Gel was stained with commassie blue.

Bands around 41 kDa are evident in 1-3 fraction from both media, at a molecular weight corresponding to the final product JAK2 JH1 (Figure 20). TB media and 2xTY media are very rich media usually used for protein expression, to have the maximum yield we decided to use both. Since fraction 1-3 from both media showed a product, they were combined for later purification.

4.8.2 SEC purification

Prior SEC purification we selected His-tag JAK2 JH1 applying Ni Sepharose Excel resin. The purification was performed through a S75 Increase 10/300GL column equilibrated in SEC buffer. As a check of the purification success, samples from each fraction were collected and run on a 12% SDS-PAGE. As visible in Figure 21, all fractions showed a band around 41 kDa corresponding to JAK2 JH1.

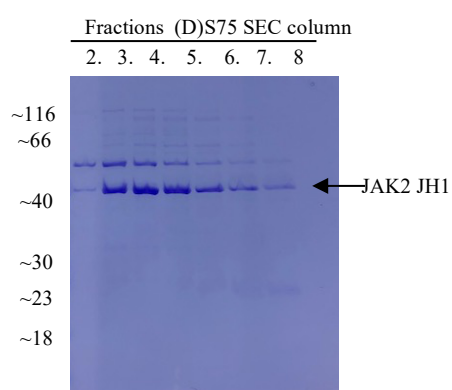


Figure 21: **Fractions from JAK2 JH1 protein purification.** Plot of samples run 12% SDS-PAGE with fractions of the SEC run. A band around 41 kDa is visible in fractions 3-8 which should correspond to JAK2 JH1 protein purified.

The purification chromatogram showed a unique peak with intensity of 180 milli-absorbance unit (mAU) suggesting a clear purification of JAK2 JH1 product. (Figure 22).

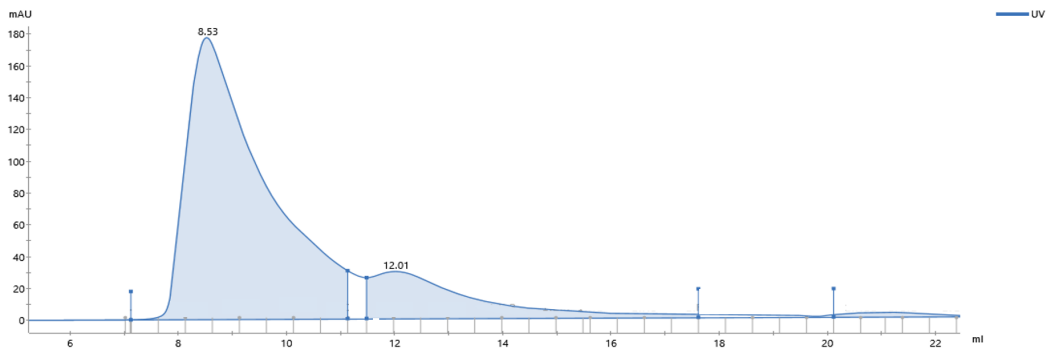
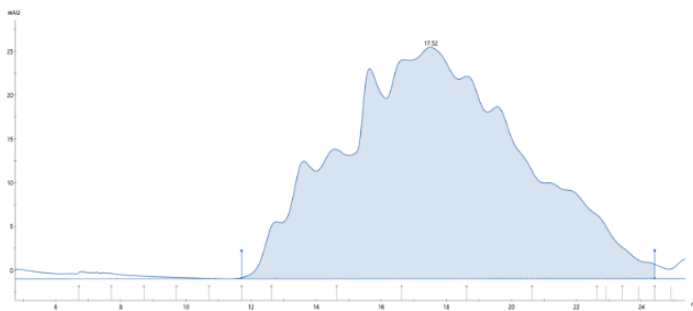


Figure 22: **SEC chromatogram of JAK2 JH1 purified protein.** The purification gave a unique peak corresponding to JAK2 JH1 protein purified.

To test the stability of purified JAK2 JH1, after 1 week at 4C, fractions 2-8 were pooled, concentrated and, re-run on a S75 Increase 10/300GL column equilibrated in SEC buffer. Unfortunately, the samples seemed to be completely degraded (Figure 23A), when run on a SDS page the bands appeared light and almost invisible (Figure 23B)

A



B

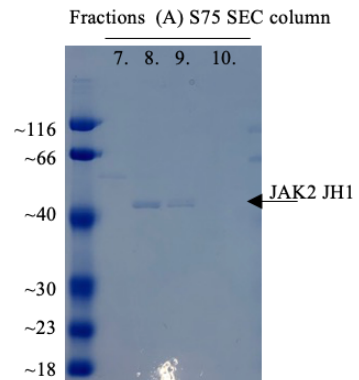


Figure 23: **JAK2 JH1 was degraded after a week.** (A). SEC chromatogram after a week of JAK2 JH1 storage. The sample appeared completely degraded. (B). SDS page of the fraction from the purification where only fraction 8-9 show a light and almost invisible band around 41kDa.

The experiment was then repeated, and the second experiment showed a completely degraded product (Figure 24)

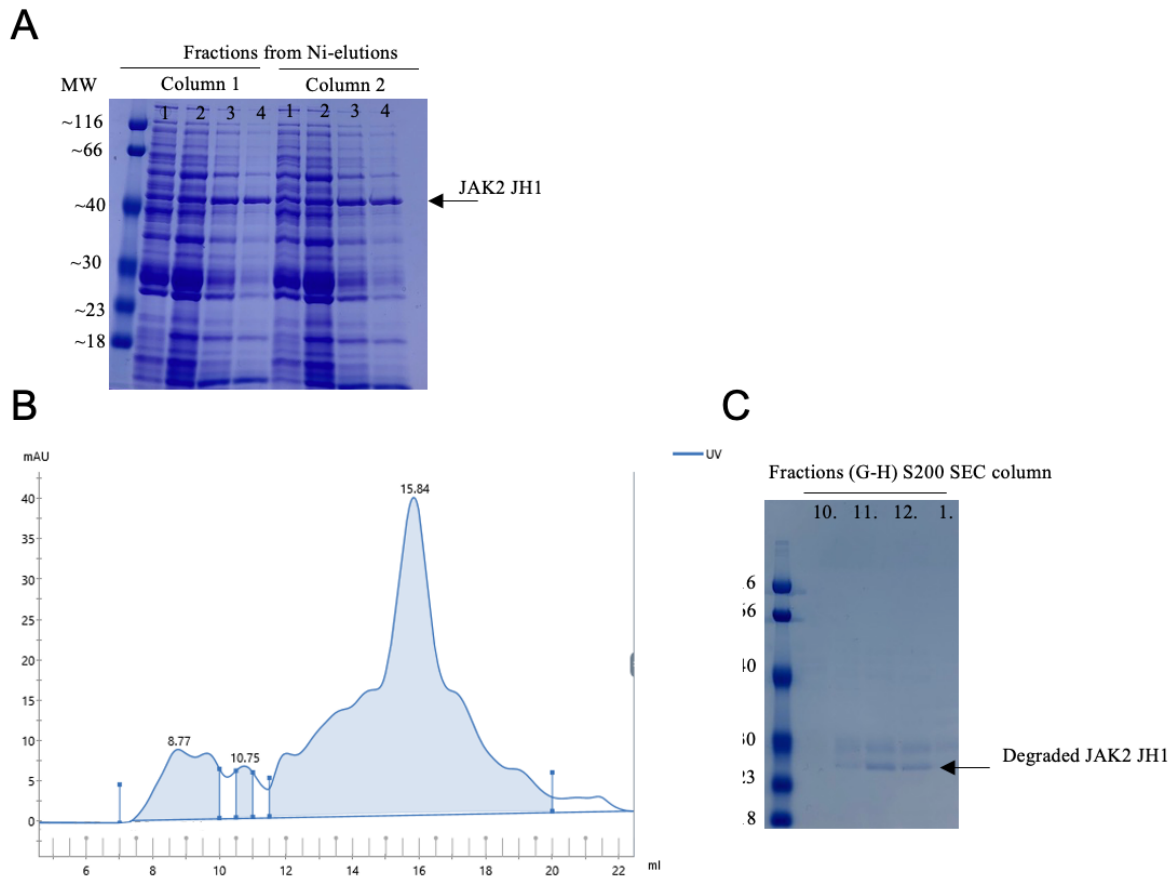


Figure 24: **Second JAK2 JH1 expression and purification.** (A). Plot of fractions from the expression loaded on a 12% SDS-PAGE, bands around 41kDa show a possible JAK2 JH1 expression (B) From the SEC chromatogram is already evident a complete degradation of the sample, confirmed in (C) in SDS page of the fraction from the purification.

4.9 Leukemic niche 2D coculture

An *in vitro* system capable to prolong primary ALL cell is lacking. To improve the viability of ALL cells, we cocultured primary leukemic cells of 10 ALL patients (2 *ETV6-RUNX1*, 6 B-others, 2 *BCR-ABL1* previously shown to not survive *in vitro*) in a 2-dimensional (2D) system on top of primary human mesenchymal stromal cells (MSC) layer on a 96 well plate for 3 days. MSCs support alone may not be enough to prolong ALL *in vitro* survival. Therefore, 8 growth factors, were added to the coculture in different combinations: interleukin 7 (IL7), granulocyte colony stimulating factor (G-CSF), Fms-related receptor tyrosine kinase 3 ligand (FLT3LG), thrombopoietin (TPO), interleukin 3 (IL3), stem cell factor (SCF), interleukin 2 (IL2), thymic stromal lymphopoietin (TSLP). All 2D experiments were performed in single; patient material is indeed limited and

precious and for this preliminary study phase we decided to first screen all the conditions and decide later to proceed with relevant results.

4.10 *In vitro* primary leukemic cell survival with different concentrations and combinations of growth factors

For the first screening three primary leukemic cell samples were selected from patients with different genetic backgrounds (2 *ETV6-RUNX1* (ER) and 1 B-other (BO)). Primary cells were cocultured on top of a human primary MSCs layer for 3 days in presence of different growth factors. In 96 wells plate the coculture was treated with 1 or 2 growth factors per well in all possible combination and in two concentration (20 or 50 ng/ml for each growth factor as final concentration). As visible in figure 25, none of the growth factors alone or in combination gave a benefit in terms of survival. Although both concentrations gave similar results, we chose to continue with 20ng/ml.

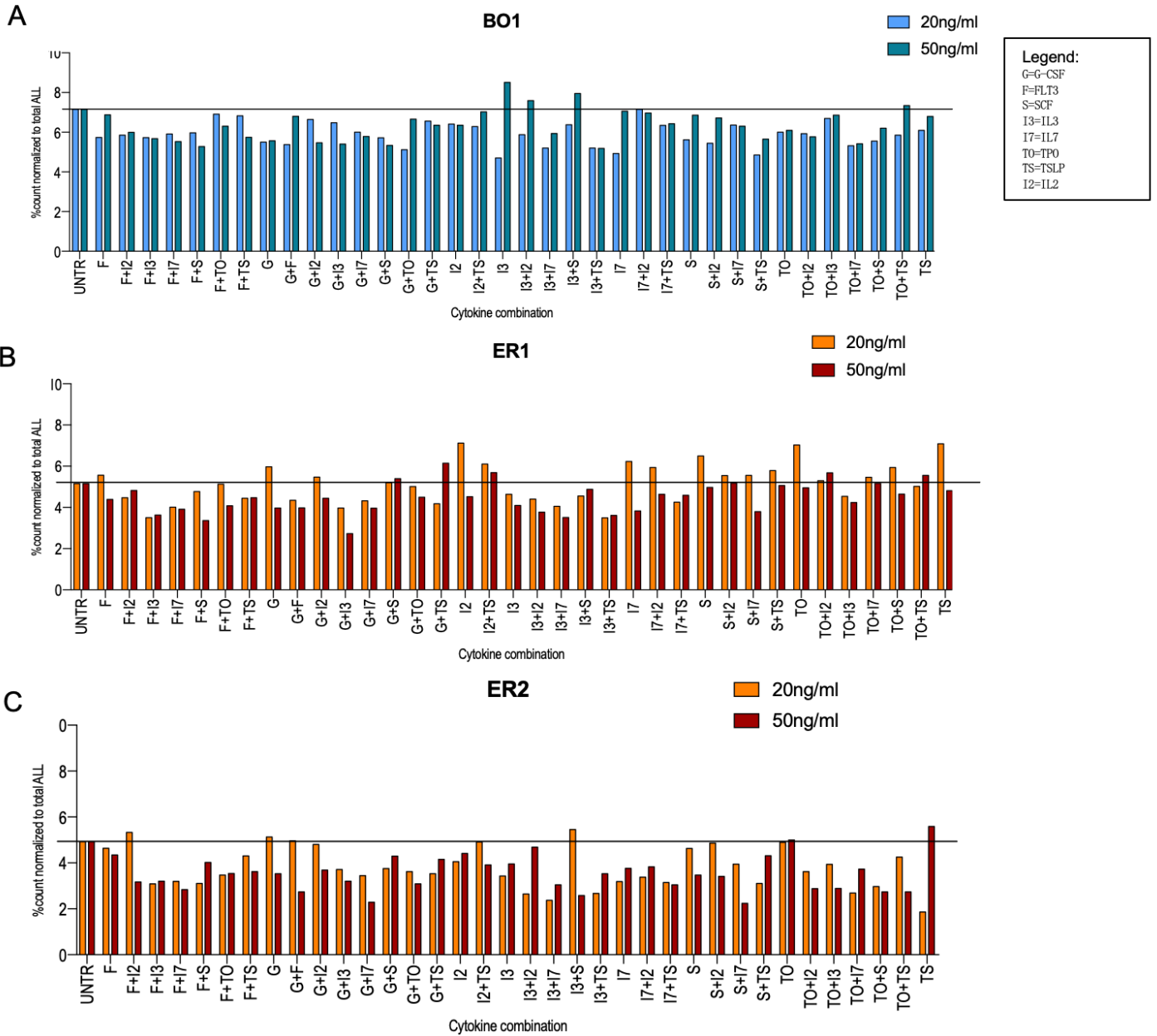


Figure 25: **Leukemic cell survival with different concentrations and combinations of growth factors.** The graphs show percentage of survival of primary leukemic cells after 72h normalized to the cell number at start of culture (day 0) with either 20ng/mL (light blue or light orange bars) or 50ng/mL (dark blue or dark orange bars) growth factor, with either one single growth factor or in combination. Solid line indicates survival of the untreated control (UNTR). For these preliminary fast screening the experiments were performed in single. (A). The graph represents the % count of viable primary leukemic cells after coculture of primary cell from patient classified as B-other (BO1). (B) and (C). Representation of results for viable primary cells after coculture of patients harboring *ETV-RUNX1*(ER1 and ER2 respectively).

4.11 Primary leukemic cells survival *in vitro* with combinations of 4 different growth factors

As the coculture of primary ALL cell with MSCs in presence of 1 or 2 growth factors did not show any benefit for ALL survival at any concentration, we tried to increase the number for each condition. Primary ALL cells from 4 patients (2 classified as B-others(BO) and 2 harboring *BCR-ABL1* (BA) fusion) were selected and cocultured on top of a layer of primary human MSCs. The cells were kept in coculture in a 96 wells plate for 3 days and each coculture was treated with the 8 growth factors listed above in all possible combinations of 4 at a concentration of 20 ng/ml (final concentration per each cytokine). In figure 26 viability is represented as percentage of viable cells normalized to the total number of primary ALL cells seeded at the start of coculture. As visible, none of the condition increased survival.

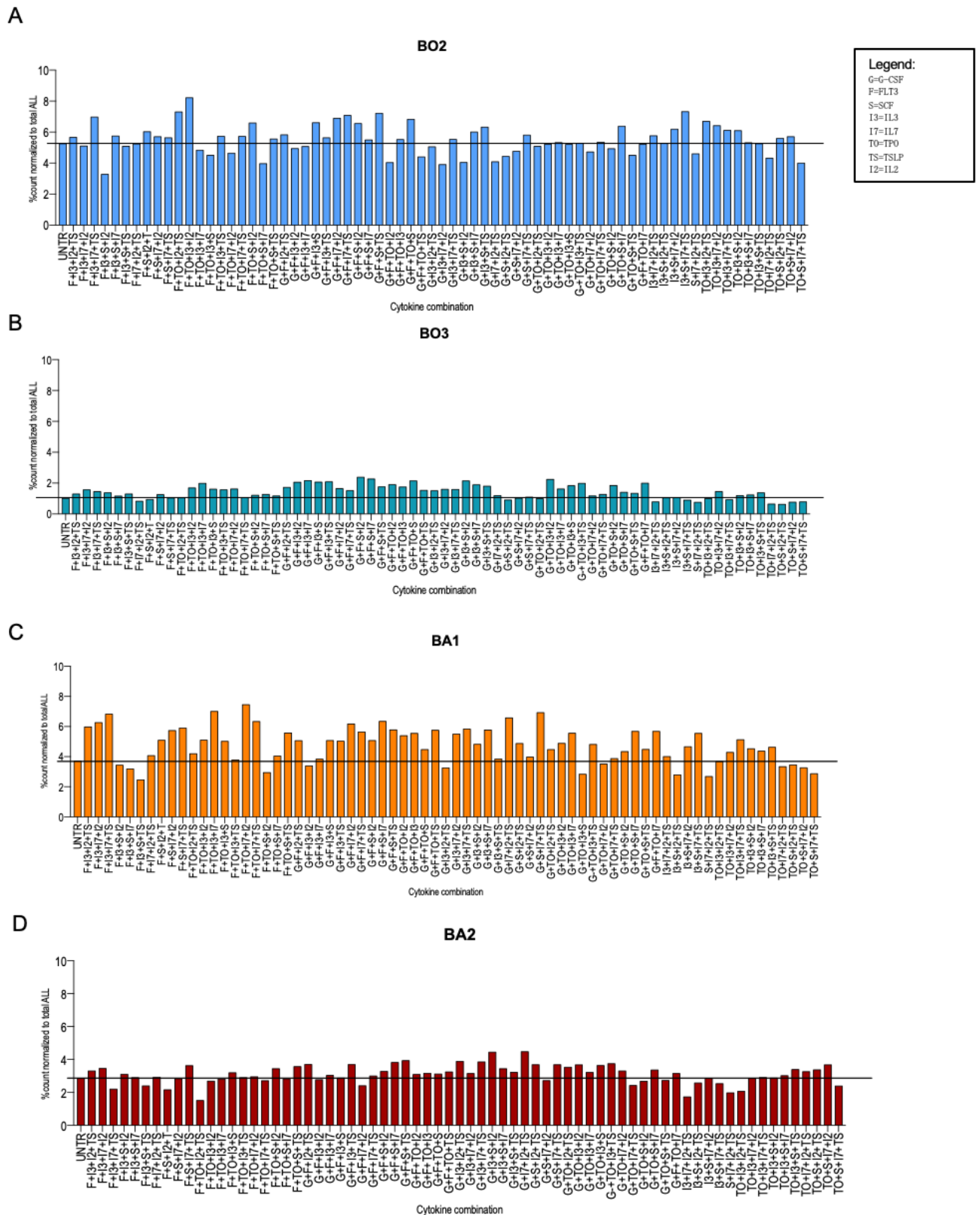


Figure 26: **Leukemic cell survival with 4 growth factors in all possible combination.** The graphs show percentage of survival of primary leukemic cells after 72hrs normalized to the cell number at start of culture (day 0) with 4 growth factors in all possible combination at a concentration of 20ng/ml (final concentration per each cytokine). The horizontal solid line indicates survival of the untreated control (UNTR). For these preliminary fast screening the experiments were performed in single. (A) and (B). The graphs represent the viability of primary leukemic cells from patients classified as B-others (BO2 and BO3). (C) and (D). Results for viable primary cells after coculture of patients harboring *BCR-ABL1* (BA1 and BA2).

4.12 The impact of different culture media on the *in vitro* survival of primary leukemic cells.

Since adding combinations of different growth factors to the culture did not impact their survival, we tested if different culture media could play a role in *in vitro* survival of primary leukemic cells. Three different culture media were used: either the culture medium used in previous experiments, RPMI Dutch modified plus 20% of FCS, L-glutamine and ITS (standard medium (SM)), serum free (SF) hematopoietic stem cells medium SFEM II or SFEM II plus 20% of FCS in presence different combination of growth factors. SFEM II is specifically designed and validated for stem cell culture. Previous published studies already showed the benefit of SFEM II in primary ALL cells⁵¹. Three primary ALL cells from patients classified as B-others (BO) were selected and cocultured on top of primary human MSCs in presence of up to 3 growth factors at a concentration of 20 ng/ml (final concentration per each) in different culture medium. When we compare the impact of SM, SF SFEM II or SFEMII 20% of FSC on ALL survival (Figure 27), none of the culture medium led to any viability improvement. The red circles in Figure 27B and C highlight the increase of BO5 ALL cells viability from 13% to 66% when cocultured with primary MSCs in SM in presence of G-CSF, FLT3LG, IL7 and even to 90% in SFEM II SF with FLT3LG, IL7, IL3.

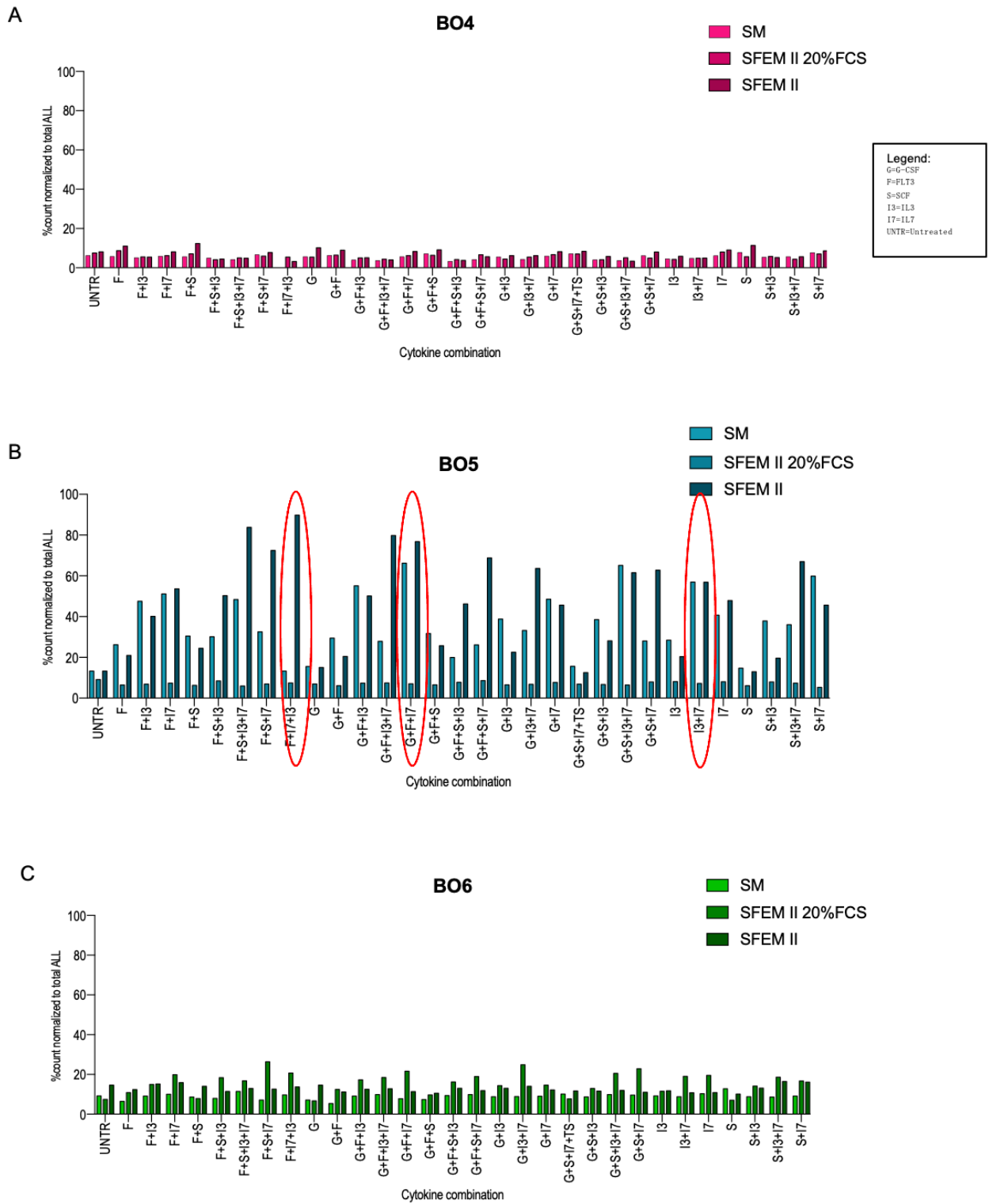


Figure 27: **Leukemic cell survival with different culture medium.** The graphs show percentage of survival of primary leukemic cells after 72hrs normalized to the cell number at start of culture (day 0) with 1 to 4 growth factors in all possible combination at a concentration of 20ng/ml (final concentration per each cytokine) and in different culture medium. The horizontal solid line indicates survival of the untreated control (UNTR). For these preliminary fast screening the experiments were performed in single. (A) and (C). Graphs of the results for the viability of primary leukemic cells from patients classified as B-other (BO4 and BO6). (B). Representation of the viability of primary ALL cells for patient BO5 (B-other) where survival increased from 13 to 66% in SM with G-CSF, FLT3LG, IL7 and to 90% in SFEM II SF with FLT3LG, IL7, IL3.

4.13 Leukemic niche 3D coculture

In this study the 2D system failed to prolong ALL *in vitro* survival and a 3D model mimicking the bone marrow organization might be a good option. To improve viability of ALL cells we cocultured human leukemia stabilized cell lines together with human primary MSCs in a synthetic matrix named Corning® PuraMatrix™ Peptide Hydrogel (PuraMatrix) used to create defined 3D microenvironments. The protocol was provided thanks to the collaboration with the University Medical Center in Utrecht (UMCU), who optimized the 3D system using primary human multiple myeloma (MM) cells in coculture with stromal layers different from MSCs in Puramatrix (not published). Unlike other hydrogels such as matrigel or Cultrex Basement Membrane Extract (BME), Puramatrix is purely synthetic and avoids batch differences problems.

4.14 Stabilized cell lines survival *in vitro* measurements by flow cytometry

The protocol provided by UMCU was optimized for coculture of human primary MM cells together with stromal cells. We wanted first to check if the parameters used for MM could be applied to the coculture of ALL cells with MSCs. The aim was to achieve the highest ALL survival. Puramatrix was prepared at a concentration of 0.25% or 0.5% and 5500 or 10000 human primary MSCs were seeded (day 0) on top of the gel and left to enter the gel for 72h when human ALL SupB15 cell line was added at a concentration of 0.4×10^6 /ml to the system. After 3 days of coculture, cells were harvested, and viability was measured by flow cytometry. In Table 5, the red square highlights 0.25% of gel concentration with 10000 MSCs seeded at day 0 which was the final condition selected for the assay. Together with 0.25% of gel concentration with 5500 MSCs condition it gave the highest number of ALL cells after recovery. As both MSCs concentration gave similar results, we chose to continue with 10000 according to previously published studies where they suggested the use of a higher number of MSCs ⁶.

	<i>Coculture count MSCs</i>	<i>Coculture count ALL</i>	<i>Count MSC only</i>	<i>Count ALL only</i>
<i>0.5% gel 5500 MSCs</i>	953	45009,5	436,5	
	407	7983	407	
	122	10807	108	
<i>0.5% gel 10000 MSC</i>	1246	26697	740	
	1182	10077	922	
	166	12874	571	
<i>0.25% gel 5500 MSCs</i>	731,5	52848	928,5	
	1306	15161	1154	
	228	30663	331	
<i>0.25% gel 10000 MSC</i>	1140,5	44305,5	1533,5	
	1895	15390	1343	
	375	34021	301	
<i>0.5% gel</i>				34332,25
				1829
				1880
<i>0.25% gel</i>				39559,67
				7896
				18352

Table 5: **Leukemic cell survival from gel recovery.** The table shows count numbers of either ALL sytoxred negative/CD19+ cells cocultured with either 5500, 10000 human primary MSCs or monoculture in 0.25 or 0.5% of Puramatrix concentration. The table also shows counts of MSCs CD146, CD76, CD166 +/-sytoxred negative after recovery in coculture and monoculture. The aim was to have the best condition for ALL survival in coculture. The red square highlights results from 3 independent experiments with the highest ALL cells number obtained from gel recovery.

When the gel was analyzed without cells and stained with CD19, the mix of CD146, CD76, CD166 or single stain, it showed a marked autofluorescence in all channels. The autofluorescence covered part of cells' signals, especially the MSCs' which usually appear in the circled gate in figure 28A. The only solution for the analysis was to exclude the contribution of the gel, as visible in figure 28B (red circle) resulting in minimal gel autofluorescence in MSCs sytoxred negative gate (orange circle). However, the intensity of gel's autofluorescence was covering the signal coming from MSCs and in part from ALL cells leading to an underestimation of the final count and therefore of the entire analysis.

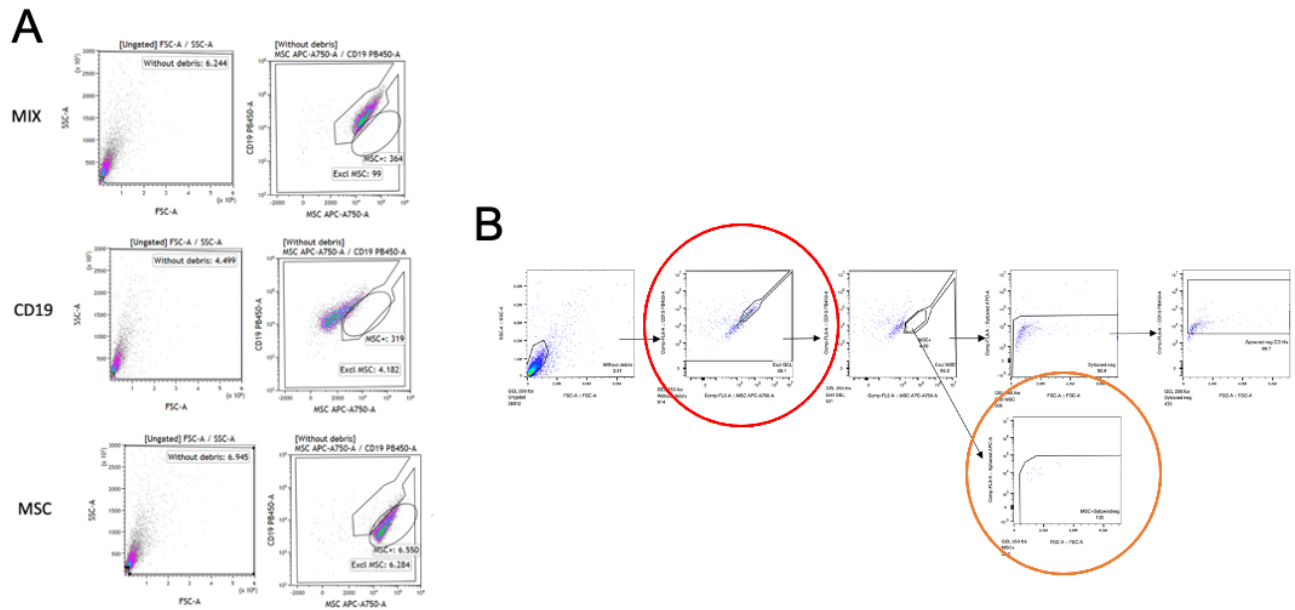


Figure 28: **Analysis of gel only in flow cytometry.** (A). Gel only was stained with the mix of antibody used for the analysis which comprises CD19, CD146, CD76, CD166; CD19 only and the mix for MSCs (CD146, CD76, CD166). In all cases a consistent population is evident. (B). when the gel population is excluded (red circle) is possible to gate the MSCs and proceed with the analysis without interference (orange circle).

4.15 Stabilized cell lines survival *in vitro* measurements by microscopy

Although flow cytometry offers high-throughput, automated quantification on a cell-by-cell basis, it showed a significant autofluorescence of the gel covering the cells (MSCs and ALL) signal and leading to an underestimation of the quantification. To overcome this issue, we introduced microscopy as second approach to the analysis. Firstly we wanted to exclude that low recovery of cells from the Puramatrix with flow cytometry was due to low viability of MSCs and ALL cells present in the 3D coculture. Cell viability was then visualized using IncuCyte® Cytotox Reagents for Counting Dead Cells stain using Leica DMI8 microscope. To better locate the two cell types during imaging, before seeding, human primary MSCs were stained with the lipophilic fluorescent dye Dil and stabilized human REH cell line with DiO. Both dyes will label all cellular membranes in a cell. Cell viability was tested using Cytotox stain. In Figure 29, Cytotox staining did not seem to overlap with Dil (MSCs) suggesting that MSCs were alive in Puramatrix hydrogel, both in coculture and in monoculture. ALL cells appeared like a cloud and overlap with Cytotox in some spots indicating the presence of dead ALL cells both in coculture and monoculture. However, the analysis of the exact number of live and dead cells could be performed due to technical limitations. Indeed, cells appeared in complex clusters where the count of single cells was difficult.

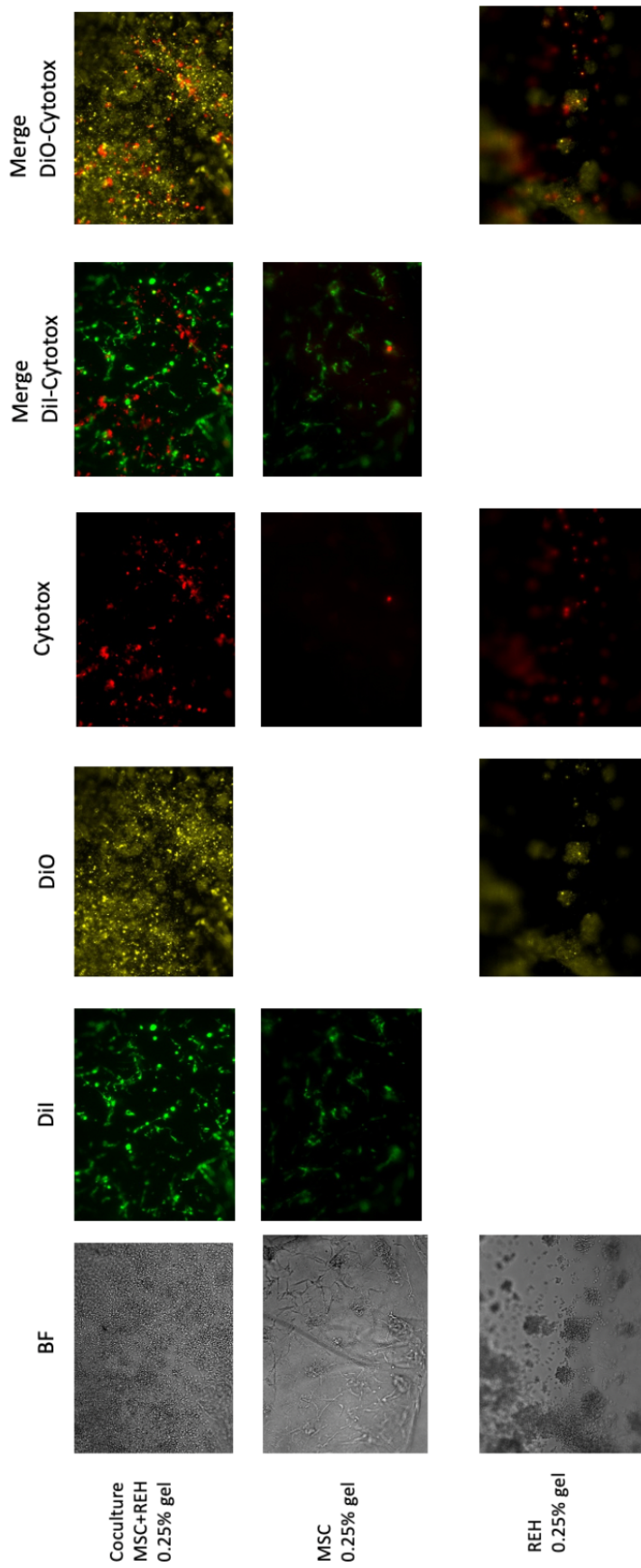


Figure 29: **MSC and ALL are alive inside Puramatrix hydrogel.** Representative images of MSC monoculture, ALL monoculture (REH cells) and coculture in 0.25% puramatrix gel. MSCs were stained in DiI (green), added to the gel and let migrated inside the gel for three days. This was followed by addition of DiO-labeled ALL cells (yellow) and incubation for three days. The coculture was stained with cytotox (red) just before imaging. BF, brightfield.

4.16 MSC migration into Puramatrix hydrogel

The chemoattractive strategy leading to migration of ALL cells toward MSCs contributes to the creation of a leukemic niche. At the moment the study of the mechanism behind this migration is limited to a 2-dimensional system which is not representative of the complex *in vivo* architecture. The 3D system should overcome this limit and allow to study the leukemic niche formation and the interaction between cells. To lately study ALL migration towards MSCs, we first investigated when MSCs were migrated completely inside the gel. 10000 of human primary MSCs were seeded on top of 0.25% Puramatrix hydrogel concentration and migration of MSCs into the gel was visualized daily. On day 1, MSCs appeared to attach on the gel surface as single cells; the shape and the distribution of single cells was similar to what was observed in 2D system⁶². From day 3, a network of cells was visible, where MSCs formed multiple compact cell clusters with different heights in the gel as visible in Figure 30. The cells were left in culture up to 6 days and no relevant changes in terms of cells shape were observed (not shown). Thus, it was chosen to add ALL cells to the gel three days after seeding MSCs.

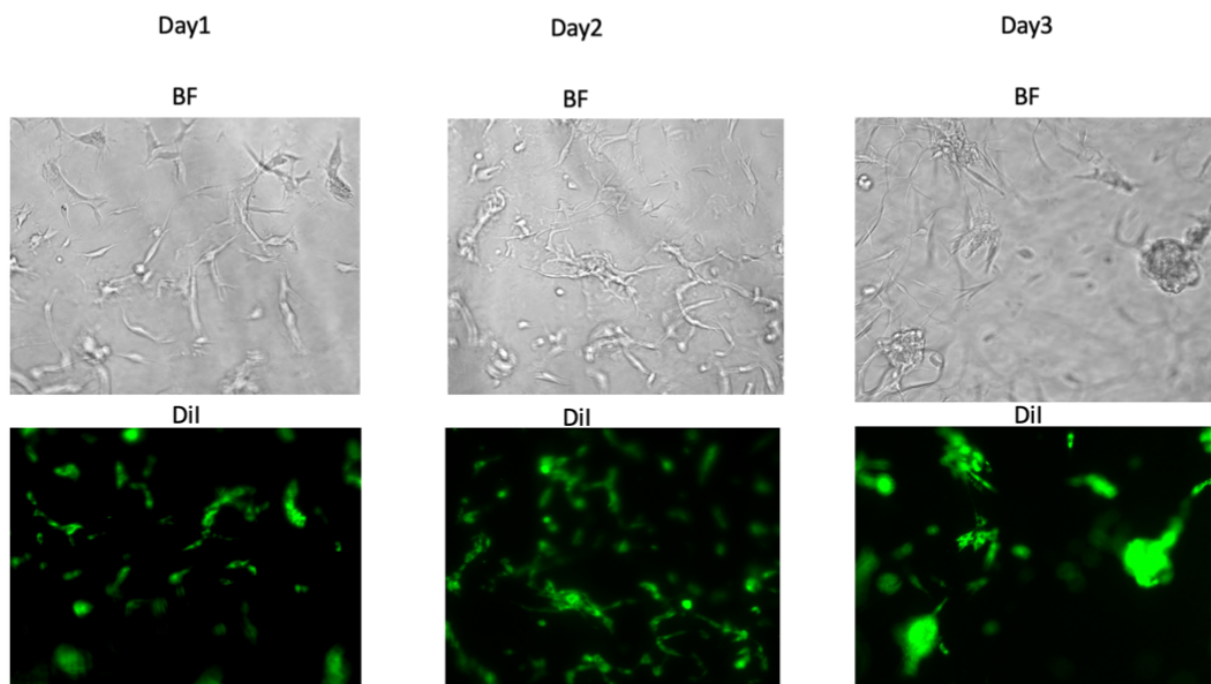


Figure 30: **MSCs migrate inside the hydrogel in three days.** Representative images of MSCs in monoculture from the first day of culture to the third. To check migration of MSCs inside the gel, MSCs were stained with Dil (green). Images of MSC migration into the hydrogel upon day 1 to 3 were shown. BF = brightfield.

4.17 ALL cells migration in coculture and monoculture into Puramatrix hydrogel

Once MSCs migration into the gel was visualized, we wanted to observe ALL migration towards MSCs in the 3D model proposed. 10000 of human primary MSCs were seeded on top of 0.25% Puramatrix hydrogel concentration. In parallel 0.1% of Puramatrix hydrogel concentration and Cultrex Basement Membrane Extract (BME) were tested as controls. Previous 3D models studies demonstrated how a less thick matrix is preferred for 3D cellular models ⁴¹, 0.1% of Puramatrix hydrogel was then introduced to check if a lower concentration could also be adopted for this model. BME on the other hand is a natural extracellular matrix that mimics the complex extracellular environment and differs from Puramatrix which is purely synthetic. MSCs were let to migrate into the gel for 72h and human ALL NALM6 cell line was then seeded on top of the 3 gels at a concentration of 0.2×10^6 /ml. We monitored ALL migration at the beginning of coculture and after three days. The first day, ALL cells were uniformly distributed on the gel surface in all gels. Three days after seeding, ALL cells appeared to be attracted by MSCs clumps forming clusters (Figure 31). The thickness of 0.1% of Puramatrix resulted anyway not appropriate since MSCs appeared also attached to the bottom surface. In Figure 31 MSCs appeared in clusters and single cells similarly in shape and distribution to what happens in 2D creating both a 3D and a 2D condition at the same time.

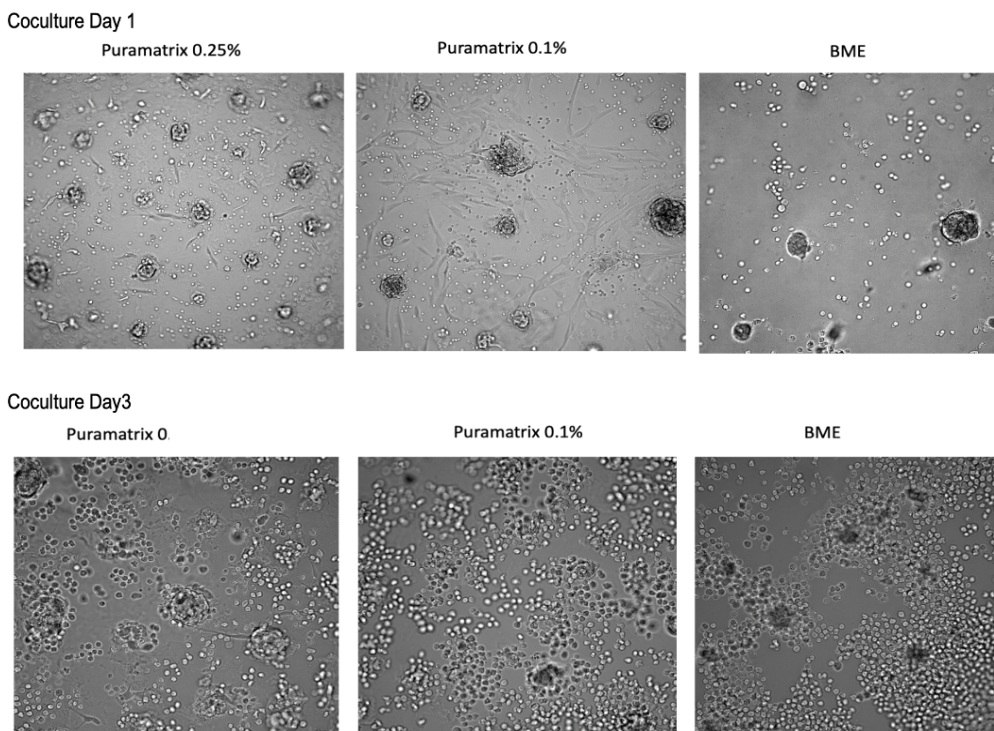
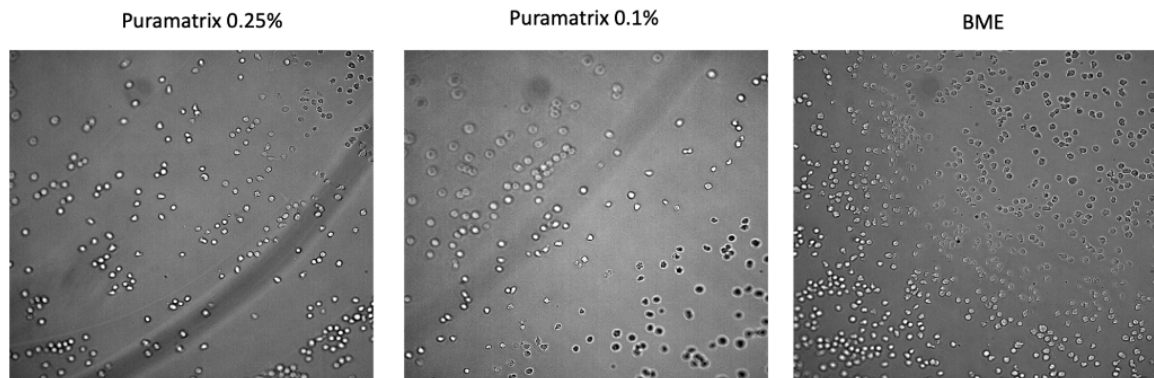


Figure 31: **ALL cells migrate inside towards MSCs creating clusters.** Representative images of ALL (NALM6 cells) migration in the gel towards MSCs in coculture in brightfield. 10000 MSCs were seeded on top of the gels and let to migrate for 72h when ALL cells were then added at a concentration of 0.2×10^6 /ml Images of ALL migration into the hydrogel upon day 1 to 3 were shown. Comparison between 0.25% puramatrix, 0.1% puramatrix and BME.

ALL cells were then seeded on top of the gels that did not contain MSCs and let to migrate for 3 days. Pictures were taken at the beginning of the culture and after 3 days. ALL cells remained randomly distributed on the surface at day 1 and inside the gel after 3 days of culture (Figure 32). The three gels showed comparable results. When coculture and monoculture are compared, the architecture of ALL cells together with MSCs looked like a big complex cluster, which differed from the monoculture.

Nalm6 only Day 1



Nalm6 only Day3

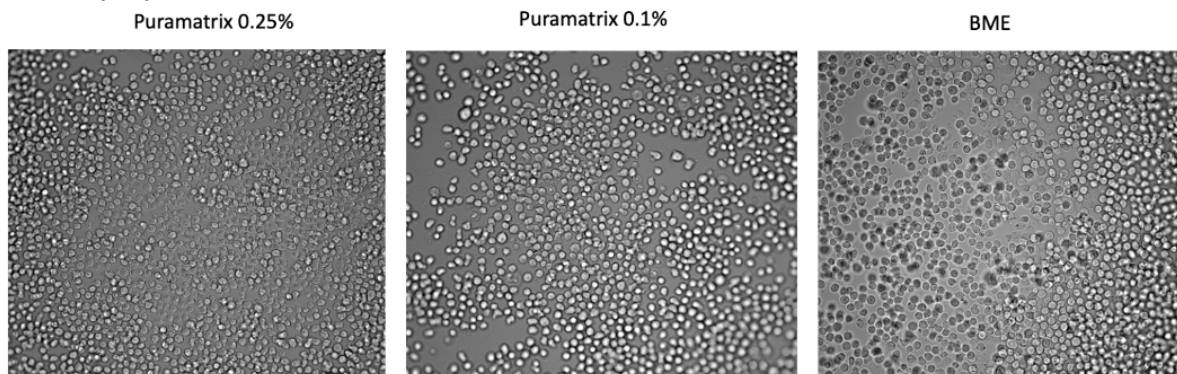


Figure 32: **In monoculture ALL cells migrate inside the hydrogel and remain randomly distributed.** Pictures of ALL (NALM6 cells) migration inside the gel in monoculture in brightfield. 0.2×10^6 /ml ALL cells were seeded on top of the gels and let to migrate for 3 days. Images of ALL migration into the hydrogel upon day 1 to 3 were shown. All images in brightfield. Comparison between 0.25% puramatrix, 0.1% puramatrix and BME.

4.18 MSC and ALL communication in the 3D architecture

When the leukemic niche is formed, TNTs and others important intercellular communication mechanisms such as extracellular vesicles, gap junctions and integrins, are involved in leukemia survival and drug resistance. Previous studies already demonstrated the capability of MSCs and ALL to communicate and the protective function of MSCs toward ALL cells ¹⁶. Similarly, we wanted to observe cell communication in this 3D model using the lipophilic carbocyanine dyes. These dyes, stain lipophilic structures in the entire cell, and exhibited very low cell toxicity. While passive transfer of these dyes is negligible, it can be transferred actively from cell to cell upon contact. When the dye is transferred, the receiver will become positive because of the fluorescent dye from the other cell type. For this experiment, NALM6 ALL cell line were labelled with Dil, and MSCs with DiD. 10000 of labelled MSCs were seeded on top of 0.25% of Puramatrix gel and let to migrate for 72h. 0.2×10^6 /ml stabilized human ALL NALM6 cell line was then added and the coculture lasted for 3 days in total. In Figure 33 shows Dil is transferred from NALM6 ALL cells towards MSCs, as MSCs become positive for Dil over time. To prove the effective dye transfer, excluding that the signal might be due to an ALL cell on top of an MSC, we checked the expression of Dil in a single MSC. In Figure 33 a single MSC is highlighted, showing

the presence of ALL-derived DiI inside MSCs. From these preliminary results we can observe that ALL cells and MSCs are also able to communicate and transfer material in the 3D structure.

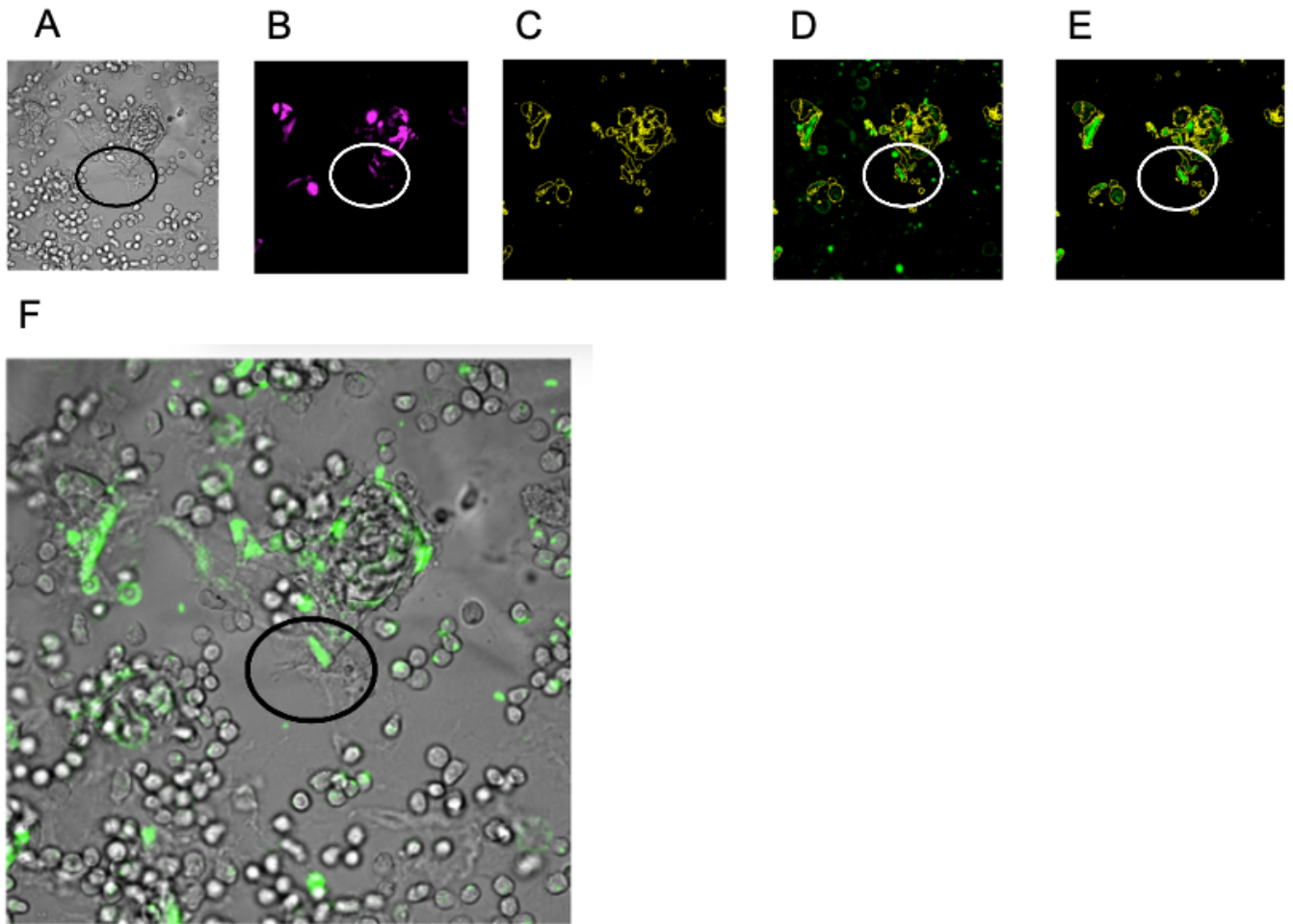


Figure 33: **ALL cells and MSCs can communicate.** To check ALL and MSCs communication 10000 MSCs were stained in DiI (magenta) seed on top of the gel and let migrated inside the gel for three days. This was followed by addition of DiI-labeled 0.2×10^6 /ml NALM6 ALL cells (green) and incubation for three days. To prove the effective dye transfer we detected a single MSC from the brightfield (A) (the circle) and created a mask around DiI signal to underline this signal (B and C). When the mask was applied to DiI signal (D) and ALL signal was deleted (E), it remained evident the dye contribution from ALL cells to a single MSC (circled) (F).

4.19 TLA

Currently, the multiplex PCR conditions have been set up for the candidate genes: *CRLF2*, *PDGFRb*, *ABL1*, *JAK2*, *TCF3*, *NR3C1*. The protocol required quality controls that guarantee the good progress of the reaction: undigested control (after the crosslinking phase), digested control (after the digestion phase) and ligation control (after the ligation phase) which, run on 1% agarose gels, appeared as a band >10kb, a smear between 0.3 and 0.2 kb and a band followed by a smear >5kb respectively (Figure 34).

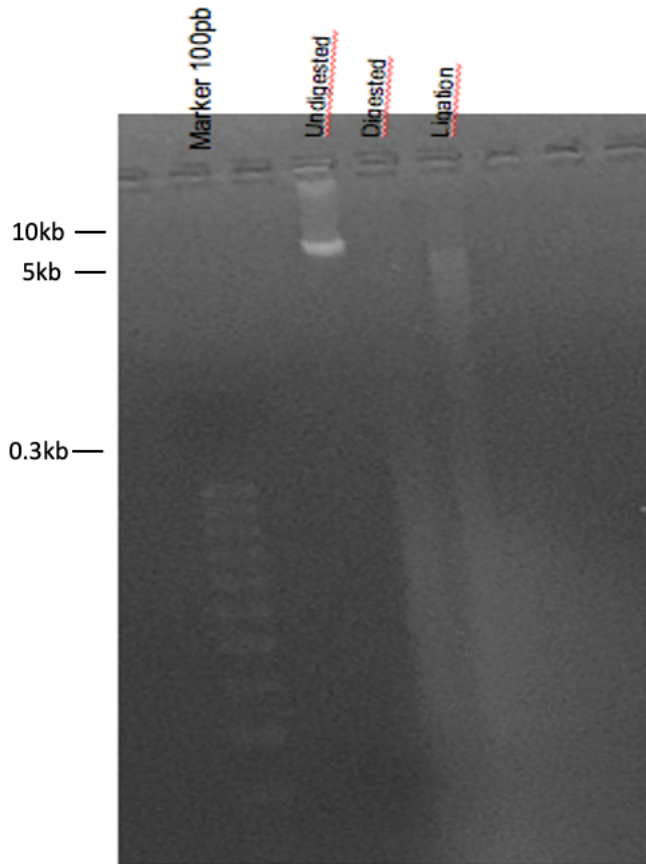


Figure 34: **TLA quality controls.** Image of undigested, digested and ligation controls run on a 1% agarose gel. Undigested control appeared as a band around 10kb, digested was a smear between 0.3 and 0.2 kb and ligation appeared as a band followed by a smear around 5kb.

Primary cell samples of 16 ALL patients in total (identified by the ONC code followed by a progressive number) stored in the laboratory of the University of Trieste were thawed, and 3-5 million cells were used for each sample. The protocol required together with quality controls, two purifications for which DNA quantification are shown in Table 6. The minimum criteria to proceed with sequencing provided: DNA concentration after 2 purifications around 10-20 μg and 3-6 μg respectively and quality controls (Figure 34).

First, 7 samples were processed (Table 6A) and sent to Cergentis for sequencing and analysis. The total number of reads obtained in each individual sample resulted in more background and less specific coverage (defined as the number of Next Generation Sequencing (NGS) reads that cover a sequence) to identify any translocation. However, according to the company, ONC10, ONC13 and ONC29 showed a better coverage and for this reason they were processed a second time and sent again for sequencing (Table 6B).

A

Sample No.	TLA 1 purification in µg	TLA 2 purification in µg
ONC29_2R	30,6	3,91
ONC10	33	15,72
ONC13	29,3	12,88
ONC14	30,6	3,6
ONC21	36	13,9
ONC23	4,5	1,9
ONC24	0,9	31,2

B

Sample No.	TLA 1 purification in µg	TLA 2 purification in µg
ONC29_2R	10,4	5,5
ONC10	16,2	4,9
ONC13	9,4	6,5

Table 6: **DNA quantity after purification.** (A). Quantity of DNA obtained after purification of the first 7 samples (B). Quantity of DNA obtained after purification of ONC10,13 and 29.

The second sequencing analysis identified translocation t(1;19)(q23.3;p13.3) resulting in the *TCF3-PBX1* fusion for patient ONC13 (not shown). Patient ONC29_2R showed t(9;22)(q34;q11) which corresponds to *BCR-ABL1* (Figure 35) and at least for patient ONC10 they did not detect any breakpoints using the multiplex primer set for *NR3C1*, *ABL1*, *JAK2*, *CRLF2*, *PDGFRB* and *TCF3*.

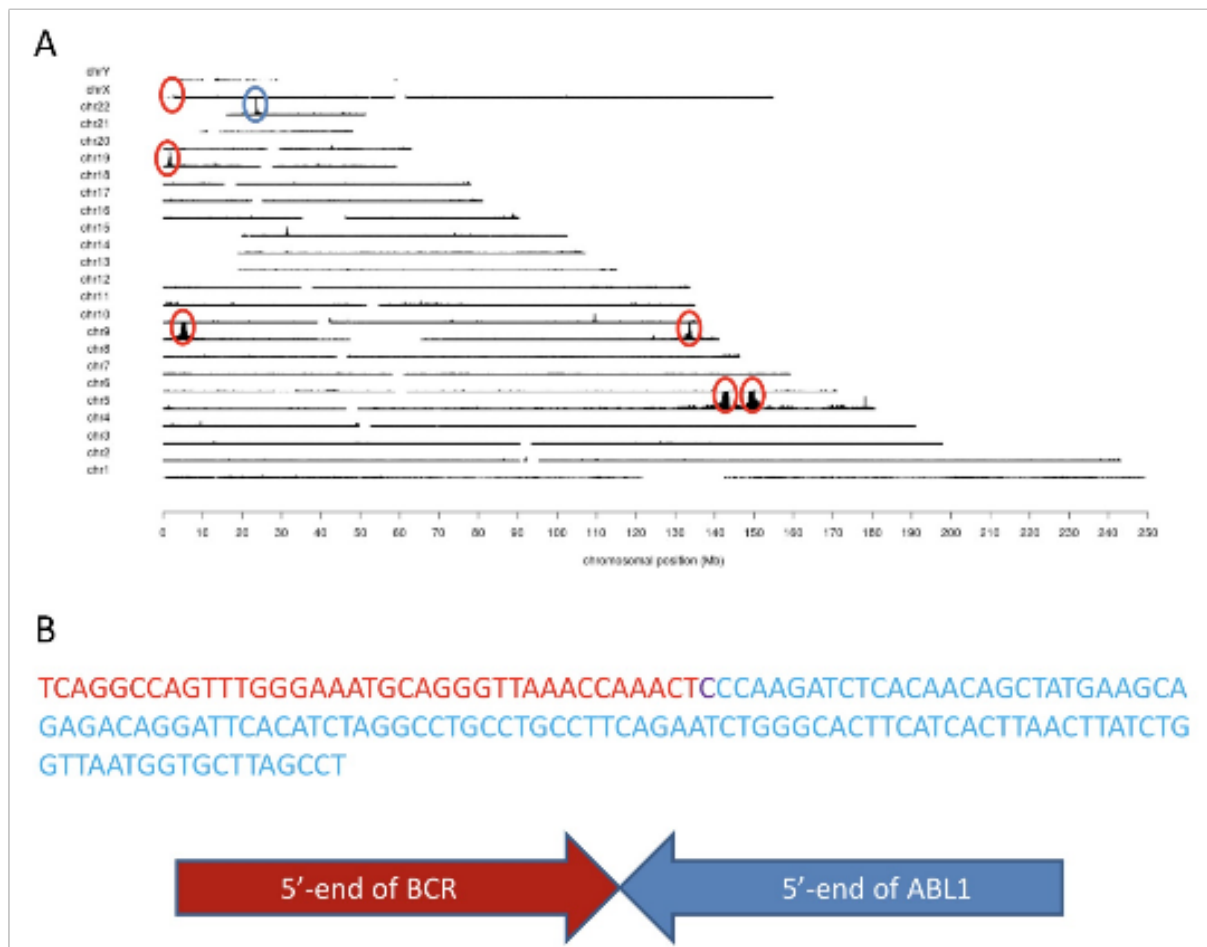


Figure 35: **ONC29 total coverage**. Panel A: The figure represents the total coverage obtained for the ONC29. Coverage is defined as the number of NGS reads that cover a sequence. All chromosomes are indicated in y-axis and the chromosomal position on the x-axis. Each peak represents a single integration site of specific view points for each single gene of interest. In blue the peak corresponding to the *BCR* gene partner of *ABL1*. Panel B: exact *BCR-ABL1* breaking point.

At the moment another 8 samples have been processed (Table 7) and from these only ONC76, ONC151, ONC25, ONC28, ONC50, ONC71 will be sent for sequencing in agreement with the company.

Sample No.	TLA 1 purification in µg	TLA 2 purification in µg
ONC25	3,43	2,08
ONC28	3,36	3
ONC50	4,5	2,42
ONC71	5,7	3,02
ONC76	2,74	2,9
ONC87	0,5	
ONC126	0,423	0,224
ONC151	3,13	2,48

Table 7: **DNA quantity after purification**. Quantity of DNA obtained after purification of 8 new samples

5 DISCUSSION

BCR-ABL like ALL are recognized as high-risk ALL subtypes across all clinical studies, being characterized by an unfavorable prognosis and a higher relapse rate in comparison to other BCP-ALL subtypes²⁰. The heterogeneity in their genetic background makes the characterization of TK *BCR-ABL like* very challenging and, currently, approaches like exome, whole genome and whole transcriptome sequencing are too expensive to be used in clinical practice¹⁰⁰. *BCR-ABL like* are TK-driven ALL that can be functionally distinguished into two major groups according to the activation of either the ABL or JAK–STAT pathway; a third, smaller group is characterized by involvement of genetic fusions that lead to altered TK in the RAS pathways¹⁷. Currently, fast and practical systems to identify the specific TKI for a direct assignment of a target therapy to patients with *BCR-ABL like* ALL is missing. Kinase activity and protein phosphorylation act as major drivers in different mechanisms such as cell cycle, differentiation and the disruption of these processes leads to malignancy. In recent years, kinases have been studied from different points of view and several potential peptides allow the study of these protein activities *in vitro* have been developed⁵⁷. In the context of the ABL-class of *BCR-ABL like* leukemia, the analysis was performed using the peptide described, initially developed to be functional for *BCR-ABL1* in CML. To validate this approach also in *BCR-ABL like* ALL, 4 ALL cell lines with different genetic backgrounds were selected and initially characterized by Western blot: NALM6 harboring *ETV6-PDGFRB*¹⁵(DSMZ, ACC-128) and ALL-SIL a T-ALL line positive for *NUP214-ABL1*, a fusion that also belongs to *BCR-ABL like* subgroup (DSMZ, ACC-128) both leading to ABL1 pathway activation; K562 and REH as positive and negative control respectively. *PDRGFB* is a cytoplasmic receptor that activates the ABL1 pathway and *PDRGFB* rearrangements (*ETV6-PDGFRB* and *EBF1-PDGFRB*) consist in about 1% of *BCR-ABL like* positive patients. Recent studies observed a reduction in signalling with imatinib in cases harbouring ABL-class rearrangements and in particular a case of refractory *EBF1-PDGFRB* ALL patient had a complete remission¹⁰¹. The chimeric protein contains the amino-terminal 154 aa of ETV6 protein fused to the transmembrane and cytoplasmic domains of PDGFRB. Western blot confirmed the presence of ETV6-PDGFRB in NALM6 which has a calculated molecular mass of 76 kDa⁹⁵ and the monomer migrates as a component approximately at 90-100 kDa in SDS gel-electrophoresis. However, in contrast to the wild-type PDGFRB which occurs as a dimer, ETV6-PDGFRB appeared to be present in NALM6 predominantly as oligomeric or multimeric complexes resulting in a band around 200 kDa²⁹. The wild type PDGFRB was also detectable in all the cell lines (a band around 100 kDa) except in K562. Some investigators report that NALM6 cell line harbors a different translocation, in particular DUX4-rearranged (t(4;14)(q35;q32)) /ERG deletion^{84,97}; however, both our Western blotting analysis and cytogenetic information on the t(5;12)(q33.2;p13.2)

translocation ⁵ (<https://www.dsmz.de/collection/catalogue/details/culture/ACC-128>) confirm the presence of the *ETV6-PDGFRB* in the NALM6 cells used in this work thesis work.

ABL is a ubiquitous tyrosine kinase that has been implicated in processes of cell differentiation, cell division, cell adhesion and migration ⁸⁵ and, according to our results, a band around 125 kDa corresponding to ABL1 was observed in all the lines. K562 is a cell line derived from a CML patient positive for *BCR-ABL1* ⁴³ and the presence of the chimeric protein was also confirmed by Western blot. Both the phosphorylated and non-phosphorylated forms of BCR-ABL1 (210 kDa) were detected in K562. Different was the situation for NUP214-ABL1 which was identified in ALL-SIL only as non-phosphorylated protein. The enzymatic activity of the ABL1 is regulated by tyrosine residues auto-phosphorylation (Y412 and Y245); phosphorylation of both tyrosines stabilizes the active conformation of the ABL1 and Y245 in particular increases the catalytic activity ⁸⁵. Studies demonstrate that BCR-ABL1 regulates a phosphorylation of more than 20 different tyrosine residues on ABL1 ⁵³, while NUP214-ABL1 displays much lower general tyrosine auto-phosphorylation (Tyr-245 is phosphorylated and Tyr-412 not). These differences might be related to the distinct subcellular localization or the recruitment of a different set of phosphatases. Indeed, whereas BCR-ABL1 is localized in the cytoplasm, NUP214-ABL1 is localized in the nuclear pore complex and is strictly dependent on this subcellular localization for its activity and oncogenic transformation ⁵³.

The peptide phosphorylation was quantified by an ELISA assay using cell lysates from the line mentioned through a neutravidin-coated plate allowing the binding of the biotin in the peptide sequence. K562 cells showed the highest fluorescence signal on P_{ABL} although comparable to that observed for ALL-SIL. Since PDGFRB is linked to ABL activation ⁴, fluorescence values for the *BCR-ABL like* cell line NALM6 should be higher than others lacking a constitutively active ABL pathway, in particular the negative control REH. The reason is still unclear, but it can be related to the ubiquitous presence of ABL1 in all cell lines ⁸⁵. Indeed, Western blot analysis with anti-human ABL1 showed the presence of non-phosphorylated ABL1 in both REH and NALM6, without detecting the phosphorylated form. The specificity of the P_{ABL} phosphorylation signal was also confirmed after treatment with TKIs. Indeed, the ABL-inhibitor imatinib was used at a concentration of 5 μ M that, as reported in the literature, that represents the steady state plasma concentration after 5-7 days of treatment in adult CML at a dose of 400 mg/day ⁴⁰ and is 20 times higher than the IC₅₀ calculated *in vitro* on cellular tyrosine phosphorylation assay ⁹². At this concentration a significant decrease of the P_{ABL} phosphorylation levels for all cell lines lysates were observed. It is known from the literature that imatinib has an unusually high selectivity to ABL1 because it targets the inactive conformation which is unique to this kinase

⁴². Mass spectrometry analysis investigating imatinib-associated proteins in K562 lysates confirmed the direct interaction of the drug with only few targets, including the known interactor BCR-ABL1 and the ABL1-related gene (ARG), Discoidin Domain Receptor Tyrosine Kinase 1 (DDR1) and the proto-oncogene receptor tyrosine kinase (KIT) ^{30,82}. DDR1 and KIT are receptor tyrosine kinases and their contribution to the ABL1 activation likely depends on extracellular stimuli. Therefore, considering that our *in vitro* system works on cell lysates rather than whole cells in the absence of specific ligands, their confounding contribution to the P_{ABL} phosphorylation, if any, is likely less important. In contrast, the contribution of ARG (closely related to ABL1) could be an issue. However, the P_{ABL} *target* region should guarantee an increased specificity for ABL1 compared to ARG. Mass spectrometry studies identified an additional off-target (non-tyrosine kinase) of imatinib, the NAD(P)H:quinone oxidoreductase NQO2, whose enzymatic function should not influence peptide phosphorylation ^{30,82}. In contrast to imatinib, the anti-JAK inhibitor ruxolitinib did not affect the phosphorylation levels at any of the concentrations selected (52 nM and 5 μM). The concentration of 52 nM was chosen in accordance to pharmacokinetic parameters measured in healthy subjects at steady state following a twice-daily administration of ruxolitinib at 15 mg and is 20 times higher than the IC₅₀ of 2.8 ± 1.2 nM calculated *in vitro* for JAK2 by a biochemical enzymatic inhibitory assay ⁷⁹. The second concentration of 5 μM is much higher than the pharmacological range and was included into the P_{ABL}-based ELISA assay in order to verify the absence of inhibition, even at this high concentration.

In our *in vitro* ELISA assay, P_{ABL}TIDE was clearly less efficient than P_{ABL}, designed to increase the specificity to ABL1 among other kinases. Besides the increased specificity of P_{ABL} over P_{ABL}TIDE, the ELISA assay proposed in this paper presents other advantages over conventional kinase assay. Firstly, the biosensor phosphorylation was quantified on a solid-phase through a neutravidin-coated plate that allows the binding of the biotin in the P_{ABL} sequence. This high specific binding greatly reduces background noise signals. Secondly, whole cell lysates can be used, avoiding tricky ABL1 purification and bypassing the problems related to the peptide penetration into intact cells. Thirdly, a unique primary antibody, i.e.: an anti-phosphotyrosine, is required. This advantage is particularly important for *BCR-ABL like* ALL because the ELISA assay conditions could be optimized regardless of the specific chimeric protein encoded by the genetic abnormalities in *BCR-ABL like* leukemic cells of the ABL-class.

Taken together, these observations suggest that the P_{ABL}-based ELISA assay is suitable for measuring the ABL1 kinase activity of cell lysates through the P_{ABL}-Y phosphorylation in the “*reporter*” region. P_{ABL} could be more suitable in detecting aberrant sustained kinase activity of ABL1-chimeric proteins rather than an over-activation of native ABL1 due to upstream signaling; however, a limitation of this study is that the difference

between basal and sustained ABL1 activity is still too tiny for the P_{ABL}-based ELISA assay to be of practical clinical interest without any further optimization. To confirm its utility, our system should be improved in sensitivity and accuracy, and results could be strengthened through the use of other TKIs, the use of different biosensors (e.g. of downstream signaling components such as STAT5 that is known to be activated by ABL-class rearrangements), and the test of patient samples of known genotype. Nonetheless, the results here described represents the first step towards the setup of a point-of-care device for diagnosis and monitoring of pediatric *BCR-ABL like* patients.

The device is also suitable for adults with ALL with even greater benefits. The incidence of *BCR-ABL like* ALL increases with age⁸⁹ and adults affected by leukemia have generally worse prognoses (survival at 5 years in Italy: ~ 39%, age considered: 15-99 years, period considered: 2005-2009 (Report AIRTUM 2018) and for myeloid leukemia (5-year survival in Italy: ~ 20% for acute form and ~ 56% for chronic, age considered: 15-99 years, period considered: 2005-2009²⁵).

In the context of the JAK-class, 2 candidate sequences were selected as described in the introduction. P1_{JAK2} represented the potential “*reporter*” region¹⁴ and was subjected to docking analysis to verify the binding potential with JAK2 and compared with the already published P2_{JAK2}⁵⁷. From extensive Molecular Dynamics (DM) analysis, P1_{JAK2} revealed better binding potential to JAK2, even when compared with P2_{JAK2}; in both cases the binding energy ΔG was negative, but P1_{JAK2} had a more favorable binding energy than P2_{JAK2}. Despite P1_{JAK2} seemed a promising “*reporter*” for a potential JAK-class biosensor, the sequence needs to be amplified for further functional analysis. Computational results must be validated and surface plasmon resonance (SPR) might be a good option. SPR is one of the most used techniques to study protein-protein interactions. The main advantage of SPR is the ability to measure the binding affinities and association/dissociation kinetics of complexes in real time, in a label-free environment, and using relatively small quantities of material⁸¹. An expression and purification protocol to obtain JAK2 Janus kinase 1 (JH1) domain from *E. coli* was established to recover substrates for the SPR experiment. After two attempts, the yields of the JAK2 kinase domain was rather low. Moreover, while the expression and purification of JAK2 seemed to have gone well in the first prep, the protein did not seem to be stable for even short period of time at 4 °C, which would be a minimal requirement for functional assays. Several vendors sell the kinase domain of JAK2, and the expression systems used is exclusive for insect cells. In addition, several crystal structures of the kinase domain of JAK2 have been determined, and an insect/mammalian expression system was exclusively used to produce the protein. Although there is no reference for this in the literature, and since

insect/mammalian cells are in general used for proteins that are not expressed well/stably in *E. coli*, we hypothesized that the protein we expressed in this experiment in *E. coli* is not fully folded into a stable domain and not fully functional. After 2 failed preps, we concluded that a functional JAK2 kinase domain cannot be expressed in *E. coli* and could not be used for downstream functional analysis. Future prospective experiments include a commercial JAK2 kinase domain for SPR analysis, P1_{JAK2} optimization and ELISA assay as described for ABL-class. The protocol used here was already rather unusual in terms of duration (around 16-20 hrs) of expression in very rich medium, and it would be very difficult to increase the expression in this system.

In collaboration with Prof. Den Boer at the Princess Maxima center for Pediatric Oncology (Utrecht, The Netherlands) attempts were made to optimize an *ex vivo* assay of primary leukemic cells in coculture with primary mesenchymal stromal cells (MSCs). *In vitro* primary leukemic cell proliferation and viability is low or undetectable even when culture media are supplemented with exogenous growth factors⁵⁹. Previous studies underline the benefit effect of the coculture of ALL cells with MSCs¹³, but it is still unclear whether or not ALL cells survival can be promoted *in vitro* and what conditions are required. The main objective of this study was to discover a condition that would result in a higher ALL cell viability, either in a two-dimensional (2D) or three-dimensional (3D) approach, favorable for the biosensor testing on primary cells. The 2D assay aimed to promote cell survival in a coculture with addition of different cocktails of growth factors. B-others *ETV6-RUNX1* and *BCR-ABL1* primary ALL cells, previously shown to not survive *in vitro*, were selected and cocultured on top of a MSC layer. The growth factors were selected according to their effect in terms of prolonging ALL cell survival when added in culture media^{31,36,44,47,48,51,52,96}: IL7, G-CSF, FLT3LG, TPO, IL3, SCF, IL2, TSLP. In total, primary leukemic cells from ten patients with B-ALL (2 *ETV6-RUNX1*, 6 B-others, 2 *BCR-ABL1*) were thawed and seeded directly on MSCs layers. The first 2 screenings, in which different concentration and different combination of growth factors were tested, showed no improvement in terms of ALL survival. However, when different culture medium such as hematopoietic stem cells medium SFEM II with or without serum were included, leukemic cells from one patient (BO5) showed an increase from 13% to 90% of survival using SFEM II serum free added with FLT3LG, IL7, IL3. Therefore, SFEM II serum free that can be used for culture of normal stem cells (manufacturer's information), could be used for *in vitro* culture of native ALL primary cells⁵¹. Strikingly, the leukemic cells of BO5 patient harbored a Ras mutation. Ras has been shown to play an important role in regulating cell proliferation in several systems. Li et al demonstrate that Flt3/Ras signals govern B cell development via effects on IL7R/STAT5 signaling². This information could explain the survival increase obtained in the third attempt and pointed the need of optimize culture condition for each

patient. However, since all these experiments were performed in single, we cannot exclude variation due to technical reasons. At this stage the aim was to quickly screen many different conditions and investigate later only those that achieved survival improvement. Primary leukemic cells is, indeed, a limited and precious material that cannot be consumed for preliminary experiment. Further studies will better investigate the results reported for BO5.

In this study the 2D system failed to prolong ALL *in vitro* survival and a 3D model mimicking the bone marrow organization might be the best option. Comparison of a traditional 2D model of cells in suspension with a 3D model showed increased resistance to chemotherapeutic-induced cell death in the 3D model as compared with the 2D model, which was hypothesized to be related to the three-dimensional architecture itself ¹. To improve viability of ALL cells we cocultured human leukemia stabilized cell lines together with human primary MSCs in a synthetic matrix named Corning® PuraMatrix™ Peptide Hydrogel (PuraMatrix). PuraMatrix has a pure synthetic composition consisting of standard amino acids (1% w/v) and 99% water used to create defined 3D microenvironments. Under physiological conditions, the peptide component self-assembles into a 3D hydrogel with a nanometer-scale fibrous structure (manufacturer's information). In contrast, Cultrex Basement Membrane Extract (BME) is the trade name for an extracellular protein mixture secreted by Engelbreth-Holm-Swarm (EHS) mouse sarcoma cells. Similarly, Matrigel, is a natural extracellular matrix that mimics the complex extracellular environment. In both cases the natural source may result in batch differences. Firstly, primary ALL cell viability was analyzed by flow cytometry, but the autofluorescence of Puramatrix hydrogel covered cells' (MSCs and ALL) signal leading to an underestimation of the final count of the entire analysis. Although flow cytometry offers high-throughput, automated quantification on a cell-by-cell basis, we introduced microscopy as second approach to the analysis. Firstly, cell viability was evaluated using IncuCyte® Cytotox Reagents for Counting Dead Cells stain and only ALL cells' death was observed. However, in Puramatrix hydrogel, cells appeared as a cloud clustered together with MSCs clumps making difficult any quantitative analysis. Interestingly imaging allowed other important observations. MSCs migrate into the gel and create complex clusters of cells attracting leukemic cells. Indeed, comparing ALL migration in monoculture and in coculture with MSCs, the different 3D cells architecture was immediately evident: in monoculture cells were homogeneously distributed while in coculture ALL cells accumulated around MSCs. The chemoattractive effect leading to migration of ALL cells toward MSCs in a 2D model has already been demonstrated. ALL cells migrate towards MSCs to create a leukemic niche and MSCs promote their survival and chemotherapy resistance ¹³. In this manuscript a similar attraction is observed, but it is still under discussion whether this

migration is related to MSCs tunnel formation into the gel. MSCs are indeed seeded on top of the Puramatrix hydrogel 72h prior of ALL cells and let to migrate into it. While migrating they may create tunnels in which ALL cells may drop, once they are added to the culture. To exclude this hypothesis and prove ALL cells active migration toward MSCs, the extracellular matrix structure may be stained as previously described⁶³. On the other hand, the chemoattractive strategy behind this migration is still under investigation in 2D. When this scenario will be clear, disrupting the chemoattractive axis will certainly prove active migration also in 3D.

Once leukemic cells create the leukemic niche, tunneling nanotubes (TNT) and other important intercellular communication mechanisms such as extracellular vesicles, gap junctions and integrins are involved in ALL and MSCs communication. Previous data already demonstrated bidirectional transfer of lipophilic dyes in a 2-dimensional system, indicating active crosstalk within the leukemic niche¹⁶. Similarly, we differentially stained ALL cells and mesenchymal stromal cells. After 3 days of coculture, we observe dye transfer from donor ALL to a single MSC. These preliminary data are promising for future investigation of the 3D structure. Unfortunately, in this 3D system, TNT formation was impossible to visualize due to limitation of the instrument. To overcome all the limitation encountered with this 3D system, other synthetic hydrogel such as VitroGel, Biogelx, Hystem gel may be considered; alternatively, wharton's jelly matrix (DWJM), the gelatinous material in the umbilical cord, would provide a more similar environment to the bone marrow extracellular matrix.

As mentioned above, the biosensor functionality needs to be tested on primary human *BCR-ABL like* ALL cells. At the University of Trieste primary leukemic cells from patients enrolled in AIEOP BFM ALL 2009 are stored, for which characterization of *BCR-ABL like* translocation is lacking. TLA identifies the presence of chromosomal translocations, ensuring the amplification and selective sequencing of regions physically close to a particular gene of interest. The advantage of this technique is that it allows the identification of fusions of the gene of interest with partner genes not yet known and therefore not detectable with current cytogenetic analyzes based on a candidate approach⁹⁰. These analyzes were performed using a sample preparation kit and sequencing service provided by the company Cergentis (Utrecht, The Netherlands). In total 16 primary leukemic samples have been processed and from these, 7 were sent for sequencing, resulting in a coverage rather low to identify any translocation. Three of these patients showed anyway a better coverage and were re-processed and sent for sequencing. The second analysis identified translocation t(1;19)(q23.3;p13.3) resulting in the *TCF3-PBX1* fusion for patient ONC13. Patient ONC29_2R showed t(9;22)(q34;q11) which corresponds to *BCR-ABL1* and at least for patient ONC10 they did not detect any breakpoints using the

multiplex primer set for *NR3C1*, *ABL1*, *JAK2*, *CRLF2*, *PDGFRB* and *TCF3*. The availability of primary cells limits the success of this procedure; the initial material consists indeed in frozen primary leukemic cells for which sufficient cell recovery for analysis is low. However, sequencing are underway for the other primary leukemic samples present in the laboratory.

6 CONCLUSION

The *in vitro* assay proposes the development of a point-of-care device that might improve the diagnosis, guide the doctor to the choice of the best TKI and monitor the clinical response also for those patients with primary resistance. Currently, pediatric *BCR-ABL1* and *BCR-ABL like* ALL have a very poor survival rate comparing to another ALL. By identifying in a timely manner, the best TKI to be used in treatment, the chances of survival for these children would be optimized and the chances of developing severe toxicities linked to exposure to high doses of inadequate drugs would also be reduced.

7 REFERENCES

1. Barboglio F, Belloni D, Scarfò L, Sbrana FV, Ponzoni M, Bongiovanni L, et al. 3D co-culture model of chronic lymphocytic leukemia bone marrow microenvironment predicts patient-specific response to mobilizing agents. *Haematologica*. 2020 Jul 30;
2. Li L-X, Goetz CA, Katerndahl CDS, Sakaguchi N, Farrar MA. A Flt3- and Ras-dependent pathway primes B cell development by inducing a state of IL-7 responsiveness. *J Immunol Baltim Md 1950*. 2010 Feb 15;184(4):1728–36.
3. Yang T-Y, Eissler CL, Hall MC, Parker LL. A multiple reaction monitoring (MRM) method to detect Bcr-Abl kinase activity in CML using a peptide biosensor. *PloS One*. 2013;8(2):e56627.
4. Plattner R, Irvin BJ, Guo S, Blackburn K, Kazlauskas A, Abraham RT, et al. A new link between the c-Abl tyrosine kinase and phosphoinositide signalling through PLC-gamma1. *Nat Cell Biol*. 2003 Apr;5(4):309–19.
5. Wlodarska I, Aventín A, Inglés-Esteve J, Falzetti D, Criel A, Cassiman JJ, et al. A new subtype of pre-B acute lymphoblastic leukemia with t(5;12)(q31q33;p12), molecularly and cytogenetically distinct from t(5;12) in chronic myelomonocytic leukemia. *Blood*. 1997 Mar 1;89(5):1716–22.
6. Jakubikova J, Cholujova D, Hideshima T, Gronosova P, Soltysova A, Harada T, et al. A novel 3D mesenchymal stem cell model of the multiple myeloma bone marrow niche: biologic and clinical applications. *Oncotarget*. 2016 Nov 22;7(47):77326–41.
7. Henriques ST, Thorstholm L, Huang Y-H, Getz JA, Daugherty PS, Craik DJ. A novel quantitative kinase assay using bacterial surface display and flow cytometry. *PloS One*. 2013;8(11):e80474.
8. Placzek EA, Plebanek MP, Lipchik AM, Kidd SR, Parker LL. A peptide biosensor for detecting intracellular Abl kinase activity using matrix-assisted laser desorption/ionization time-of-flight mass spectrometry. *Anal Biochem*. 2010 Feb 1;397(1):73–8.
9. Gnanasambandan K, Sayeski PP. A structure-function perspective of Jak2 mutations and implications for alternate drug design strategies: the road not taken. *Curr Med Chem*. 2011;18(30):4659–73.
10. Den Boer ML, van Slegtenhorst M, De Menezes RX, Cheok MH, Buijs-Gladdines JGCAM, Peters STCJM, et al. A subtype of childhood acute lymphoblastic leukaemia with poor treatment outcome: a genome-wide classification study. *Lancet Oncol*. 2009 Feb;10(2):125–34.
11. Kirshner J, Thulien KJ, Martin LD, Debes Marun C, Reiman T, Belch AR, et al. A unique three-dimensional model for evaluating the impact of therapy on multiple myeloma. *Blood*. 2008 Oct 1;112(7):2935–45.
12. De Braekeleer E, Douet-Guilbert N, Rowe D, Bown N, Morel F, Berthou C, et al. ABL1 fusion genes in hematological malignancies: a review. *Eur J Haematol*. 2011 May;86(5):361–71.
13. de Rooij B, Polak R, van den Berk LCJ, Stalpers F, Pieters R, den Boer ML. Acute lymphoblastic leukemia cells create a leukemic niche without affecting the CXCR4/CXCL12 axis. *Haematologica*. 2017 Oct;102(10):e389–93.
14. Sanz A, Ungureanu D, Pekkala T, Ruijtenbeek R, Touw IP, Hillhorst R, et al. Analysis of Jak2 catalytic function by peptide microarrays: the role of the JH2 domain and V617F mutation. *PloS One*. 2011 Apr 18;6(4):e18522.
15. Matheson EC, Hall AG. Assessment of mismatch repair function in leukaemic cell lines and blasts from children with acute lymphoblastic leukaemia. *Carcinogenesis*. 2003 Jan;24(1):31–8.
16. Polak R, de Rooij B, Pieters R, den Boer ML. B-cell precursor acute lymphoblastic leukemia cells use tunneling nanotubes to orchestrate their microenvironment. *Blood*. 2015 Nov 19;126(21):2404–14.

17. Ofran Y, Izraeli S. BCR-ABL (Ph)-like acute leukemia-Pathogenesis, diagnosis and therapeutic options. *Blood Rev.* 2017 Mar;31(2):11–6.
18. An X, Tiwari AK, Sun Y, Ding P-R, Ashby CR, Chen Z-S. BCR-ABL tyrosine kinase inhibitors in the treatment of Philadelphia chromosome positive chronic myeloid leukemia: a review. *Leuk Res.* 2010 Oct;34(10):1255–68.
19. Cario G, Leoni V, Conter V, Baruchel A, Schrappe M, Biondi A. BCR-ABL1-like acute lymphoblastic leukemia in childhood and targeted therapy. *Haematologica.* 2020 Sep 1;105(9):2200–4.
20. Boer JM, Marchante JRM, Evans WE, Horstmann MA, Escherich G, Pieters R, et al. BCR-ABL1-like cases in pediatric acute lymphoblastic leukemia: a comparison between DCOG/Erasmus MC and COG/St. Jude signatures. *Haematologica.* 2015 Sep;100(9):e354-357.
21. Chiaretti S, Messina M, Foà R. BCR/ABL1-like acute lymphoblastic leukemia: How to diagnose and treat? *Cancer.* 2019 Jan 15;125(2):194–204.
22. Izraeli S. Beyond Philadelphia: 'Ph-like' B cell precursor acute lymphoblastic leukemias - diagnostic challenges and therapeutic promises. *Curr Opin Hematol.* 2014 Jul;21(4):289–96.
23. Pieters R, Carroll WL. Biology and treatment of acute lymphoblastic leukemia. *Pediatr Clin North Am.* 2008 Feb;55(1):1–20, ix.
24. Bhojwani D, Yang JJ, Pui C-H. Biology of childhood acute lymphoblastic leukemia. *Pediatr Clin North Am.* 2015 Feb;62(1):47–60.
25. Iavarone I, Buzzoni C, Stoppa G, Steliarova-Foucher E, SENTIERI-AIRTUM Working Group. Cancer incidence in children and young adults living in industrially contaminated sites: from the Italian experience to the development of an international surveillance system. *Epidemiol Prev.* 2018 Dec;42(5-6S1):76–85.
26. Songyang Z, Carraway KL, Eck MJ, Harrison SC, Feldman RA, Mohammadi M, et al. Catalytic specificity of protein-tyrosine kinases is critical for selective signalling. *Nature.* 1995 Feb 9;373(6514):536–9.
27. Braham MVJ, Minnema MC, Aarts T, Sebestyen Z, Straetemans T, Vyborova A, et al. Cellular immunotherapy on primary multiple myeloma expanded in a 3D bone marrow niche model. *Oncoimmunology.* 2018;7(6):e1434465.
28. Cox CV, Evely RS, Oakhill A, Pamphilon DH, Goulden NJ, Blair A. Characterization of acute lymphoblastic leukemia progenitor cells. *Blood.* 2004 Nov 1;104(9):2919–25.
29. Sjöblom T, Boureux A, Rönstrand L, Heldin CH, Ghysdael J, Ostman A. Characterization of the chronic myelomonocytic leukemia associated TEL-PDGF beta R fusion protein. *Oncogene.* 1999 Nov 25;18(50):7055–62.
30. Rix U, Hantschel O, Dürnberger G, Remsing Rix LL, Planyavsky M, Fernbach NV, et al. Chemical proteomic profiles of the BCR-ABL inhibitors imatinib, nilotinib, and dasatinib reveal novel kinase and nonkinase targets. *Blood.* 2007 Dec 1;110(12):4055–63.
31. Corazza F, Hermans C, D'Hondt S, Ferster A, Kentos A, Benoît Y, et al. Circulating thrombopoietin as an in vivo growth factor for blast cells in acute myeloid leukemia. *Blood.* 2006 Mar 15;107(6):2525–30.
32. Aricò M, Schrappe M, Hunger SP, Carroll WL, Conter V, Galimberti S, et al. Clinical outcome of children with newly diagnosed Philadelphia chromosome-positive acute lymphoblastic leukemia treated between 1995 and 2005. *J Clin Oncol Off J Am Soc Clin Oncol.* 2010 Nov 1;28(31):4755–61.
33. Saltzman A, Stone M, Franks C, Searfoss G, Munro R, Jaye M, et al. Cloning and characterization of human Jak-2 kinase: high mRNA expression in immune cells and muscle tissue. *Biochem Biophys Res Commun.* 1998 May 29;246(3):627–33.

34. Suri C, Naik PK. Combined molecular dynamics and continuum solvent approaches (MM-PBSA/GBSA) to predict noscapiinoid binding to γ -tubulin dimer. *SAR QSAR Environ Res.* 2015 Jun;26(6):507–19.
35. Laurini E, Marson D, Aulic S, Fermeglia M, Pricl S. Computational Alanine Scanning and Structural Analysis of the SARS-CoV-2 Spike Protein/Angiotensin-Converting Enzyme 2 Complex. *ACS Nano.* 2020 Sep 22;14(9):11821–30.
36. Takatsu K. Cytokines involved in B-cell differentiation and their sites of action. *Proc Soc Exp Biol Med Soc Exp Biol Med N Y N.* 1997 Jun;215(2):121–33.
37. Mullighan CG, Su X, Zhang J, Radtke I, Phillips LAA, Miller CB, et al. Deletion of IKZF1 and prognosis in acute lymphoblastic leukemia. *N Engl J Med.* 2009 Jan 29;360(5):470–80.
38. Tang J, Wang JY, Parker LL. Detection of early Abl kinase activation after ionizing radiation by using a peptide biosensor. *Chembiochem Eur J Chem Biol.* 2012 Mar 19;13(5):665–73.
39. van den Berk LCJ, van der Veer A, Willemse ME, Theeuwes MJGA, Lujendijk MW, Tong WH, et al. Disturbed CXCR4/CXCL12 axis in paediatric precursor B-cell acute lymphoblastic leukaemia. *Br J Haematol.* 2014 Jul;166(2):240–9.
40. Druker BJ, Talpaz M, Resta DJ, Peng B, Buchdunger E, Ford JM, et al. Efficacy and safety of a specific inhibitor of the BCR-ABL tyrosine kinase in chronic myeloid leukemia. *N Engl J Med.* 2001 Apr 5;344(14):1031–7.
41. Lueckgen A, Garske DS, Ellinghaus A, Mooney DJ, Duda GN, Cipitria A. Enzymatically-degradable alginate hydrogels promote cell spreading and in vivo tissue infiltration. *Biomaterials.* 2019 Oct;217:119294.
42. Lee SJ, Wang JYJ. Exploiting the promiscuity of imatinib. *J Biol.* 2009;8(3):30.
43. Wu SQ, Voelkerding KV, Sabatini L, Chen XR, Huang J, Meisner LF. Extensive amplification of bcr/abl fusion genes clustered on three marker chromosomes in human leukemic cell line K-562. *Leukemia.* 1995 May;9(5):858–62.
44. Lisovsky M, Estrov Z, Zhang X, Consoli U, Sanchez-Williams G, Snell V, et al. Flt3 ligand stimulates proliferation and inhibits apoptosis of acute myeloid leukemia cells: regulation of Bcl-2 and Bax. *Blood.* 1996 Nov 15;88(10):3987–97.
45. Roberts KG, Morin RD, Zhang J, Hirst M, Zhao Y, Su X, et al. Genetic alterations activating kinase and cytokine receptor signaling in high-risk acute lymphoblastic leukemia. *Cancer Cell.* 2012 Aug 14;22(2):153–66.
46. Kratz CP, Stanulla M, Cavé H. Genetic predisposition to acute lymphoblastic leukemia: Overview on behalf of the I-BFM ALL Host Genetic Variation Working Group. *Eur J Med Genet.* 2016 Mar;59(3):111–5.
47. Day RB, Bhattacharya D, Nagasawa T, Link DC. Granulocyte colony-stimulating factor reprograms bone marrow stromal cells to actively suppress B lymphopoiesis in mice. *Blood.* 2015 May 14;125(20):3114–7.
48. Crooks GM, Hao QL, Petersen D, Barsky LW, Bockstoce D. IL-3 increases production of B lymphoid progenitors from human CD34+CD38- cells. *J Immunol Baltim Md 1950.* 2000 Sep 1;165(5):2382–9.
49. Nakasone ES, Askautrud HA, Kees T, Park J-H, Plaks V, Ewald AJ, et al. Imaging tumor-stroma interactions during chemotherapy reveals contributions of the microenvironment to resistance. *Cancer Cell.* 2012 Apr 17;21(4):488–503.
50. Biondi A, Schrappe M, De Lorenzo P, Castor A, Lucchini G, Gandemer V, et al. Imatinib after induction for treatment of children and adolescents with Philadelphia-chromosome-positive acute lymphoblastic leukaemia (EsPhALL): a randomised, open-label, intergroup study. *Lancet Oncol.* 2012 Sep;13(9):936–45.

51. Bruserud Ø, Glenjen N, Ryningen A, Ulvestad E. *In vitro* culture of human acute lymphoblastic leukemia (ALL) cells in serum-free media; a comparison of native ALL blasts, ALL cell lines and virus-transformed B cell lines. *Leuk Res*. 2003 May;27(5):455–64.
52. Barata JT, Cardoso AA, Nadler LM, Boussiotis VA. Interleukin-7 promotes survival and cell cycle progression of T-cell acute lymphoblastic leukemia cells by down-regulating the cyclin-dependent kinase inhibitor p27(kip1). *Blood*. 2001 Sep 1;98(5):1524–31.
53. De Keersmaecker K, Versele M, Cools J, Superti-Furga G, Hantschel O. Intrinsic differences between the catalytic properties of the oncogenic NUP214-ABL1 and BCR-ABL1 fusion protein kinases. *Leukemia*. 2008 Dec;22(12):2208–16.
54. AIRTUM Working Group, CCM, AIEOP Working Group. Italian cancer figures, report 2012: Cancer in children and adolescents. *Epidemiol Prev*. 2013 Feb;37(1 Suppl 1):1–225.
55. Jatiani SS, Baker SJ, Silverman LR, Reddy EP. Jak/STAT pathways in cytokine signaling and myeloproliferative disorders: approaches for targeted therapies. *Genes Cancer*. 2010 Oct;1(10):979–93.
56. Rane SG, Reddy EP. JAKs, STATs and Src kinases in hematopoiesis. *Oncogene*. 2002 May 13;21(21):3334–58.
57. Lipchik AM, Perez M, Bolton S, Dumrongprechachan V, Ouellette SB, Cui W, et al. KINATEST-ID: a pipeline to develop phosphorylation-dependent terbium sensitizing kinase assays. *J Am Chem Soc*. 2015 Feb 25;137(7):2484–94.
58. Colmone A, Amorim M, Pontier AL, Wang S, Jablonski E, Sipkins DA. Leukemic cells create bone marrow niches that disrupt the behavior of normal hematopoietic progenitor cells. *Science*. 2008 Dec 19;322(5909):1861–5.
59. Pal D, Blair HJ, Elder A, Dormon K, Rennie KJ, Coleman DJL, et al. Long-term *in vitro* maintenance of clonal abundance and leukaemia-initiating potential in acute lymphoblastic leukaemia. *Leukemia*. 2016 Aug;30(8):1691–700.
60. Locatelli F, Moretta F, Rutella S. Management of relapsed acute lymphoblastic leukemia in childhood with conventional and innovative approaches. *Curr Opin Oncol*. 2013 Nov;25(6):707–15.
61. Villarino AV, Kanno Y, O'Shea JJ. Mechanisms and consequences of Jak-STAT signaling in the immune system. *Nat Immunol*. 2017 Mar 22;18(4):374–84.
62. Lo Sicco C, Reverberi D, Balbi C, Ulivi V, Principi E, Pascucci L, et al. Mesenchymal Stem Cell-Derived Extracellular Vesicles as Mediators of Anti-Inflammatory Effects: Endorsement of Macrophage Polarization. *Stem Cells Transl Med*. 2017 Mar;6(3):1018–28.
63. Leonard AK, Loughran EA, Klymenko Y, Liu Y, Kim O, Asem M, et al. Methods for the visualization and analysis of extracellular matrix protein structure and degradation. *Methods Cell Biol*. 2018;143:79–95.
64. Cohen GB, Ren R, Baltimore D. Modular binding domains in signal transduction proteins. *Cell*. 1995 Jan 27;80(2):237–48.
65. Ghazavi F, Lammens T, Van Roy N, Poppe B, Speleman F, Benoit Y, et al. Molecular basis and clinical significance of genetic aberrations in B-cell precursor acute lymphoblastic leukemia. *Exp Hematol*. 2015 Aug;43(8):640–53.
66. Schmah J, Fedders B, Panzer-Grümayer R, Fischer S, Zimmermann M, Dagdan E, et al. Molecular characterization of acute lymphoblastic leukemia with high CRLF2 gene expression in childhood. *Pediatr Blood Cancer*. 2017 Oct;64(10).
67. Cilloni D, Saglio G. Molecular pathways: BCR-ABL. *Clin Cancer Res Off J Am Assoc Cancer Res*. 2012 Feb 15;18(4):930–7.

68. Khatri A, Wang J, Pendergast AM. Multifunctional Abl kinases in health and disease. *J Cell Sci.* 2016 Jan 1;129(1):9–16.
69. Meijerink JPP, den Boer ML, Pieters R. New genetic abnormalities and treatment response in acute lymphoblastic leukemia. *Semin Hematol.* 2009 Jan;46(1):16–23.
70. Saini L, Brandwein J. New Treatment Strategies for Philadelphia Chromosome-Positive Acute Lymphoblastic Leukemia. *Curr Hematol Malig Rep.* 2017 Apr;12(2):136–42.
71. Oh I-H, Jeong S-Y, Kim J-A. Normal and leukemic stem cell niche interactions. *Curr Opin Hematol.* 2019 Jul;26(4):249–57.
72. Zhou M-H, Yang Q-M. NUP214 fusion genes in acute leukemia (Review). *Oncol Lett.* 2014 Sep;8(3):959–62.
73. Aricò M, Valsecchi MG, Camitta B, Schrappe M, Chessells J, Baruchel A, et al. Outcome of treatment in children with Philadelphia chromosome-positive acute lymphoblastic leukemia. *N Engl J Med.* 2000 Apr 6;342(14):998–1006.
74. Roberts KG, Pei D, Campana D, Payne-Turner D, Li Y, Cheng C, et al. Outcomes of children with BCR-ABL1-like acute lymphoblastic leukemia treated with risk-directed therapy based on the levels of minimal residual disease. *J Clin Oncol Off J Am Soc Clin Oncol.* 2014 Sep 20;32(27):3012–20.
75. Den Boer ML, Harms DO, Pieters R, Kazemier KM, Gobel U, Körholz D, et al. Patient stratification based on prednisolone-vincristine-asparaginase resistance profiles in children with acute lymphoblastic leukemia. *J Clin Oncol Off J Am Soc Clin Oncol.* 2003 Sep 1;21(17):3262–8.
76. Wu D, Sylvester JE, Parker LL, Zhou G, Kron SJ. Peptide reporters of kinase activity in whole cell lysates. *Biopolymers.* 2010;94(4):475–86.
77. Tasian SK, Loh ML, Hunger SP. Philadelphia chromosome-like acute lymphoblastic leukemia. *Blood.* 2017 Nov 9;130(19):2064–72.
78. Palmi C, Vendramini E, Silvestri D, Longinotti G, Frison D, Cario G, et al. Poor prognosis for P2RY8-CRLF2 fusion but not for CRLF2 over-expression in children with intermediate risk B-cell precursor acute lymphoblastic leukemia. *Leukemia.* 2012 Oct;26(10):2245–53.
79. Quintás-Cardama A, Vaddi K, Liu P, Manshouri T, Li J, Scherle PA, et al. Preclinical characterization of the selective JAK1/2 inhibitor INCB018424: therapeutic implications for the treatment of myeloproliferative neoplasms. *Blood.* 2010 Apr 15;115(15):3109–17.
80. Tefferi A. Primary myelofibrosis: 2021 update on diagnosis, risk-stratification and management. *Am J Hematol.* 2021 Jan;96(1):145–62.
81. Douzi B. Protein-Protein Interactions: Surface Plasmon Resonance. *Methods Mol Biol Clifton NJ.* 2017;1615:257–75.
82. Bantscheff M, Eberhard D, Abraham Y, Bastuck S, Boesche M, Hobson S, et al. Quantitative chemical proteomics reveals mechanisms of action of clinical ABL kinase inhibitors. *Nat Biotechnol.* 2007 Sep;25(9):1035–44.
83. Bloom M, Maciaszek JL, Clark ME, Pui C-H, Nichols KE. Recent advances in genetic predisposition to pediatric acute lymphoblastic leukemia. *Expert Rev Hematol.* 2020 Jan;13(1):55–70.
84. Yasuda T, Tsuzuki S, Kawazu M, Hayakawa F, Kojima S, Ueno T, et al. Recurrent DUX4 fusions in B cell acute lymphoblastic leukemia of adolescents and young adults. *Nat Genet.* 2016 May;48(5):569–74.
85. Greuber EK, Smith-Pearson P, Wang J, Pendergast AM. Role of ABL family kinases in cancer: from leukaemia to solid tumours. *Nat Rev Cancer.* 2013 Aug;13(8):559–71.

86. Prici S, Cortelazzi B, Dal Col V, Marson D, Laurini E, Fermeiglia M, et al. Smoothened (SMO) receptor mutations dictate resistance to vismodegib in basal cell carcinoma. *Mol Oncol*. 2015 Feb;9(2):389–97.
87. Neculai D, Neculai AM, Verrier S, Straub K, Klumpp K, Pfitzner E, et al. Structure of the unphosphorylated STAT5a dimer. *J Biol Chem*. 2005 Dec 9;280(49):40782–7.
88. Kronenberg E, Weber F, Brune S, Schepmann D, Almansa C, Friedland K, et al. Synthesis and Structure-Affinity Relationships of Spirocyclic Benzopyrans with Exocyclic Amino Moiety. *J Med Chem*. 2019 Apr 25;62(8):4204–17.
89. Roberts KG, Li Y, Payne-Turner D, Harvey RC, Yang Y-L, Pei D, et al. Targetable kinase-activating lesions in Ph-like acute lymphoblastic leukemia. *N Engl J Med*. 2014 Sep 11;371(11):1005–15.
90. de Vree PJP, de Wit E, Yilmaz M, van de Heijning M, Klous P, Verstegen MJAM, et al. Targeted sequencing by proximity ligation for comprehensive variant detection and local haplotyping. *Nat Biotechnol*. 2014 Oct;32(10):1019–25.
91. Franca R, Kuzelicki NK, Sorio C, Toffoletti E, Montecchini O, Poropat A, et al. Targeting Kinase-activating Genetic Lesions to Improve Therapy of Pediatric Acute Lymphoblastic Leukemia. *Curr Med Chem*. 2018;25(24):2811–25.
92. Deininger M, Buchdunger E, Druker BJ. The development of imatinib as a therapeutic agent for chronic myeloid leukemia. *Blood*. 2005 Apr 1;105(7):2640–53.
93. Schinnerl D, Fortschegger K, Kauer M, Marchante JRM, Kofler R, Den Boer ML, et al. The role of the Janus-faced transcription factor PAX5-JAK2 in acute lymphoblastic leukemia. *Blood*. 2015 Feb 19;125(8):1282–91.
94. Lucet IS, Fantino E, Styles M, Bamert R, Patel O, Broughton SE, et al. The structural basis of Janus kinase 2 inhibition by a potent and specific pan-Janus kinase inhibitor. *Blood*. 2006 Jan 1;107(1):176–83.
95. Carroll M, Tomasson MH, Barker GF, Golub TR, Gilliland DG. The TEL/platelet-derived growth factor beta receptor (PDGF beta R) fusion in chronic myelomonocytic leukemia is a transforming protein that self-associates and activates PDGF beta R kinase-dependent signaling pathways. *Proc Natl Acad Sci U S A*. 1996 Dec 10;93(25):14845–50.
96. Scheeren FA, van Lent AU, Nagasawa M, Weijer K, Spits H, Legrand N, et al. Thymic stromal lymphopoietin induces early human B-cell proliferation and differentiation. *Eur J Immunol*. 2010 Apr;40(4):955–65.
97. Tanaka Y, Kawazu M, Yasuda T, Tamura M, Hayakawa F, Kojima S, et al. Transcriptional activities of DUX4 fusions in B-cell acute lymphoblastic leukemia. *Haematologica*. 2018 Nov;103(11):e522–6.
98. Pui C-H, Evans WE. Treatment of acute lymphoblastic leukemia. *N Engl J Med*. 2006 Jan 12;354(2):166–78.
99. Abou Dalle I, Jabbour E, Short NJ, Ravandi F. Treatment of Philadelphia Chromosome-Positive Acute Lymphoblastic Leukemia. *Curr Treat Options Oncol*. 2019 Jan 24;20(1):4.
100. Boer JM, Steeghs EMP, Marchante JRM, Boeree A, Beaudoin JJ, Beverloo HB, et al. Tyrosine kinase fusion genes in pediatric BCR-ABL1-like acute lymphoblastic leukemia. *Oncotarget*. 2017 Jan 17;8(3):4618–28.
101. Weston BW, Hayden MA, Roberts KG, Bowyer S, Hsu J, Fedoriw G, et al. Tyrosine kinase inhibitor therapy induces remission in a patient with refractory EBF1-PDGFRB-positive acute lymphoblastic leukemia. *J Clin Oncol Off J Am Soc Clin Oncol*. 2013 Sep 1;31(25):e413-416.
102. Pettersen EF, Goddard TD, Huang CC, Couch GS, Greenblatt DM, Meng EC, et al. UCSF Chimera—a visualization system for exploratory research and analysis. *J Comput Chem*. 2004 Oct;25(13):1605–12.

103. Songyang Z, Blechner S, Hoagland N, Hoekstra MF, Piwnica-Worms H, Cantley LC. Use of an oriented peptide library to determine the optimal substrates of protein kinases. *Curr Biol CB*. 1994 Nov 1;4(11):973–82.
104. Case, D. A.; Ben-Shalom, I. Y.; Brozell, S. R.; Cerutti, D. S.; Cheatham III, T. E.; Cruzeiro, V. W. D.; Darden, T. A.; Duke, R. E.; Ghoreishi, D.; Giambasu, G.; Giese, T.; Gilson, M. K.; Gohlke, H.; Goetz, A. W.; Greene, D.; Harris, R.; Homeyer, N.; Huang, Y.; Izadi, S.; Kovalenko, A.; Krasny, R.; Kurtzman, T.; Lee, T. S.; LeGrand, S.; Li, P.; Lin, C.; Liu, J.; Luchko, T.; Luo, R.; Man, V.; Mermelstein, D. J.; Merz, K. M.; Miao, Y.; Monard, G.; Nguyen, C.; Nguyen, H.; Onufriev, A.; Pan, F.; Qi, R.; Roe, D. R.; Roitberg, A. E.; Sagui, C.; Schott-Verdugo, S.; Shen, J.; Simmerling, C. L.; Smith, J.; Swails, J.; Walker, R. C.; Wang, J.; Wei, H.; Wilson, L.; Wolf, R. M.; Wu, X.; Xiao, L.; Xiong, Y.; York, D. M.; Kollman, P. A. AMBER 2019, University of California, San Francisco., 2019.